Supplementary Materials for

Regional and global sea-surface temperatures during the last interglaciation

Jeremy S. Hoffman,* Peter U. Clark, Andrew C. Parnell, Feng He

*Corresponding author. Email: jhoffman@smv.org

Published 20 January 2017, *Science* **355**, 276 (2017)
DOI: 10.1126/science.aai8464

This PDF file includes:

Materials and Methods
Figs. S1 to S43
Tables S1 and S2
References

Other Supplementary Materials for this manuscript includes the following:
(available at www.sciencemag.org/content/355/6322/276/suppl/DC1)

Data File S1

Materials and Methods

1. LIG Proxy Database

We compiled published data from 83 marine sedient core sites with co-registered proxy-based sea surface temperature (SST) and benthic foraminiferal $\delta^{18}O$ records that span the Last Interglaciation (LIG), which is defined as the interval (129-116 ka) when global mean sea level was above present (*21*). We restricted records to those that have a resolution of <4,000 years on their published age models (Table S1, Fig. S1). These selection criteria yielded a database containing 104 independent time series of proxy-based SSTs during the LIG (Table S1). Proxies used to estimate SSTs include the alkenone unsaturation index ($U^{K'}_{37}$) (n=20), planktonic foraminiferal Mg/Ca (n=12), and microfossil bioassemblages (census counts of planktonic foraminifera [n=59], radiolaria [n=8], coccoliths [n=6], and diatoms [n=2]).

Geochemical proxies of SST (Mg/Ca, $U^{K'}_{37}$) are inferred to reflect either summer season or mean annual SST. Where the inferred season of the geochemical SST estimate is not made explicit in the primary publication, we assume either summer or annual SST based on the calibration dataset cited by the authors. Altogether, our database includes 19 records from 19 sites that reflect summer SSTs and 85 records from 72 sites that reflect mean annual SSTs (Table S1).

SST estimates based on microfossil assemblages are generally reported as a "August-summer" and "February-winter" SST estimate (*5*). Following methods used for global SST compilations for Termination 1 (*32*) and the Holocene (*33*), we assume that average of these two seasonal estimates is equivalent to the mean annual SST. To assess this assumption, we subtracted the observed average annual SSTs from the average of "summer" (August) plus "winter" (February) SSTs over the period 1870-2015 from the HadlSST1.1 data set (*17*) for each

of the grid boxes containing the microfossil SST records (Fig. S2). To assess the sensitivity of this relationship to changing boundary conditions, we did the same calculation for the last 6,000 years of the TRACE21 experiment, which most closely approximates the LIG with respect to ice-sheet extent but still captures changes in insolation and greenhouse gases (*34*) (Fig. S2).

In general, the HadlSST1.1 data agree with the TRACE21 data, with average summer-plus-winter SSTs at Southern Hemisphere extratropical sites showing a warm bias relative annual SSTs and a cold bias in the tropics. There is a minor difference in the Northern Hemisphere extratropical sites, with the TRACE21 data not showing the warm bias suggested by the HadlSST1.1 data, but we attribute this difference to a known cold bias in the TRACE21 results for the North Atlantic (*34*), where most of our sites are located.

To account for this bias, we added or subtracted the HadlSST1.1 SST Aug/Feb bias from our proxy records at these locations and added the SST bias uncertainty (1 □) in quadratu proxy SST uncertainty.

2. Data density

The resolution of the records on their published age models ranges from centennial to multi-millennial with a median resolution of 1100 years (Table S1, Figure S1). Where the primary authors did not report mean age-model resolution across the LIG, we estimated the published age-model resolution by dividing the duration of the LIG (13 kyr) by the number of proxy SST data points.

3. How well can 72 core sites capture global mean annual SST?

To assess how well the annual proxy-based SSTs from 72 marine core sites represent the global mean annual SST, we first calculated 1°x1° SST anomalies using observational data from HadISST1.1 (*17*), subtracting the 1870-1889 mean values from the 1995-2014 mean values. We

subsampled these anomalies 1000 times at an increasing number (up to 500) of random pseudo-core locations (1°x1° grid boxes), ensuring that the same site was not selected more than once, and averaged the SST anomaly for each number of pseudo-core locations. We then computed the root-mean-square deviation (RMSD) from the global mean SST anomaly for each number of pseudo-core sites (Fig. S3). Selecting ~26 unique pseudo-core sites yields an RMSD that falls below 0.05°C from the true global anomaly. These results are comparable to those presented in previous studies (*32*, *33*, *35*) in demonstrating that only a sparse array of locations (in this case, ≥ 26 unique core sites) is required to accurately capture a global signal of ocean temperature changes (Fig. S3).

4. LIG age models

Due to the lack of radiometric age control in marine sediment records spanning the LIG, LIG age models are commonly based on stratigraphic correlation ("tuning") of the core-site benthic $\delta^{18}O$ record to a master $\delta^{18}O$ record whose age model is largely based on orbital tuning (*36*-*38*). More recently, age models for the LIG interval have been constructed by correlating millennial-scale variability in a proxy-based SST record reconstructed from a marine sediment core to similar variability in a Greenland (*39*) or Antarctic ice-core temperature record (*9*, *40*, *41*). We combine these two strategies for this study and, in the following, define our underlying assumptions and how we propagate all uncertainties.

4a. Assumptions

Our age-model construction strategy relies on two primary assumptions.

1. Benthic $\delta^{18}O$ changes occur broadly synchronously within the major ocean basins (defined here as North Atlantic, South Atlantic, Pacific, and Indian), but may be diachronous between basins, with some work suggesting that differences may approach 5,000 years between the

Pacific and Atlantic basins during Termination 1 (*13*, *14*). We note that $\delta^{18}O$ records from the same basins spanning Termination 1 suggest that smaller diachronous $\delta^{18}O$ signals may occur at varying ocean depths, on the order of a few hundred years (*15*). We thus define basin-specific reference cores (herein reference cores) for intra-basin $\delta^{18}O$ alignment (Fig. S4) in order to reduce stratigraphic uncertainties related to potential diachronous inter-basin benthic $\delta^{18}O$ signals, recognizing that some depth-dependent changes within a basin may not be accounted for.

2. We assume that millennial- and orbital-scale changes in subpolar ocean SSTs at our reference core sites occur simultaneously with air-temperature variations over Antarctica and Greenland, as has been inferred for the last, penultimate, and earlier deglaciations (*9-11*, *42-45*). We thus align our SSTs at our three high-latitude Southern Ocean reference core sites with the European Project for Ice Coring in Antarctica Dome C (EDC) ice core and our North Atlantic reference core site with the Greenland synthetic temperature record (*11*) (Fig. S4).

Both of these ice-core records are on the "Speleo-Age" model, which is based on correlation of these ice cores to radiometrically dated Asian speleothems (*11*). Linking the ice cores from the two hemispheres within this chronology relies on (1) the temporal stationarity of the observed lead/lag relationships between Greenland and Antarctic ice-core temperatures during the canonical millennial-scale climate events of the last glacial cycle associated with the thermal bipolar seesaw (*46*) and (2) that North Atlantic cold events are correlative with radiometrically dated Asian monsoon minimum intervals (*47*). This Speleo-Age chronology agrees with the EDC3 time scale (*48*) within ±2-3 kyr and the orbitally tuned LR04 time scale (*38*) within ±5 kyr from the present to 400 ka, which is well within the uncertainties of both records for the LIG interval.

We evaluate the assumption of aligning SSTs with the ice-core records by sampling transient modeling results at the locations of our three Southern Ocean reference core sites and at the location of the EDC ice core for the last deglaciation simulated by CCSM3 (*49*) and the penultimate deglaciation and LIG simulated by LOVECLIM (*50*). Lagged cross-correlations between the raw and linearly detrended model-based SSTs at the locations of our basin-specific reference cores and 2-m air temperatures over EDC reveal the highest lagged cross-correlation is centered at zero lag (Figure S5), thus supporting this assumption.

4b. Basin reference-core alignment strategy

Each of our four high-latitude reference cores has high-resolution benthic $\delta^{18}O$ and proxy-based SST records (Table S1 and S2, bolded). Proxy-based SST reconstructions from these core sites have previously been climatostratigraphically aligned with Antarctic ice-core records (*9*, *40*) or the Greenland synthetic temperature record (*11*, *39*). To generate LIG age models for each reference core site, we followed the climatostratigraphic strategy by using AnalySeries (*51*) to graphically align each reference SST and corresponding ice-core record using clearly defined features of the SST record on its depth scale and the EDC ice-core or Greenland synthetic temperature record on its Speleo-Age scale (Fig. S4). The alignment features included glacial/interglacial transition midpoints, marine isotope substages as described in the SPECMAP protocol (*36*, *37*), or tie points previously used by the primary authors (*9*, *39*). Lagged cross-correlations between the aligned basin-specific reference cores and the corresponding ice-core record reveal the highest lagged cross-correlation is centered at zero lag (Fig. S5c), thus supporting our alignment. The resulting reference-record age model is then applied to the co-registered benthic $\delta^{18}O$ record from the same reference core site, which this is then used as the basin-reference $\delta^{18}O$ record (Figure S6).

4c. Within-basin alignment strategy and uncertainties

With the baseline alignment uncertainty for any given ocean basin established, we then progress through the following steps to generate LIG age models for the other core sites in our database within each basin.

1. The basin-reference benthic $\delta^{18}O$ record is used as the alignment target for all of the other benthic $\delta^{18}O$ records within the same ocean basin (Table S1, Fig. S6). To do these benthic $\delta^{18}O$ alignments, we follow the same strategy as for aligning the reference SST records by aligning common $\delta^{18}O$ features (glacial/interglacial transition midpoints, marine isotope substages as described in the SPECMAP protocol (*36*, *37*)). These tie points become age-control points (ACPs) for the reference cores, with an uncertainty from the Speleo-Age scale at that time. In essence, these ACPs are equivalent to radiocarbon ages (with their uncertainties) that are used to construct age models.

2. We generate 1000 possible age models for each benthic $\delta^{18}O$ record with its ACPs using Bchron (4.2.5, default values, uncertainty modeled as Gaussian from Speleo-Age model uncertainty, iterations=10000, burn=5000, thin=5, maxExtrap=100000) (*16*) (Fig. S7a). Bchron models sediment accumulation as a continuous, monotonic, stochastic process, with minimal assumptions about the smoothness of sedimentation. In doing so, it also allows for increasing uncertainty between age horizons. This step is crucial because the depths that are sampled for benthic $\delta^{18}O$ analyses can be of very different resolution from those sampled for proxy-based SSTs, and vice-versa, within the same core.

4. Next, we generate 1000 realizations of the site-specific proxy-based SST record (e.g., Fig. S7b) by perturbing the published proxy record with the quoted uncertainties in the proxy-specific calibrations or transfer functions as follows.

a) **Mg/Ca from planktonic foraminifera** – All Mg/Ca-based temperature estimates were calibrated using a global multispecies relationship (*52*) and its uncertainties where:

$$Mg/Ca\ (mmol/mol) = (0.38 \pm 0.02) * exp((0.09 \pm 0.003) * SST)$$

b) **$U^{K'}_{37}$ from alkenones** - All $U^{K'}_{37}$ records were calibrated using a global relationship (*53*) and its uncertainties in slope and intercept:

$$U^{K'}_{37} = SST * (0.033 \pm 0.0001) + (0.044 \pm 0.016)$$

c) **Microfossil reconstructions** – All faunal reconstructions were perturbed with the uncertainty reported in the original publication drawn from a zero-mean Gaussian distribution.

5. We reference each core site in the database as the anomaly from the SST value in the nearest 1°×1° grid cell in the HadlSST1.1 1870-1889 and 1995-2014 data sets (*17*) (Fig. S7c).

At the end of this process, we have 1000 realizations of each of our 104 LIG proxy-based SST records that combine the uncertainties introduced from the alignments in our technique and the proxy-based SST calibration uncertainties.

5. Stacking LIG proxy-based SSTs

With 1000 realizations of each proxy-based SST record on 1000 possible age models, we then stack (that is, average) each of the first realizations of the 104 SST records to generate one realization of the global stack, then stack each of the 2nd realizations, then the 3rd, and so on, until we have 1000 realizations of the global LIG proxy-based SST stack (ten iterations are shown in Fig. S8). The proxy-based SST stack and its uncertainty shown in the paper are the 5°x5° gridded, area-weighted mean and two standard deviations of these 1000 realizations. This stacking procedure is identical to those presented in other recent proxy compilations for Termination 1 (*32*) and the Holocene (*33*).

6. How sensitive is the LIG stack?

We investigate the sensitivity of the temperature stack to the resolution of the chosen interpolation scheme, the type of areal weighting used, the number of proxy records, the types of proxy records, and the reference dataset used to calculate the proxy-based SST anomalies.

6a. Resolution

Recalculating the global temperature stack at 500- and 1000-year resolution yields essentially identical stack anomalies and error bars, only at lower resolution (Fig. S9). Uncertainty estimates for the global stack at any given time (t) are based on the standard deviation of 1000 realizations of the global temperature anomaly estimated from perturbing the LIG proxy records, interpolating them onto a constant resolution, and then stacking them. So, for example, 1000-year interpolation of the proxy records results in 1000 global ΔSST estimates at 129 ka and at 128 ka, which are essentially identical to those estimated at 129 ka and 128 ka in the 500-year and 100-year interpolation schemes.

6b. Areal weighting

Figure S10 shows the results of three different schemes: (1) the area-weighted 5°x5° gridded average used in the paper; (2) average of the non-gridded proxy records by cosine (latitude); (3) the area-weighted 30°x30° gridded average. The three stacks have similar magnitude and timing of the LIG proxy SST anomaly, suggesting that the maximum LIG anomaly is relatively insensitive to the weighting scheme.

6c. Jackknifing

We recalculated the LIG proxy SST stack using two jackknifing approaches to examine the sensitivity of the stack to the number of records used. The 5x5° stack was recalculated 1000 times after randomly excluding 50% of the records each time. This process was then repeated but

excluding 90% of the records 1000 times. Because the proxy records were perturbed with proxy and chronological uncertainty before jackknifing, these results include both sources of uncertainty. The uncertainty of the jackknifed stacks is greater than the full proxy stack, but the overall temporal structure is retained and are essentially identical (Fig. S11), suggesting that the maximum LIG anomaly is relatively insensitive to the number of records included.

6d. Proxy type

In order to assess how our temperature stack may be affected by disagreement among the different proxies included in the database, we calculated separate proxy-specific global SST stacks (Fig. S12). We also calculated proxy jackknife stacks by leaving out one group of the major proxy types (microfossil, Mg/Ca, and $U^{K'}_{37}$) each time and then recalculating the global and regional stacks (Fig. S13). Different temperature histories shown by the proxy stacks in part reflect the geographical distribution and number of each proxy type in the database (Fig. 1a), with one group of proxy records sampling a different region (and thus possible climate response) than another. There is an indication that the geochemical SST estimates are on the whole warmer than the microfossil SST estimates during the LIG, and that this difference is especially prevalent in the Southern Hemisphere extratropics, where the geochemical proxies alone would suggest >4.2°C LIG warming relative to the 1870-1889 average (Fig. S13).

To further assess apparent proxy disagreement we compare SST estimates from multiple proxies, including geochemical/microfossil pairs that occur in individual cores in the database (n=12) (Figure S14). No systematic or consistent pattern of SST estimate offsets is apparent the 16 core sites (Fig. S14), but appears at the basin scale (Figs. S13, S19). The spatial pattern of anomalies recorded by the individual proxy groups during specific time periods (Figs 2, S15-S17, S19) identifies coherent regional SSTs among proxies. The only area where proxies are

substantially different from each other is in the tropics, where the $U^{K'}_{37}$ SST proxy suggests a tendency for warmer tropical SSTs than Mg/Ca or microfossil proxies (Figs. 2, S19). This may reflect a spring-summer dependence of $U^{K'}_{37}$ and a bias towards higher unsaturation ratios (and thus warmer SSTs) in areas of dynamic oceanographic settings (*19*).

6e. SST anomaly reference dataset

SST anomalies calculated for proxy compilations are referenced to different time periods and/or different observational datasets (*5*, *7*, *8*, *54*). We assess the sensitivity of our global temperature stack to three different reference periods: (1) HadISST1.1 1870-1889 mean SST (the period of SSTs in this database closest to preindustrial) at the nearest 1°x1° grid box to the core sites in the database; (2) HadISST1.1 1995-2014 mean SST (most recent period of global SSTs with anthropogenic influence) at the nearest 1°x1° grid box to the core sites in the database (*17*); (3) core top/Holocene proxy SSTs at the same or nearest available core site with a core top or mid-Holocene SST estimate (*55*) (Table S1). We note that core-top ages may differ significantly from each other. Following the recommendation of the primary authors (*56*), we reference core ODP 1089 SSTs to the core-top value. We were able to reference to core top/mid-Holocene proxy SSTs for all but three of our core sites (Table S2). In those three cases, we reference the core-site anomaly from the HadISST1.1 1870-1889 mean SST at the nearest 1°x1° grid box.

This assessment shows that the magnitude of LIG global annual SST is dependent on the choice of reference period (Fig. S18). For example, LIG temperatures at 125 ka are 0.5±0.3°C relative to the 1870-1889 climatological mean, 0.1±0.3°C relative to the 1995-2014 mean, and 0.8±0.3°C relative to the core top/Holocene reference. McKay et al. (2011) (*8*) established their LIG SST anomaly by averaging SSTs over a 5-kyr period centered on the warmest temperature between 135 and 118 ka, and derived a value of 0.7±0.6°C, in agreement with our estimate based

on a similar reference. We note that the warmest temperature in our stacks is at or near 125 ka, so following the same method as McKay et al. of averaging over a 5-kyr window and referenced to core top or Holocene values should result in a lower estimate than our estimate of 0.8±0.3°C.

Figure S 1. Histogram of the mean resolution of proxy records in the LIG database for 129-116 ka on their published age models (Table S1). Yellow vertical line denotes the median age model resolution (1,100 years).

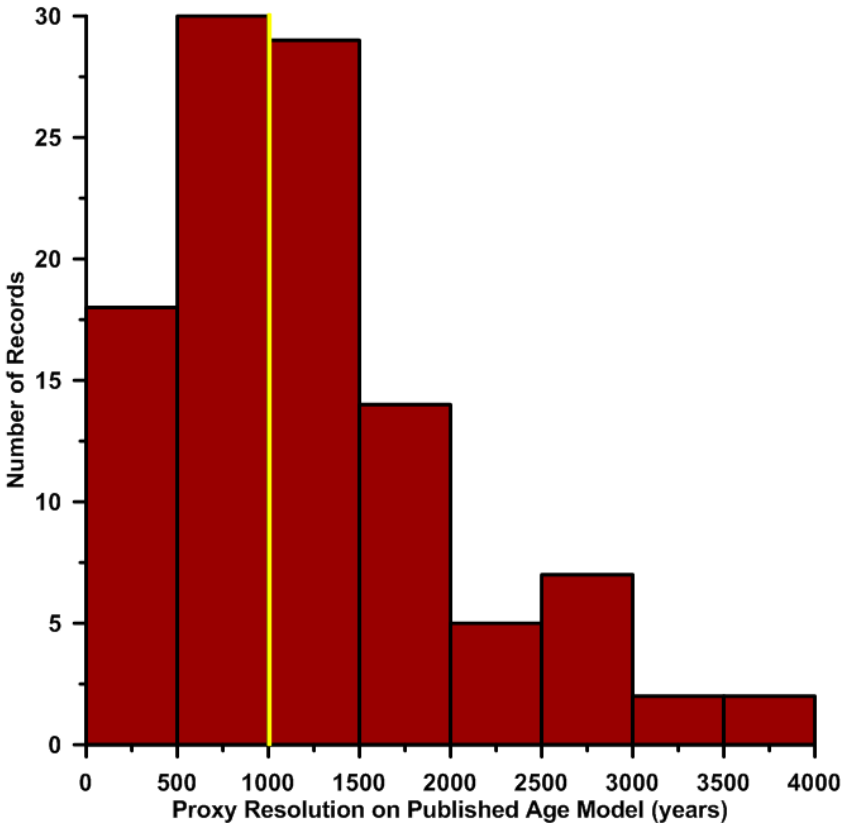

Figure S 2. HadlSST1.1 and SynTraCE seasonal-average SST bias. Blue circles are the "seasonal bias" estimated by subtracting the HadlSST1.1 August-summer/February-winter approximation of the annual SST (August & February average SSTs) from the observed annual SST from 1870-2015 at the locations of the core sites where we average summer/winter proxy temperatures (Table S1). Red circles are calculated the same as the blue circles only from the SynTraCE simulation over 6ka-0ka ***(34)***. Uncertainties are the 1σ deviation from the mean bias values.

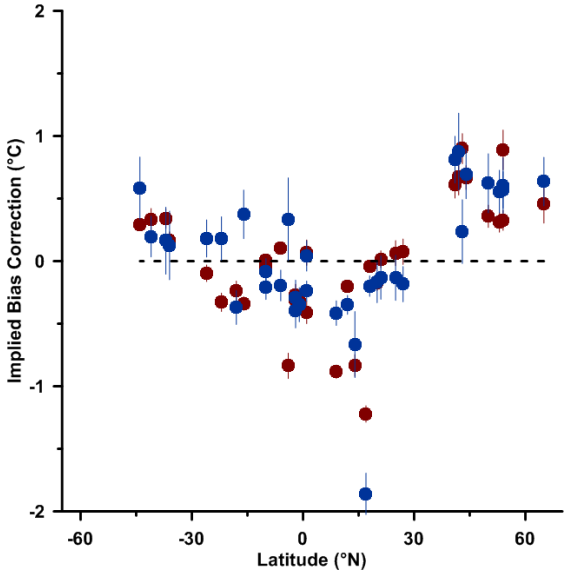

Fig. S3

Root-mean squared deviation (RMSD) of pseudo-core sites from global SST anomaly. These are calculated from the true global weighted mean SST anomaly achieved from selecting increasing numbers of randomly chosen and independent pseudo-core sites. The global reference anomaly was calculated from HadISST1.1 1995-2014 mean SST – 1870-1889 mean SST. Star shows the RMSD (°C) at 72 randomly chosen pseudo-core sites to reflect the number of annual proxy reconstructions in our database.

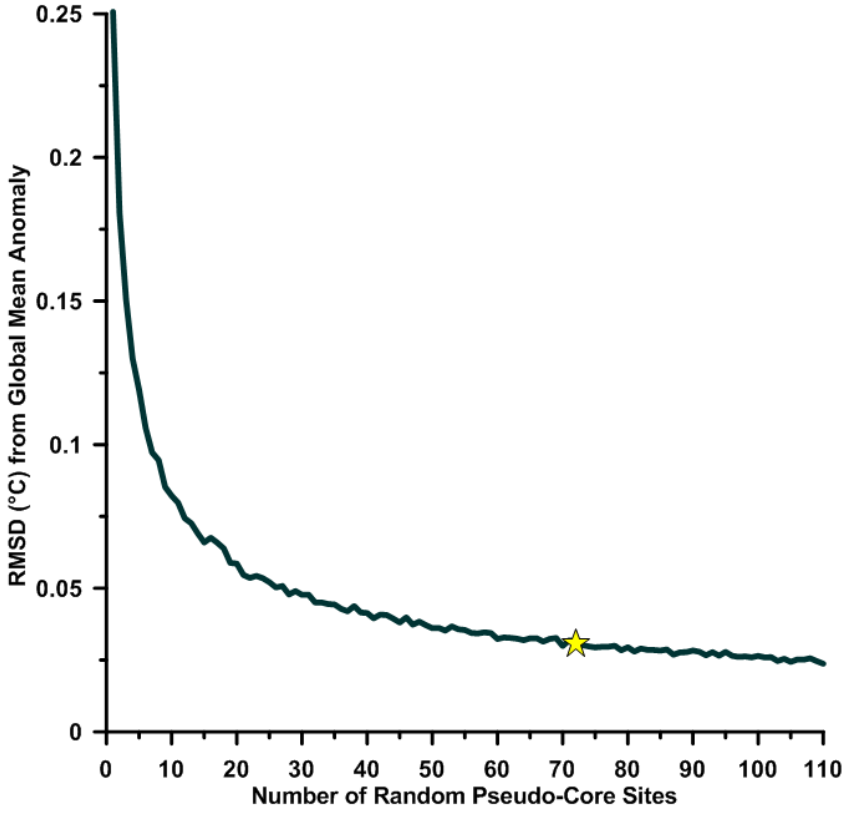

Fig. S4

Illustration of the age control points used for alignment of the basin reference records to the Speleo-Age ice core records. Green lines illustrate the tie points used in the basin reference core alignments. A) Black line, piston core MD97-2120 Mg/Ca-based SSTs on its depth scale (*44*), blue line, the EDC deuterium record on the Speleo-Age model (*11*). B) Black line, piston core MD01-2444 alkenone-based SSTs on its depth scale (*39*), blue line, the Grn_T_syn record on the Speleo-Age model (*11*). C) Black line, piston core MD02-2488 faunal-based SSTs on its depth scale (*9*, *40*), blue line, the EDC deuterium record on the "Speleo-Age" timescale (*11*). D) Black line, the ODP1089 alkenone-based SST record on its depth scale (*56*), blue line, the EDC deuterium record on the "Speleo-Age" timescale (*11*).

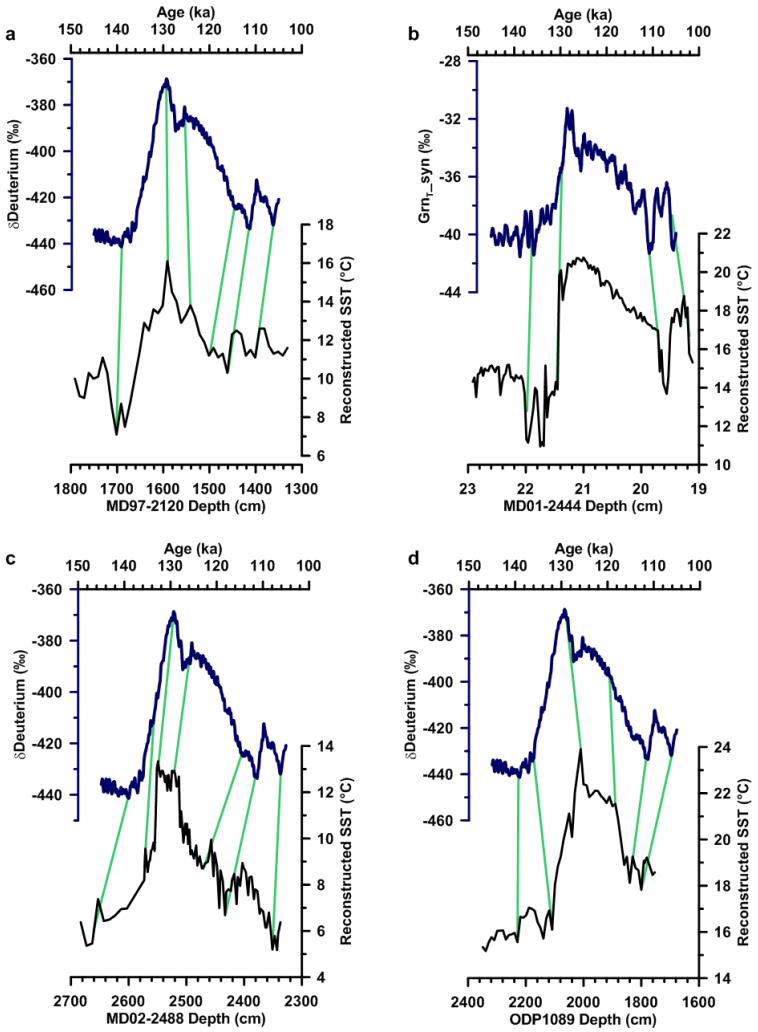

Fig. S5

Lagged cross-correlation function estimates for climatostratigraphic alignment assumption investigation. These are calculated between the raw (solid lines) and linearly detrended (hatched lines) modeled 2-meter air temperature variations at the location of EPICA Dome C and the model-based SSTs at our Southern Ocean basin reference core sites for two transient modeling experiments and the proxy reconstructions on the Speleo-age model (*11*). A) Termination 2 and the LIG simulated in LOVECLIM (*50*). B) Termination 1 simulated in NCAR CCSM3 (*49*). C) Termination 2 and LIG (145-115ka) observed in the proxy reconstructions. Gray bar denotes ±500 year lags.

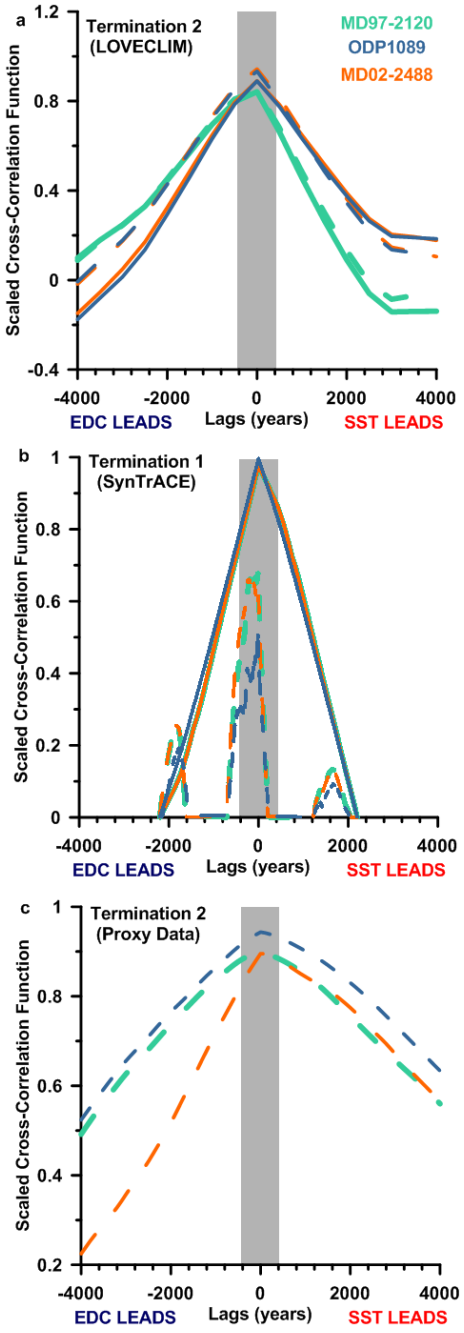

Fig. S6

Comparison of basin-reference core $\delta^{18}O$ records on Bchron age models. 1000 realizations of each record were perturbed with an assumed ±0.05‰ $\delta^{18}O$ uncertainty and were then interpolated onto 1000 age models predicted by Bchron using the depth/Speleo-Age/uncertainty constraints from the tie points prescribed in Fig. S4. Light blue line, piston core MD97-2120 (*44*), black line, the LR04 stack and its standard error on its published age model (*38*), green line, piston core MD01-2444 (*39*), dark blue line, piston core MD02-2488 (*9*, *40*), orange line, ODP1089 (*56*).

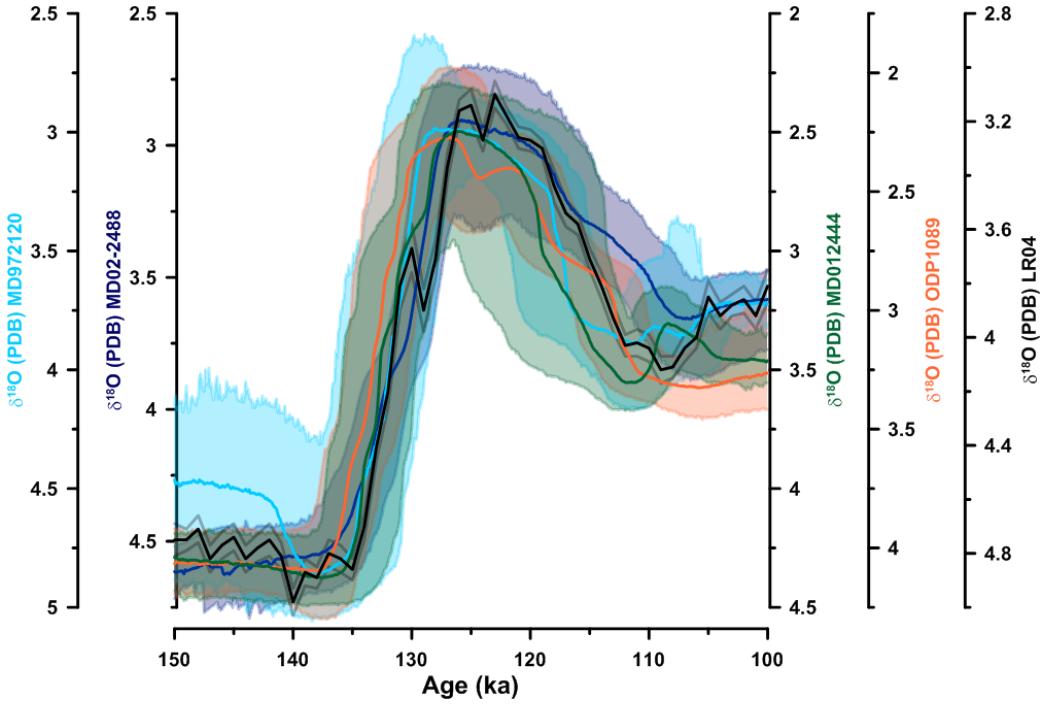

Fig. S7

Example of 10 Monte Carlo realizations for ODP846. **A)** 10 realizations of the ODP846 age-depth relationship predicted by Bchron (*16*) with the ACPs shown (black dots and bars). **B)** Ten realizations of the alkenone-based SST estimate from ODP 846 (*58*) perturbed with its proxy uncertainty on its depth scale. **C)** Five realizations of the ODP846 SST anomaly from HadISST1.1 1870-1889 on the propagated LIG age model predicted by Bchron and after perturbing it with its proxy uncertainty.

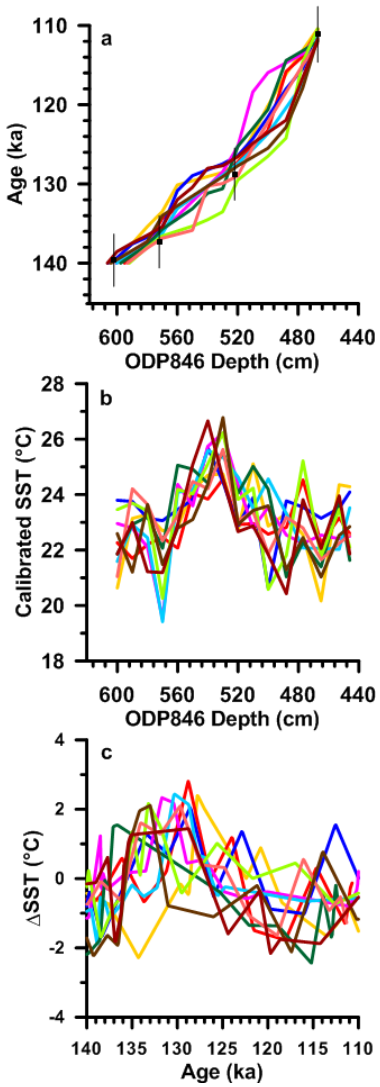

Fig. S8

Five realizations of the 5x5° gridded cos(latitude)-weighted proxy-based LIG global stack. One realization is derived from perturbing all of the proxy records (n=85) with both chronological uncertainties and their reported temperature calibration errors.

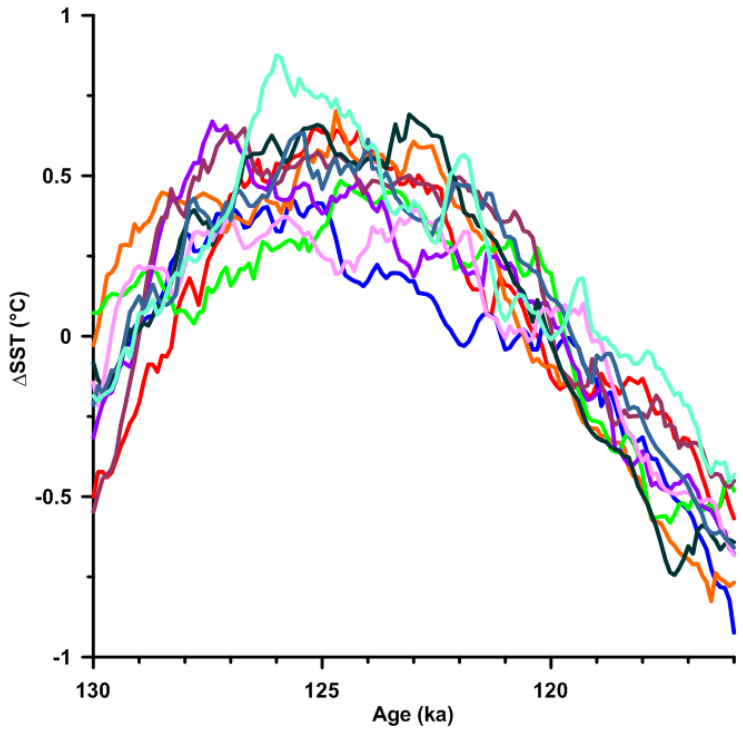

Fig. S9

The global 5x5° gridded cos(latitude)-weighted LIG temperature stack based on proxy records interpolated onto different resolutions after predicting their age models in Bchron. The colors are 100- (black), 500- (blue), and 1000-year (yellow) resolution. Errors (2σ) include both the age model and proxy calibration uncertainties.

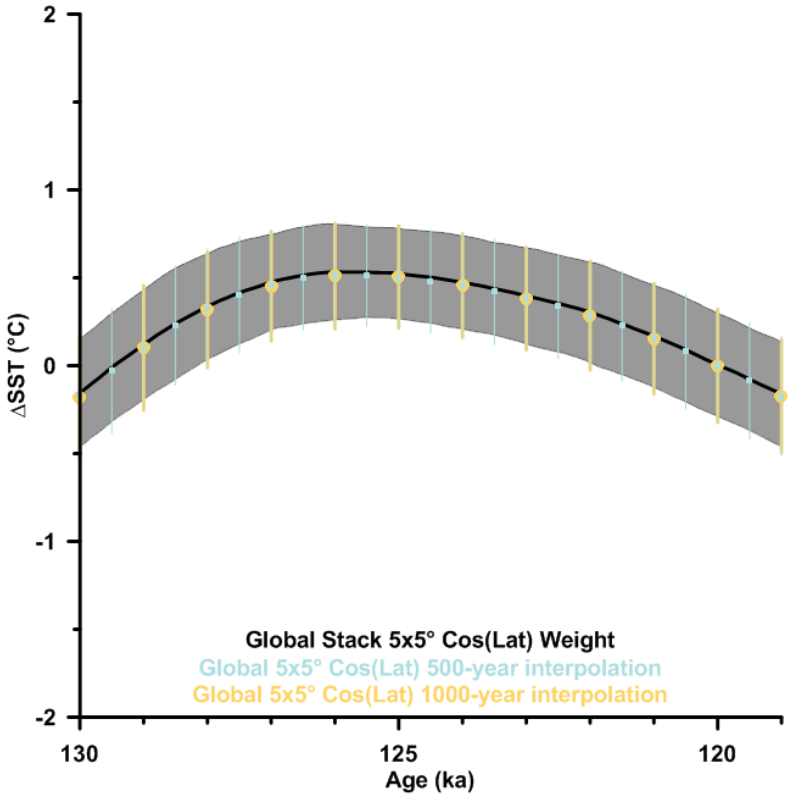

Fig. S10

The global LIG SST stack calculated by: area-weighted cos(latitude) and 5°x5° gridding (light blue), area-weighted cos(latitude) 30°x30° gridding (dark blue), and cos(latitude)-weighted mean of proxy records without gridding (black). Errors (2σ) are based on perturbing the proxy records with chronological and calibration uncertainties. We present the 5°x5° cos(latitude)-weighted stack in the manuscript (Fig 1c).

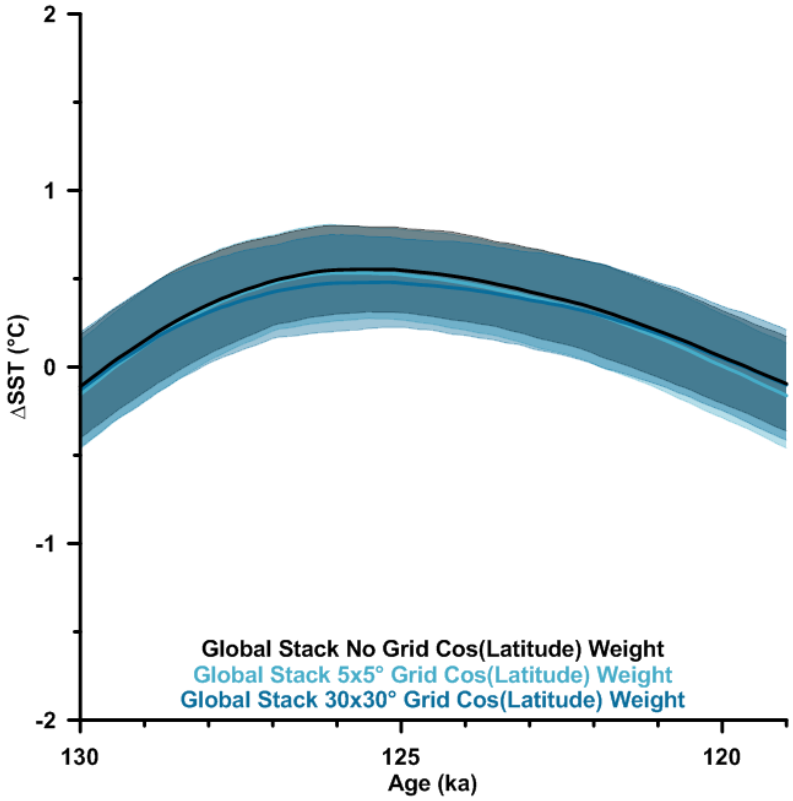

Fig. S11

The 2σ uncertainty bounds 5x5° cos(latitude)-weighted global LIG proxy SST stack recalculated after randomly leaving out 50% (dark blue) and 90% (light blue) of the proxy records 1000 times. Also shown is the 5x5° cos(latitude)-weighted global LIG proxy SST stack with its 2σ uncertainties (black).

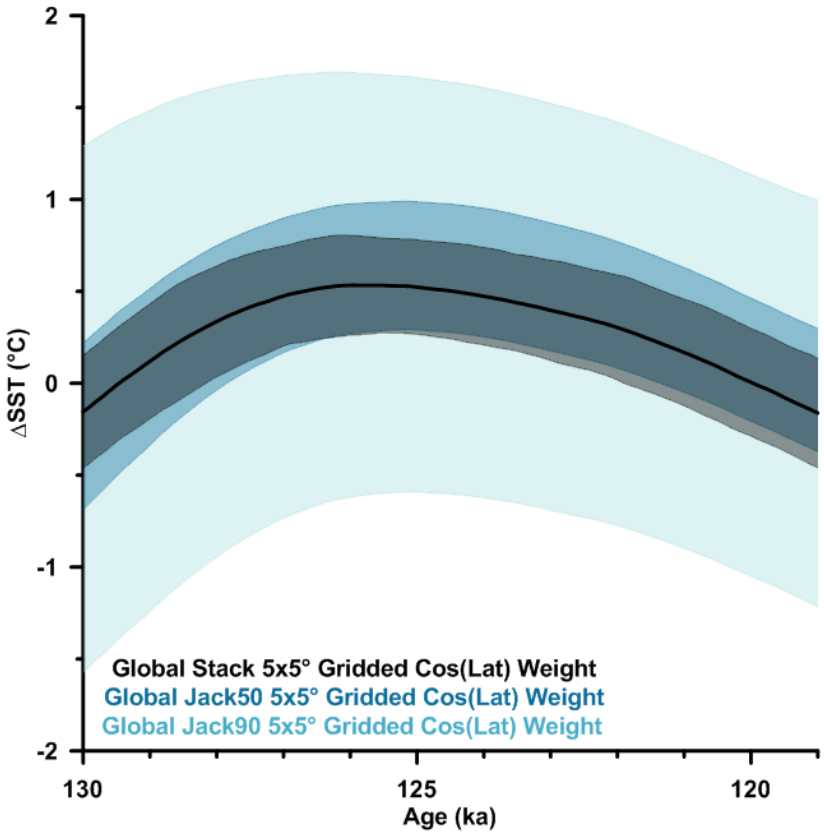

Fig. S12

Proxy-specific 5x5° gridded, cos(latitude)-weighted global LIG SST stacks with 2σ errors. The global stack is shown at the top for reference.

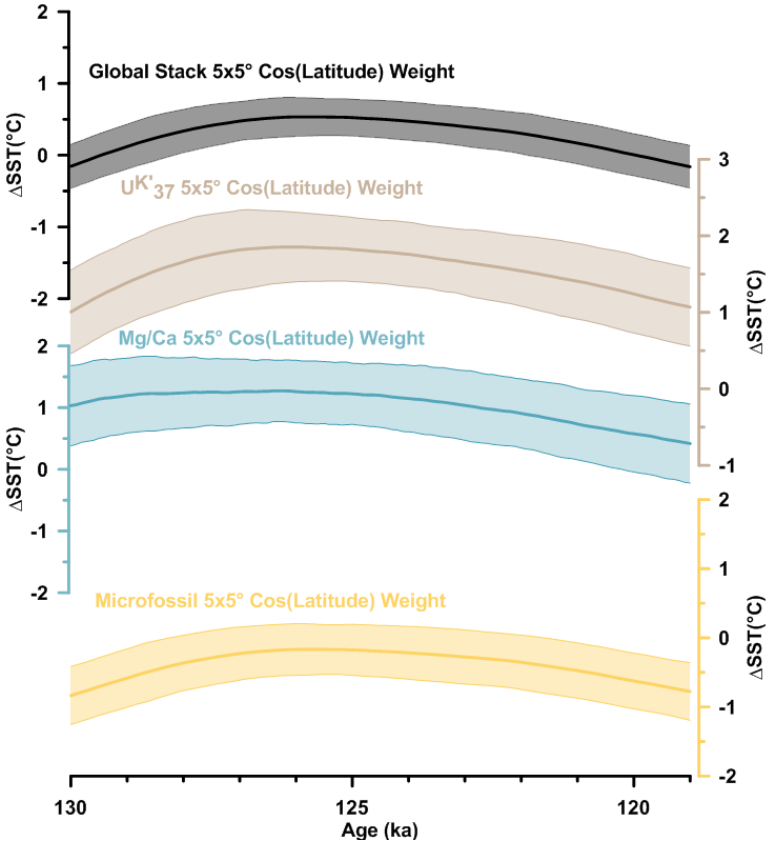

Fig. S13

Jackknifing global and regional stacks by leaving out an entire proxy type and then recalculating the 5x5°gridded stack relative to HadlSST1.1 1870-1889. a) Jackknifed 5x5° gridded and cos(latitude)-weighted global stacks. b) Jackknifed 5x5° gridded and cos(latitude)-weighted Tropical stacks. c) Jackknifed 5x5° gridded and cos(latitude)-weighted Southern Hemisphere extratropical stacks. d) Jackknifed 5x5° gridded and cos(latitude)-weighted Northern Hemisphere extratropical stacks.

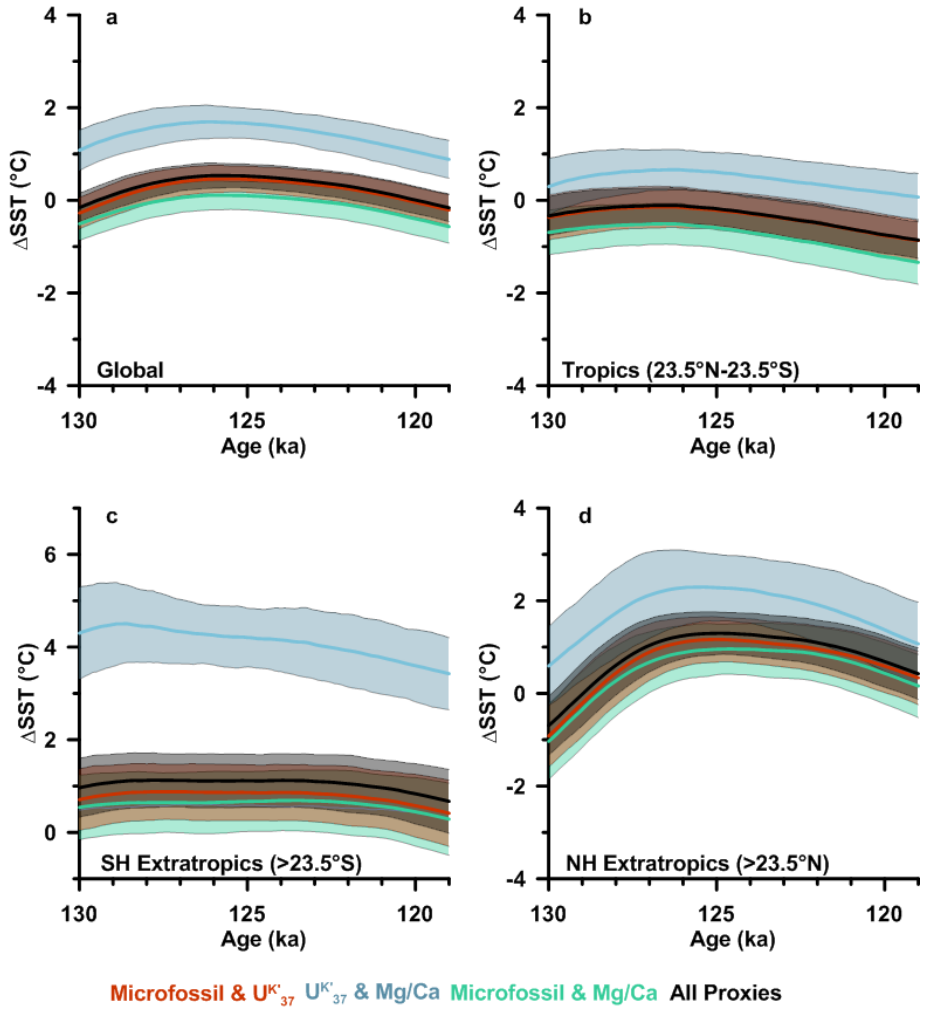

Fig. S14

Site-specific proxy record comparisons. For $\delta^{18}O$ or SST proxy record references for these cores, see **Table S2**. a) RC11-86 b) RC12-294 c) GeoB10038-4 d) V22-182 e) RC13-229 f) RC13-228 g) GeoB1112 h) MD01-2444 i) V22-38 j) V22-174 k) RC13-205 l) GeoB1105

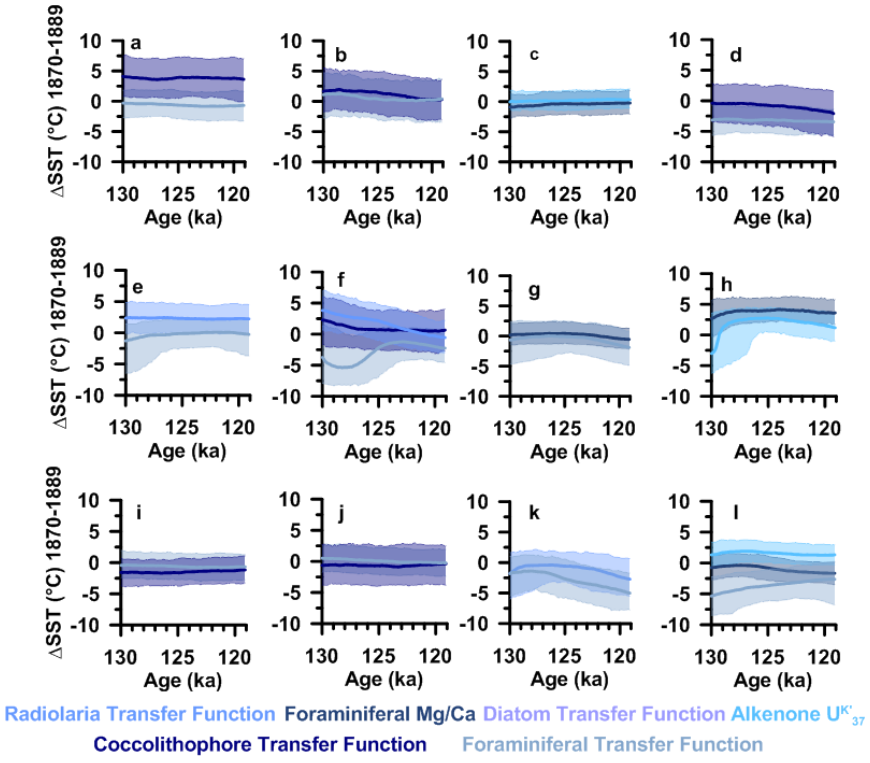

Fig. S15

Map of proxy-based SST anomalies at 129ka relative to HadlSST1.1 1870-1889. A) Microfossil SST anomalies only. B) $U^{K'}_{37}$ SST anomalies only. C) Planktonic foraminferal Mg/Ca SST anomalies only. Average anomaly uncertainties at time slice are shown in bottom left corner.

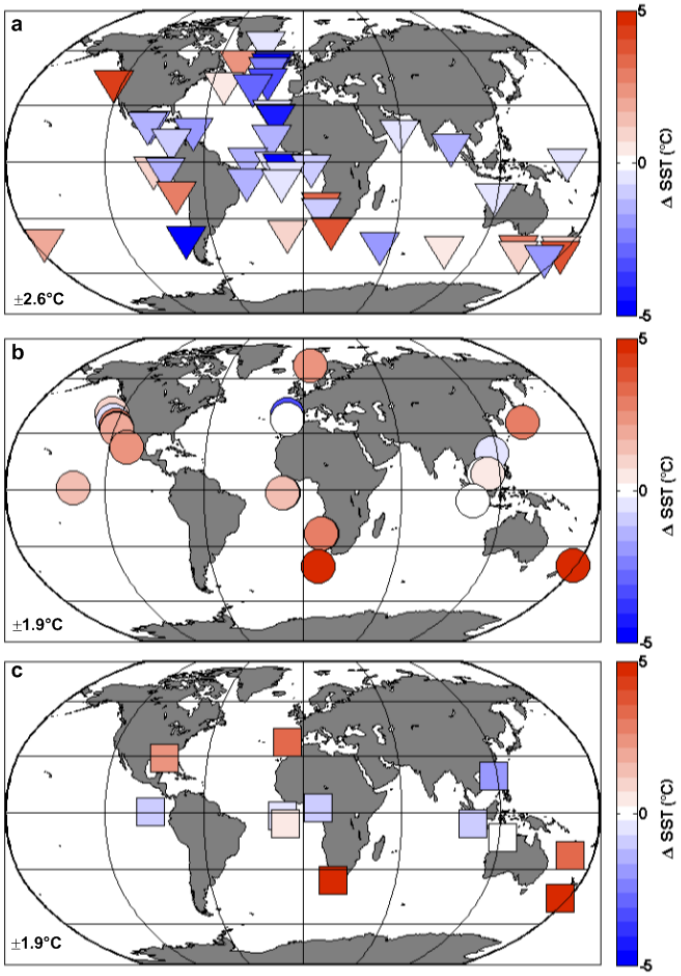

Fig. S16

Map of proxy-based SST anomalies at 125ka relative to HadlSST1.1 1870-1889. A) Microfossil SST anomalies only. B) $U^{K'}_{37}$ SST anomalies only. C) Planktonic foraminferal Mg/Ca SST anomalies only. Average anomaly uncertainties at time slice are shown in bottom left corner.

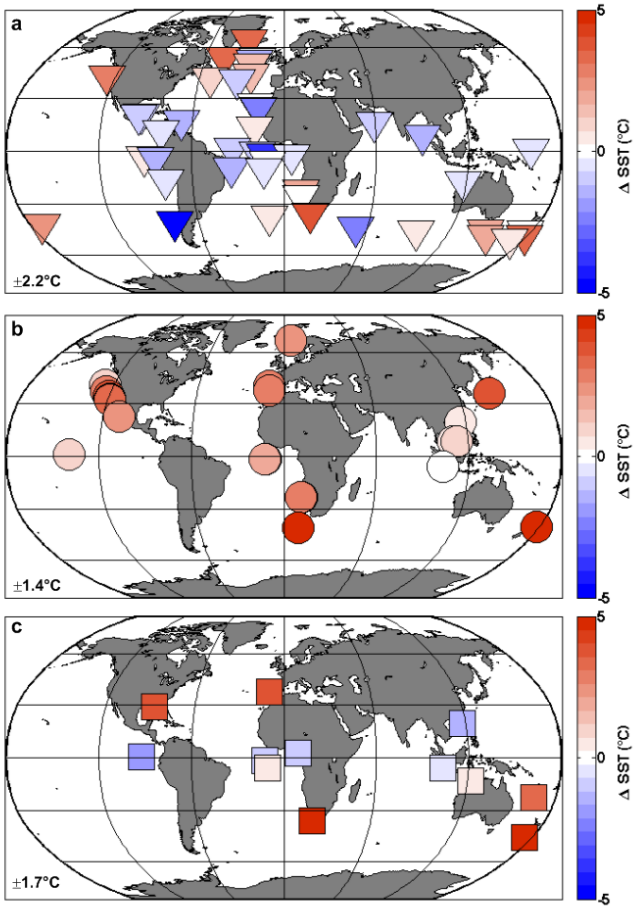

Fig. S17

Map of proxy-based SST anomalies at 120ka relative to HadlSST1.1 1870-1889. A) Microfossil SST anomalies only. B) $U^{K'}_{37}$ SST anomalies only. C) Planktonic foraminferal Mg/Ca SST anomalies only. Average proxy uncertainties at time slice are shown in bottom left corner.

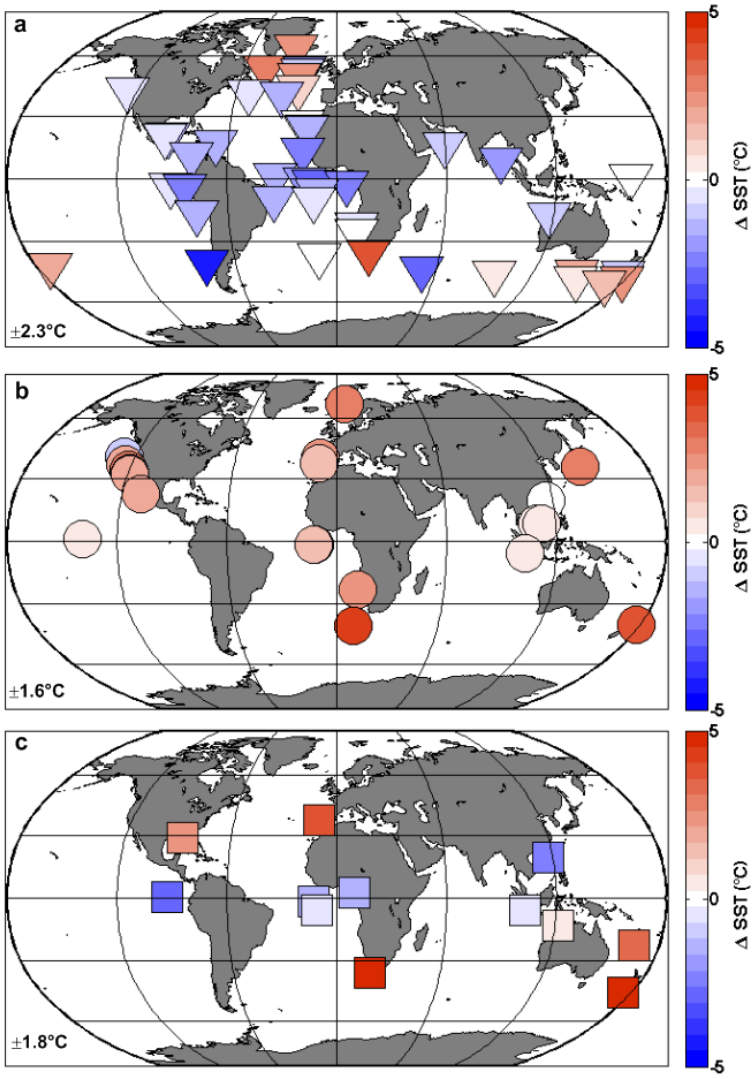

Fig. S18

Global 5x5° gridded cosine(latitude)-weighted LIG proxy SST stacks calculated as anomalies from different reference SST datasets. Blue line and shading: Proxy SSTs as anomaly from Core Top/Holocene proxy value, CT/Holocene proxies are identified in Table S1. Green line and shading: Proxy SSTs as anomaly from HadISST1.1 1870-1889 average. Red line and shading: Proxy SSTs as anomaly from HadISST1.1 1995-2014 average. Uncertainty bounds (2σ) reflect both chronological and temperature calibration uncertainties.

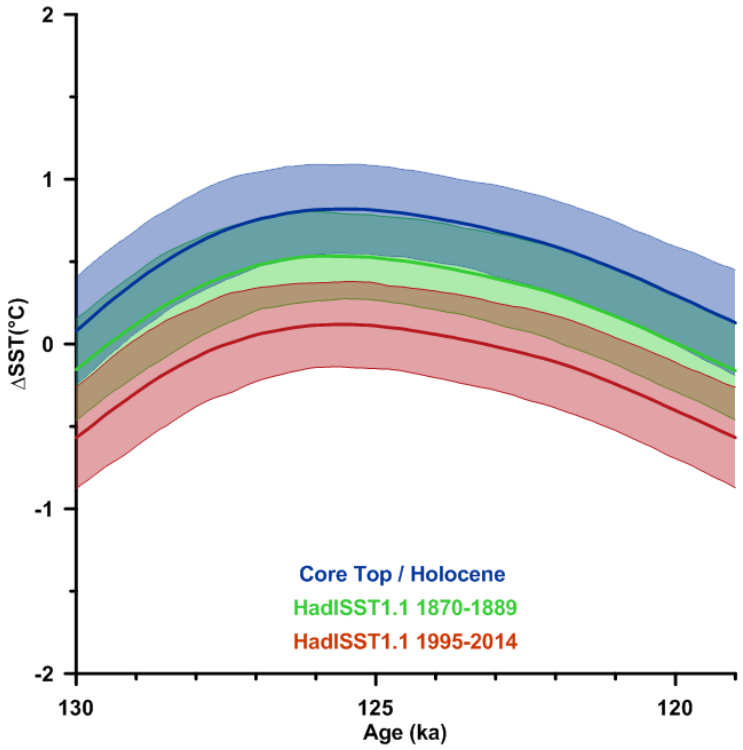

Fig. S19

Tropical (sites between 23.5°N-S) proxy-based SST reconstructions at time slices by longitude. a) 130ka, b) 125ka, c) 120ka.

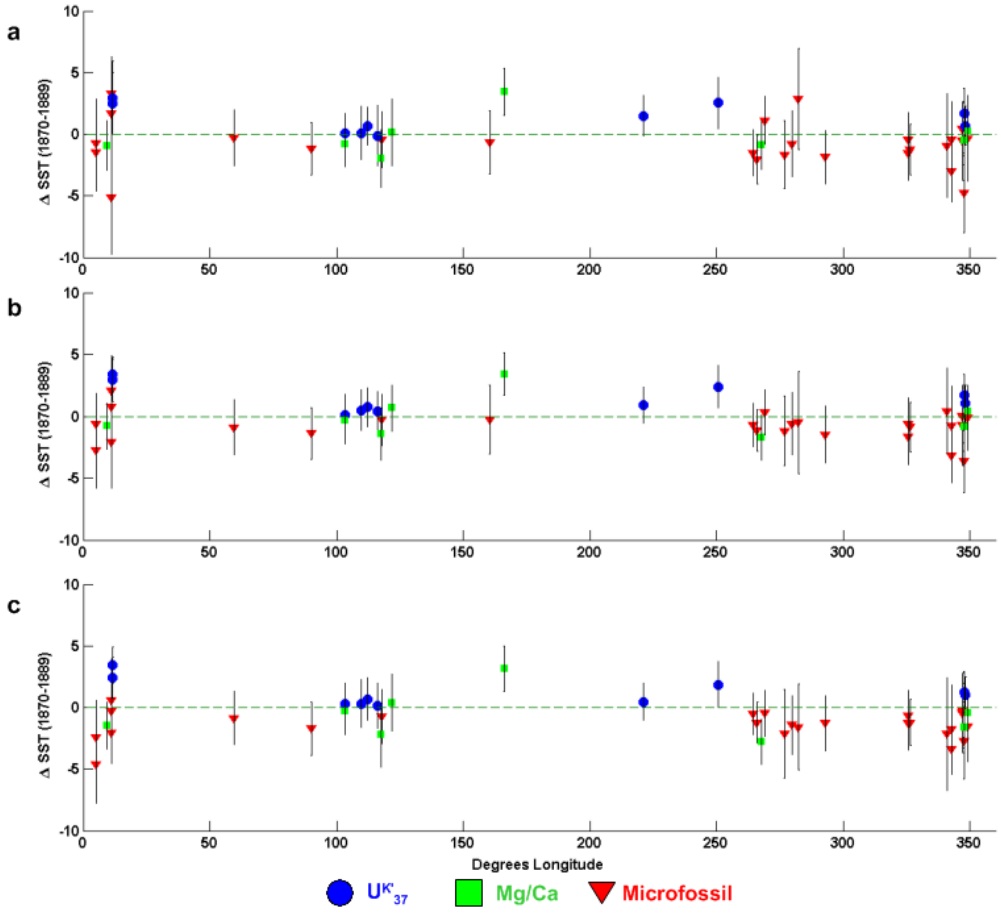

Fig. S20

Map and latitude transect timeslices comparing locations of annual and summer proxy-based SSTs compiled for this study. a) Map of proxy-based SST locations with symbols identifying summer (red triangles) and annual (black triangles) proxies. b) Proxy-based LIG SST anomaly compared with core site latitude at 129ka. c) Same as in b) but for 125ka. d) Same as in b) but for 120ka.

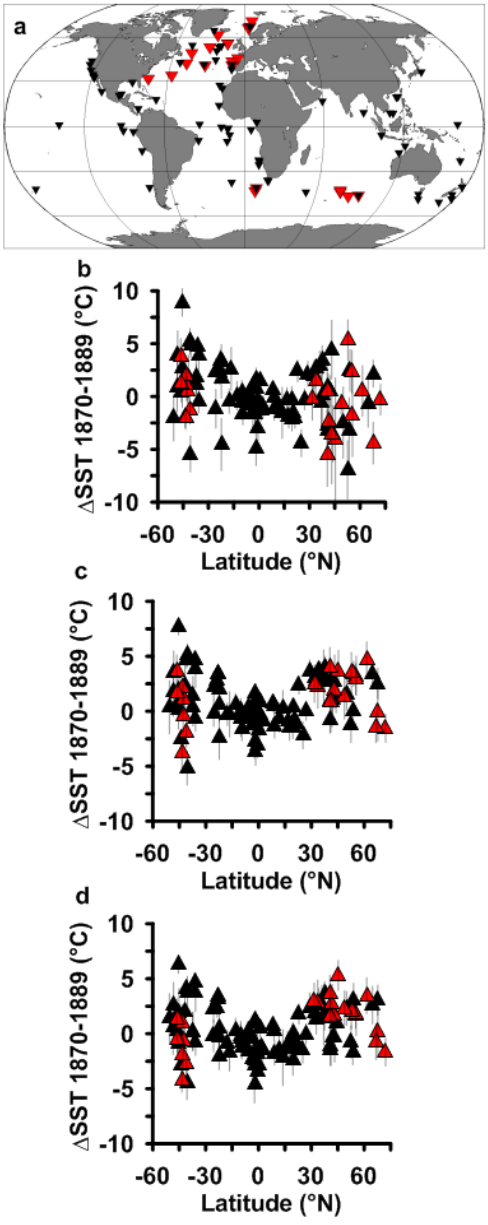

Fig. S21

Benthic $\delta^{18}O$ alignments for the Indian Ocean basin. In all figures the blue time series is the benthic $\delta^{18}O$ time series is from MD02-2488 (*9*) on the "Speleo-Age" model constructed using tie points from Figure S5. Correlation coefficients (R^2) are also shown. Metadata on the cores on their depth scales is available in Table S2. a) MD84-527 b) MD94-102 c) MD73-025 d) MD01-2378 e) V28-345 f) MD94-101 g) V34-88 h) RC12-339 i) GeoB10038-4 j) MD88-770

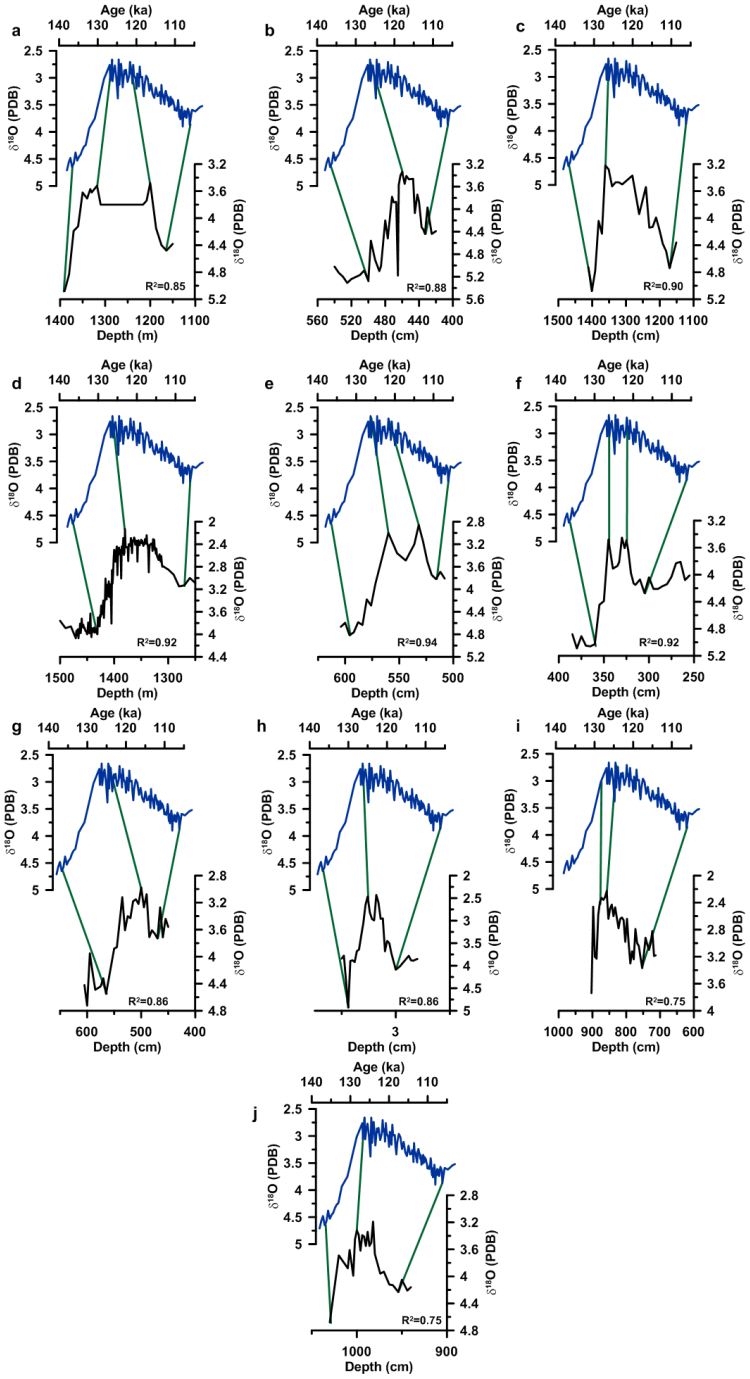

Fig. S22

Age models for Indian Ocean basin cores. In all figures the blue lines are the 95% confidence interval for age models predicted using Bchron (*16*). In all figures the black lines are the 95% confidence intervals using the age model uncertainty propagation method from (*10*). Each plot gives the core site and metadata on these cores is available in Table S1 & S2.

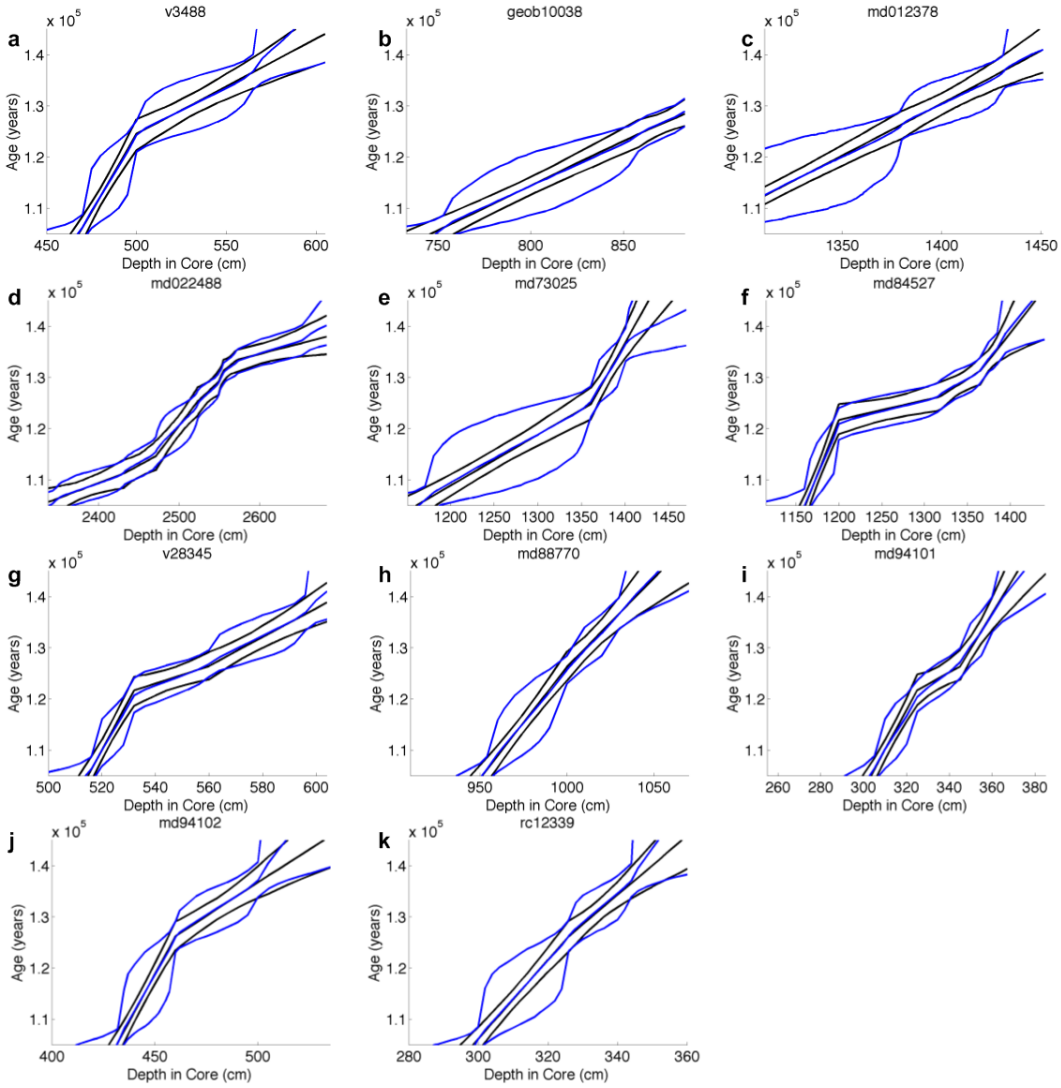

Fig. S23

Time series of calibrated SSTs for Indian Ocean basin cores. Core sites are listed at the top of each panel and metadata is available for each site in Table S1&S2. In all figures the mean and 95% confidence intervals are shown. Green vertical lines demarcate the 125ka and 120ka time intervals.

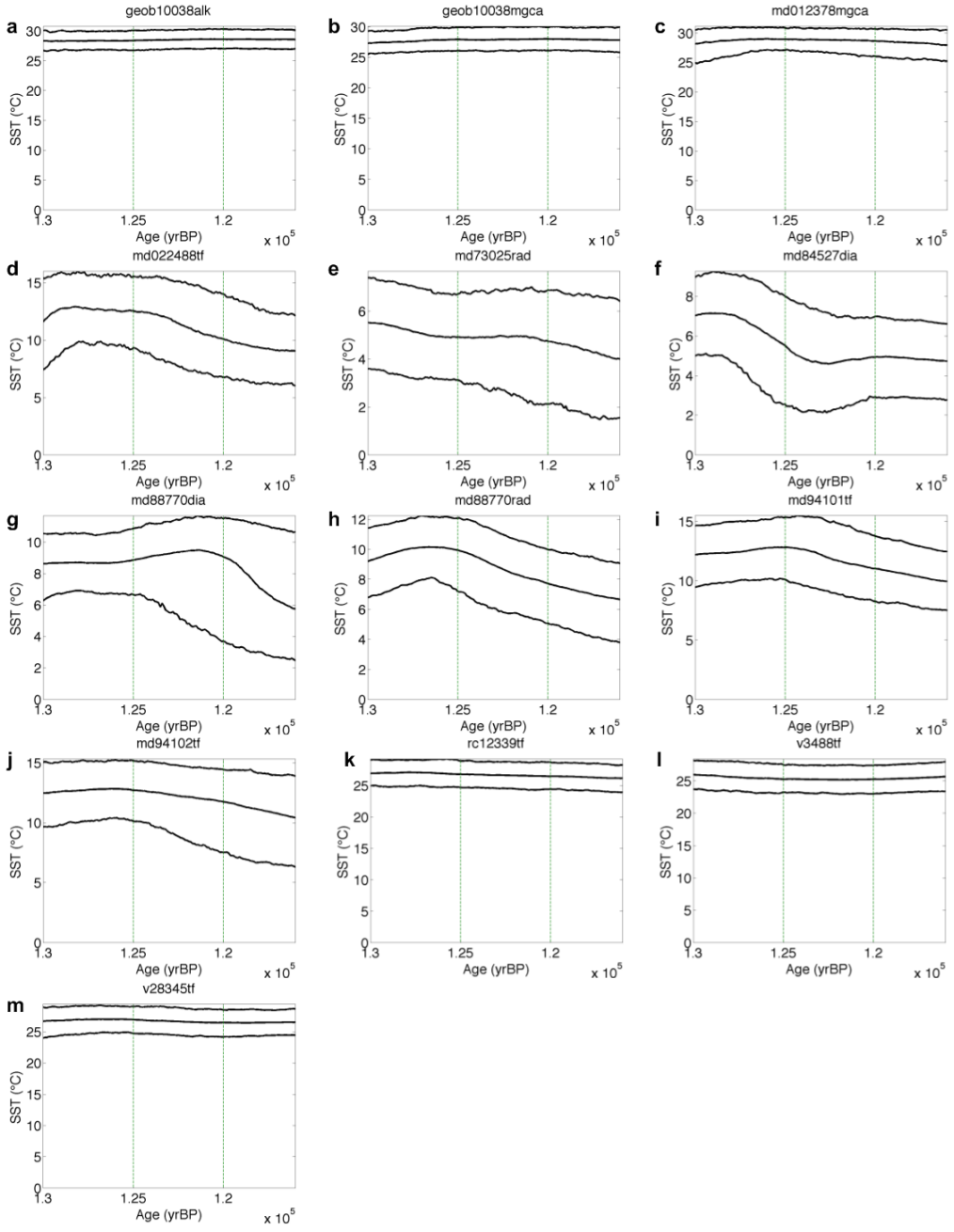

Fig. S24

Benthic $\delta^{18}O$ alignments for the South Atlantic basin. In all figures the blue time series is the benthic $\delta^{18}O$ time series from ODP1089(*59*) on the "Speleo-Age" model developed from the tie-points in Figure S5. Correlation coefficients (R^2) are also shown. Metadata for the cores on their depth scales is available in Tables S1 and S2. a) V22-174 b) RC13-228 c) GeoB1711 d) RC13-205 e) GeoB1112 f) V22-38 g) V22-182 h) ODP662 i) GeoB1105.

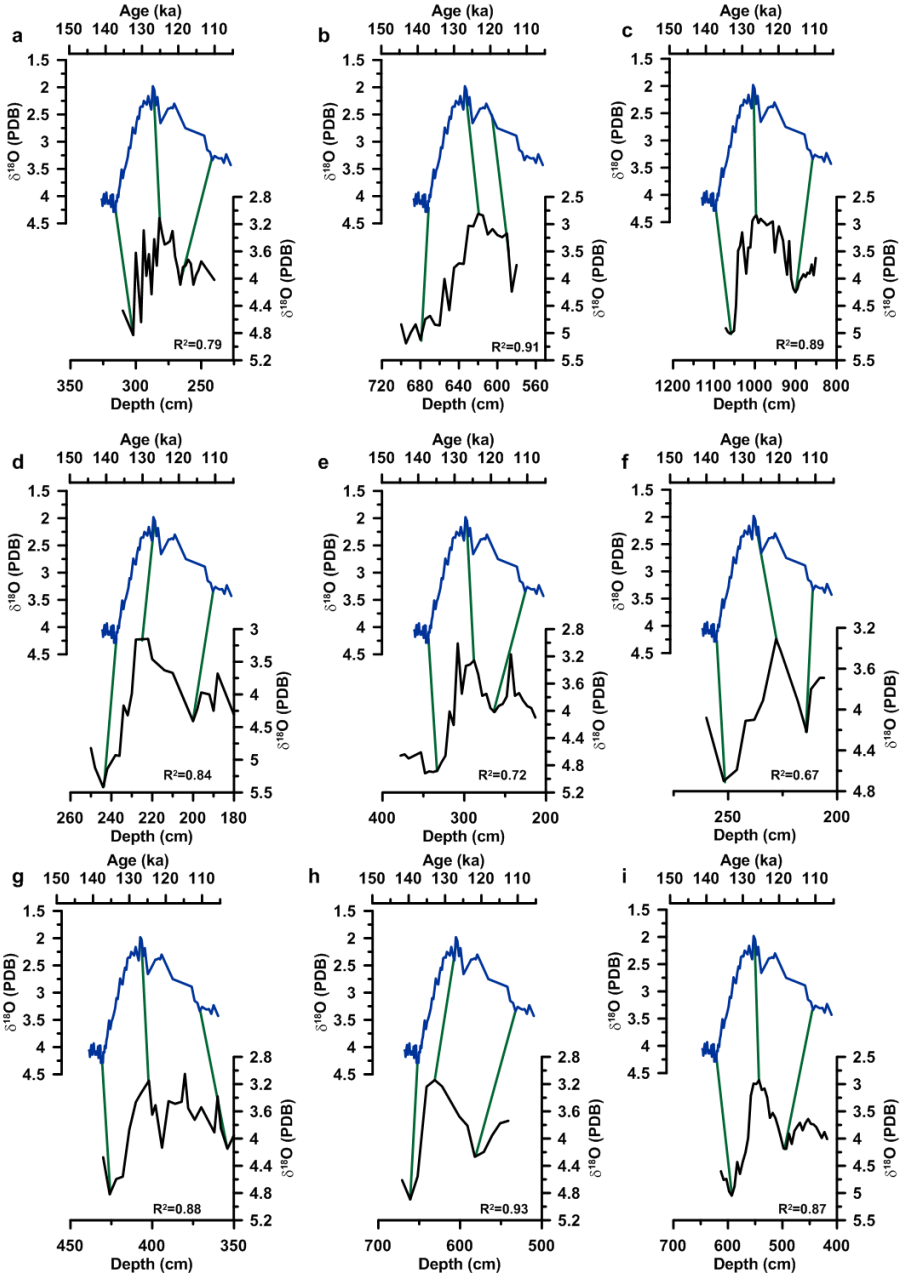

Fig. S25

Additional benthic $\delta^{18}O$ alignments for the South Atlantic basin. In all figures the blue time series is the benthic $\delta^{18}O$ time series from ODP1089(*59*) on the "Speleo-Age" model developed from the tie-points in Figure S5. Correlation coefficients (R^2) are also shown. Metadata for the cores on their depth scales is available in Tables S1 and S2. a) MD96-2080 b) RC12-294 c) PS-2489 d) GeoB1710-3 e) RC13-229 f) RC11-86.

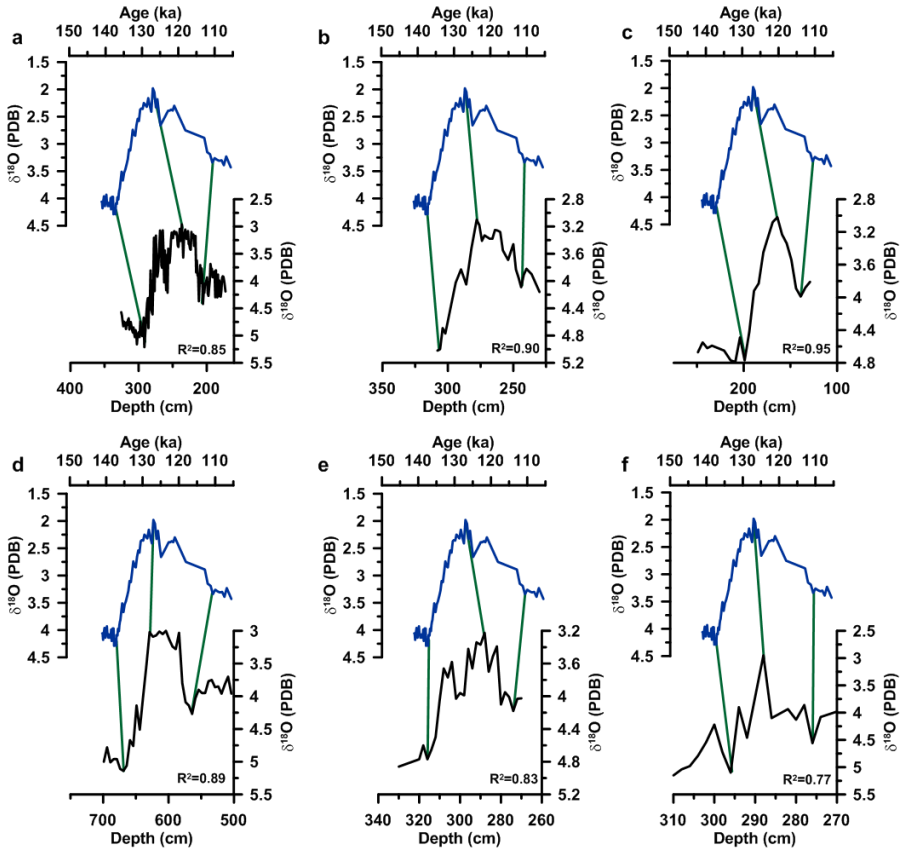

Fig. S26

Age models for South Atlantic basin cores. In all figures the blue lines are the 95% confidence interval for age models predicted using Bchron (*16*). In all figures the black lines are the 95% confidence intervals using the age model uncertainty propagation method from (*10*). Each plot gives the core site and metadata on these cores is available in Table S1 & S2.

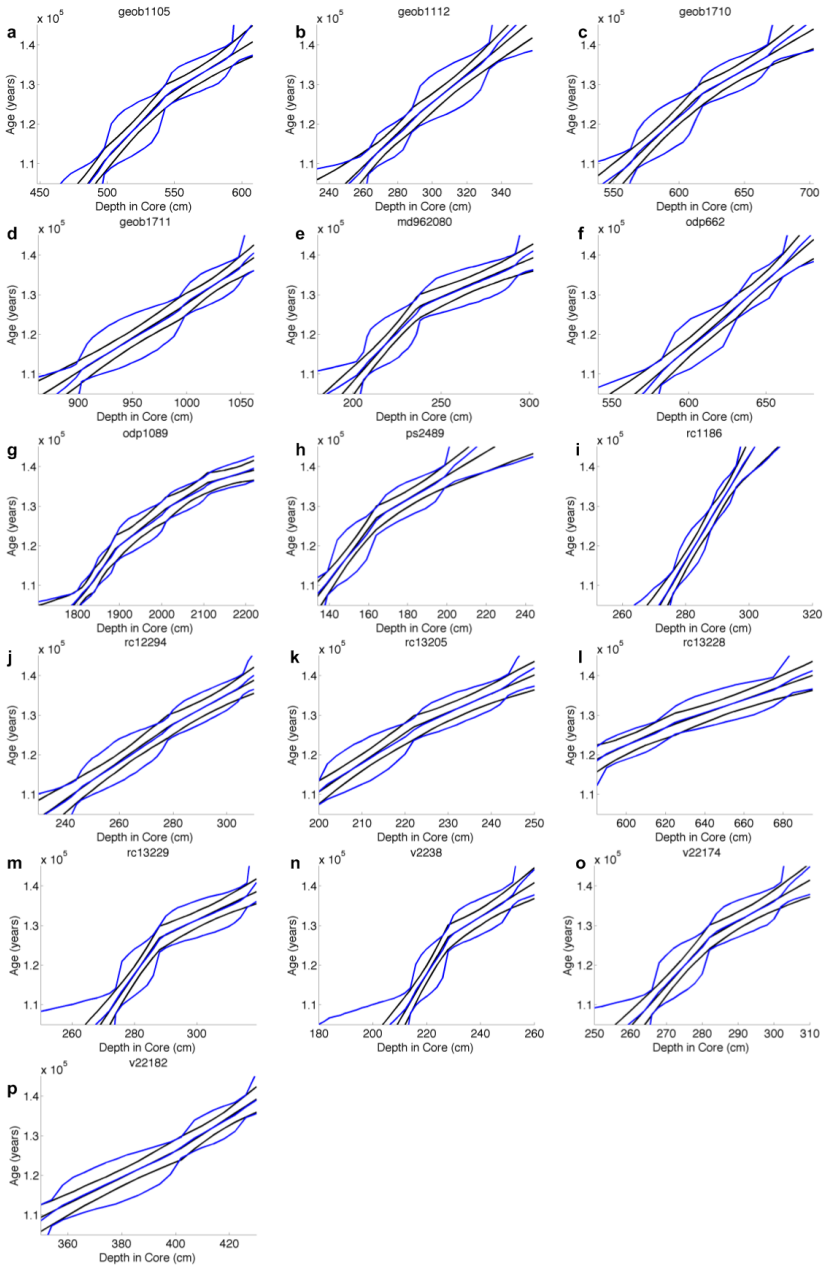

Fig. S27

Time series of calibrated SSTs for South Atlantic basin cores. Core sites are listed at the top of each panel and metadata is available for each site in Table S1&S2. In all figures the mean and 95% confidence intervals are shown. Green vertical lines demarcate the 125ka and 120ka time intervals.

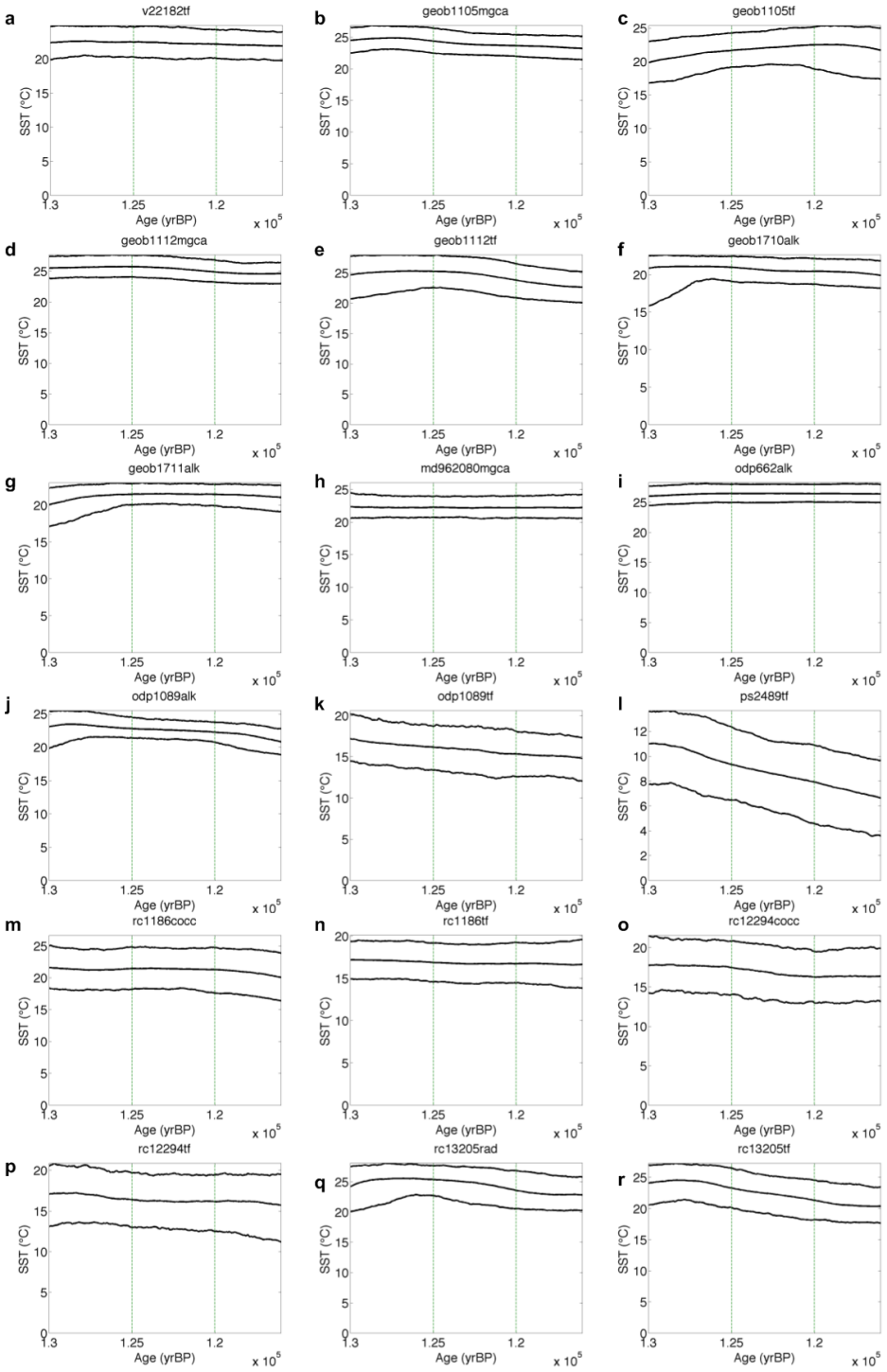

Fig. S28

Additional time series of calibrated SSTs for South Atlantic basin cores. Core sites are listed at the top of each panel and metadata is available for each site in Table S1&S2. In all figures the mean and 95% confidence intervals are shown. Green vertical lines demarcate the 125ka and 120ka time intervals.

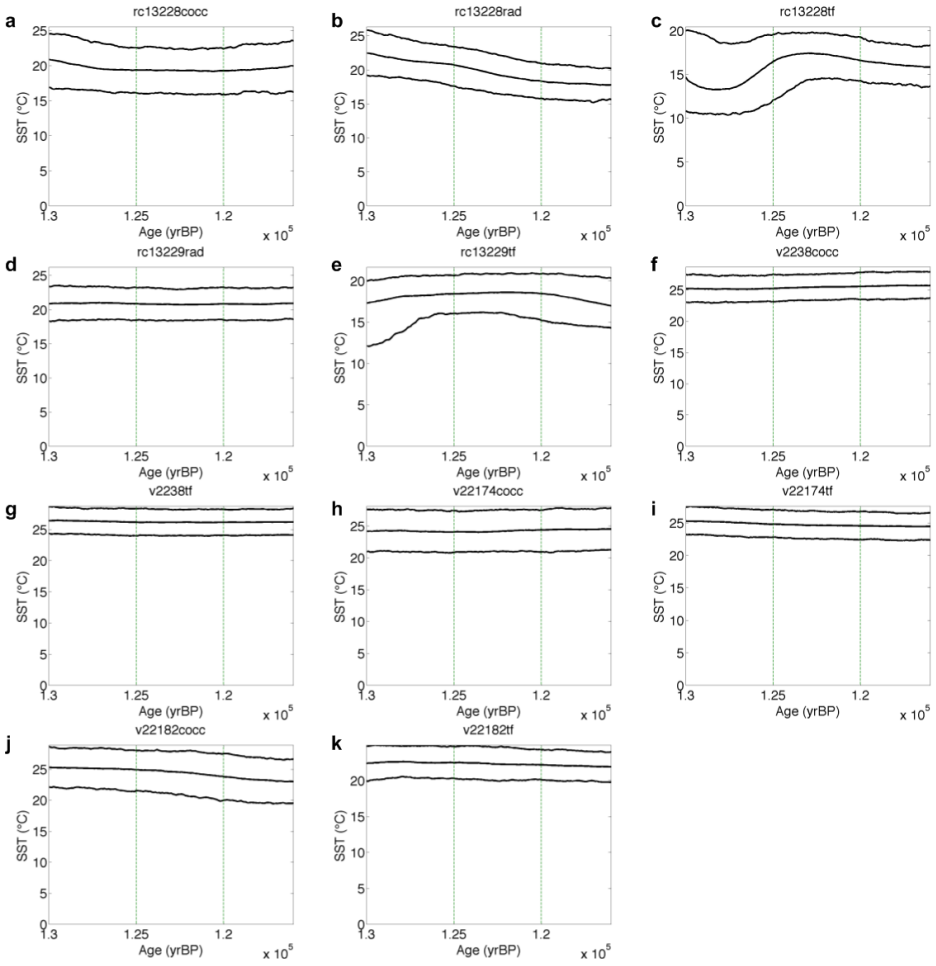

Fig. S29

Benthic $\delta^{18}O$ alignments for the Pacific Ocean basin. In all figures the blue time series is the benthic $\delta^{18}O$ time series from MD97-2120 (*60*) on the "Speleo-Age" model developed from the tie-points in Figure S5. Correlation coefficients (R^2) are also shown. Metadata for the cores on their depth scales is available in Tables S1 and S2. a) ODP1012 b) LPAZ-21 c) ODP1145 d) MD01-2421 e) ODP893 f) ODP1014 g) Y-72-111 h) ODP1020 i) ODP1018.

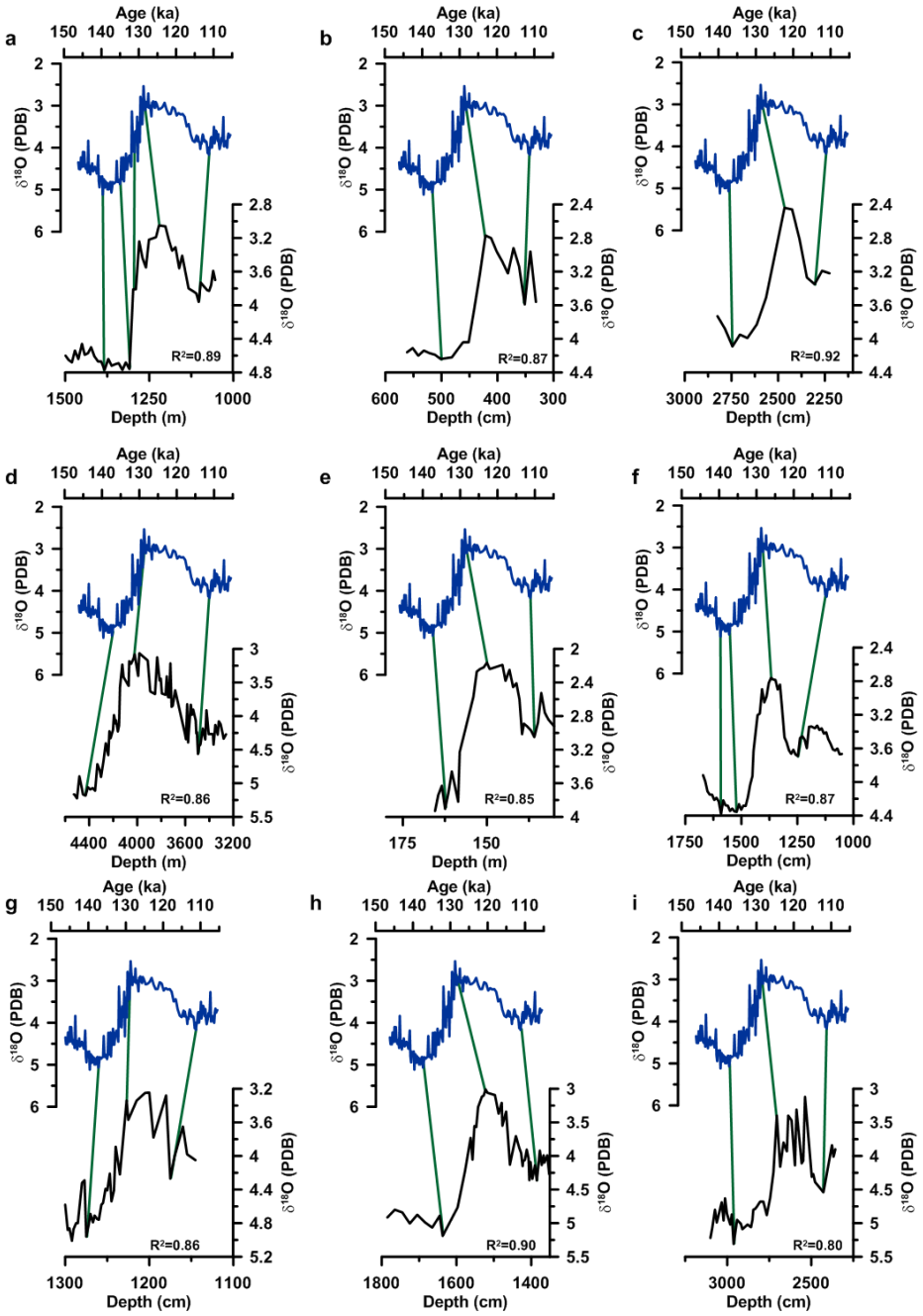

Fig. S30

Additional benthic $\delta^{18}O$ alignments for the Pacific Ocean basin. In all figures the blue time series is the benthic $\delta^{18}O$ time series from MD97-2120 (*60*) on the "Speleo-Age" model developed from the tie-points in Figure S5. Correlation coefficients (R^2) are also shown. Metadata for the cores on their depth scales is available in Tables S1 and S2. a) ODP846 b) V19-29 c) Y71-6-12 d) V28-238 e) W8402a f) TR163-22 g) ODP1146 h) MD97-2151 i) GIK17961.

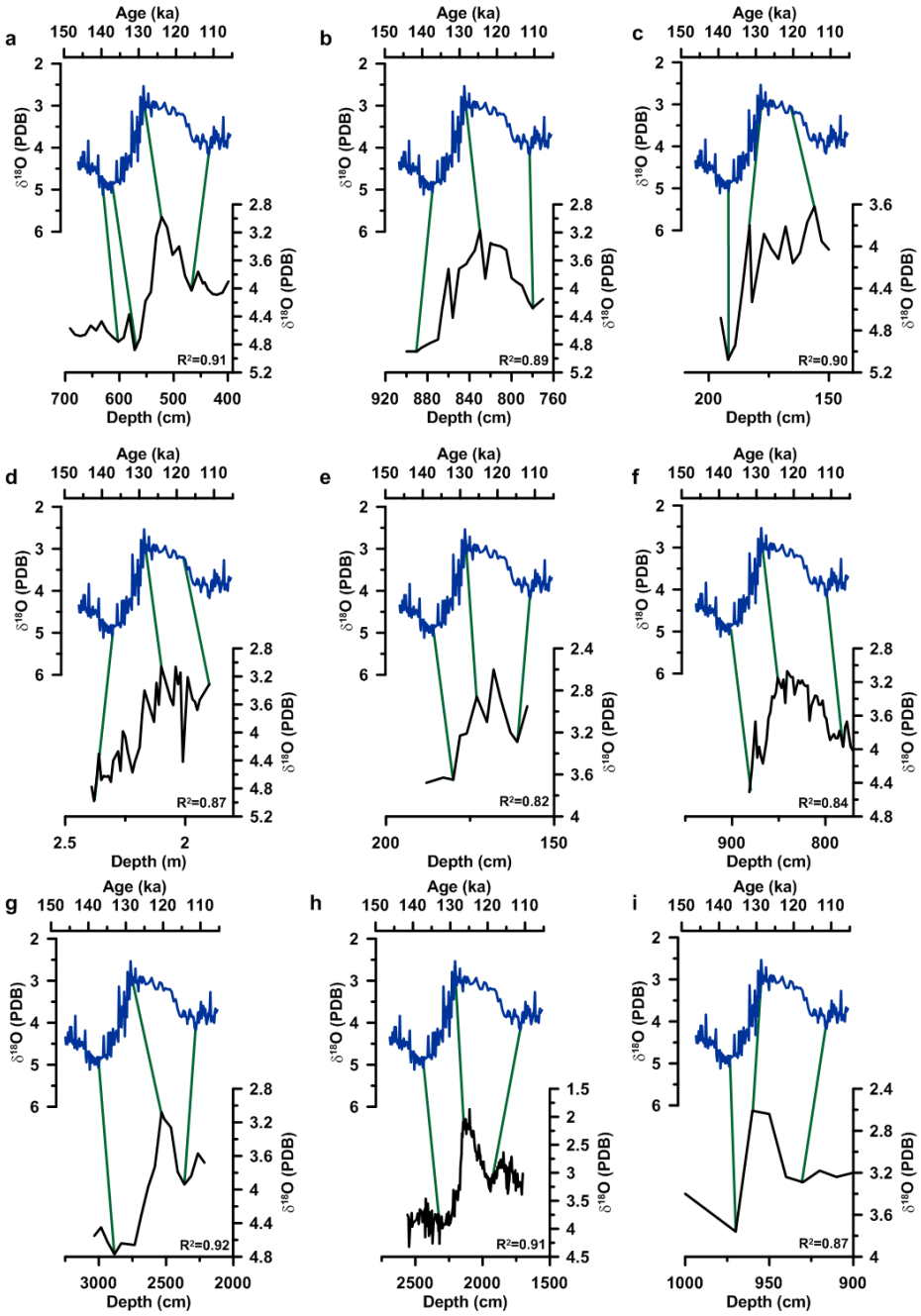

Fig. S31

Additional benthic $\delta^{18}O$ alignments for the Pacific Ocean basin. In all figures the blue time series is the benthic $\delta^{18}O$ time series from MD97-2120 (*60*) on the "Speleo-Age" model developed from the tie-points in Figure S5. Correlation coefficients (R^2) are also shown. Metadata for the cores on their depth scales is available in Tables S1 and S2. a) ODP846 b) V19-29 c) Y71-6-12 d) V28-238 e) W8402a f) TR163-22 g) ODP1146 h) MD97-2151 i) GIK17961.

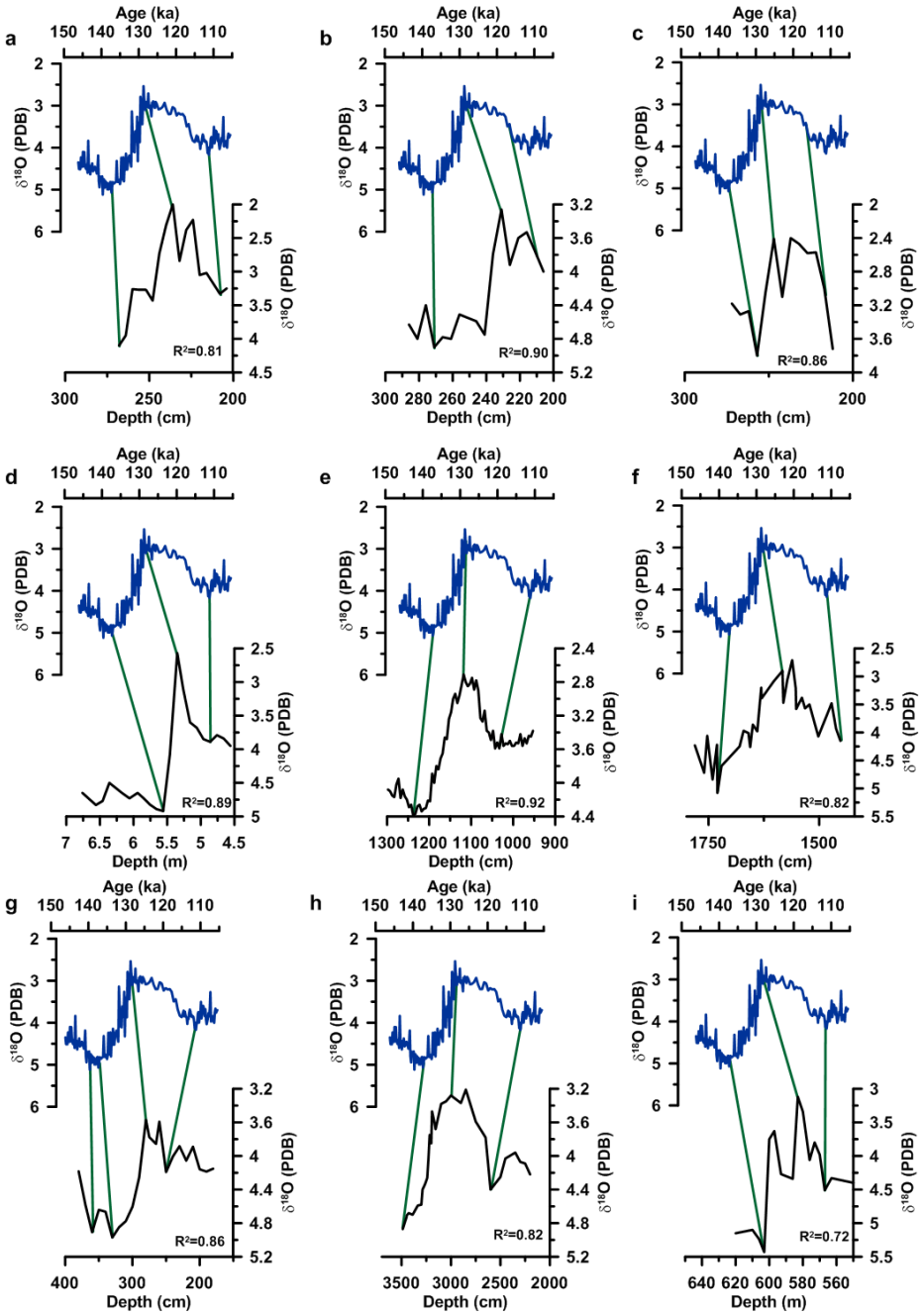

Fig. S32

Age models for Pacific Ocean basin cores. In all figures the blue lines are the mean and 95% confidence interval for age models predicted using Bchron (*16*). In all figures the black lines are the mean and 95% confidence intervals using the age model uncertainty propagation method from (*10*). Each plot gives the core site and metadata on these cores is available in Table S1 & S2.

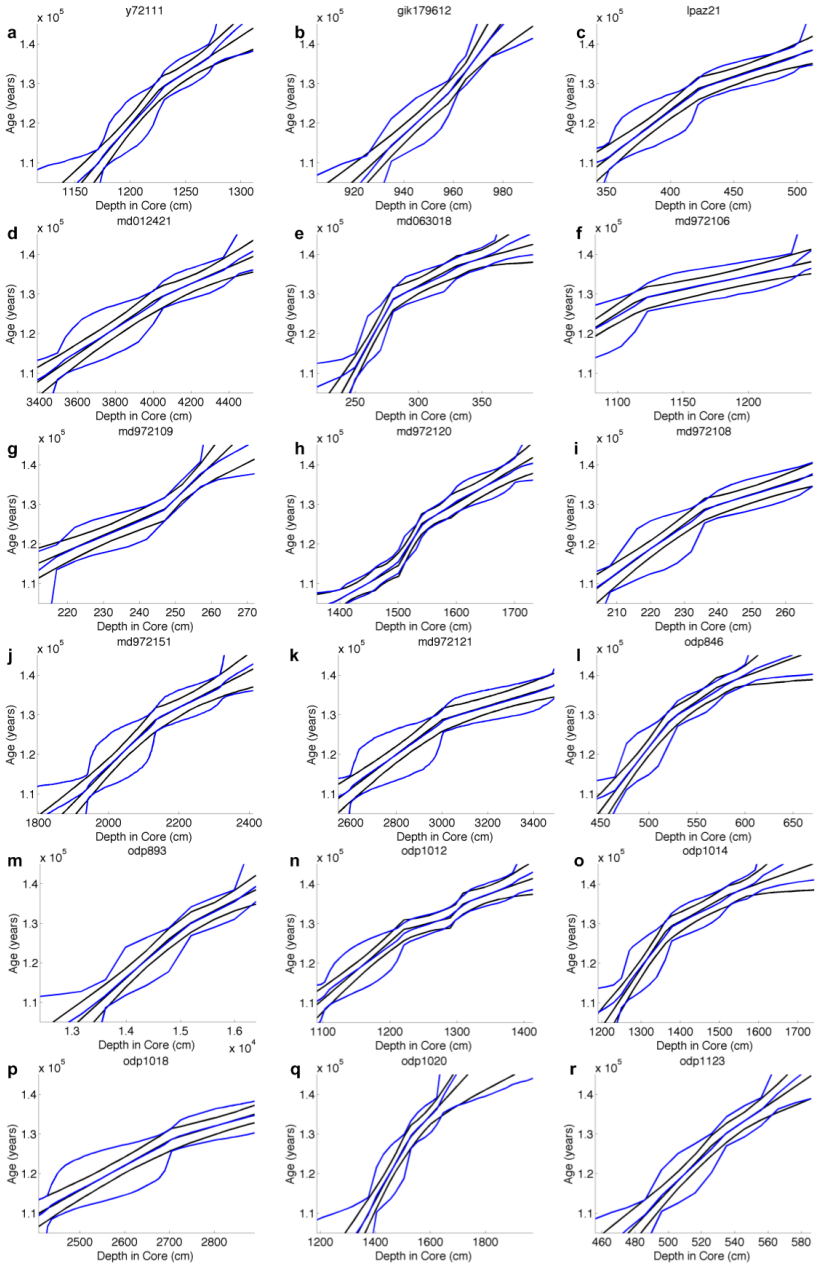

Fig. S33

Additional age models for Pacific Ocean basin cores. In all figures the blue lines are the mean and 95% confidence interval for age models predicted using Bchron (*16*). In all figures the black lines are the mean and 95% confidence intervals using the age model uncertainty propagation method from (*10*). Each plot gives the core site and metadata on these cores is available in Table S1 & S2.

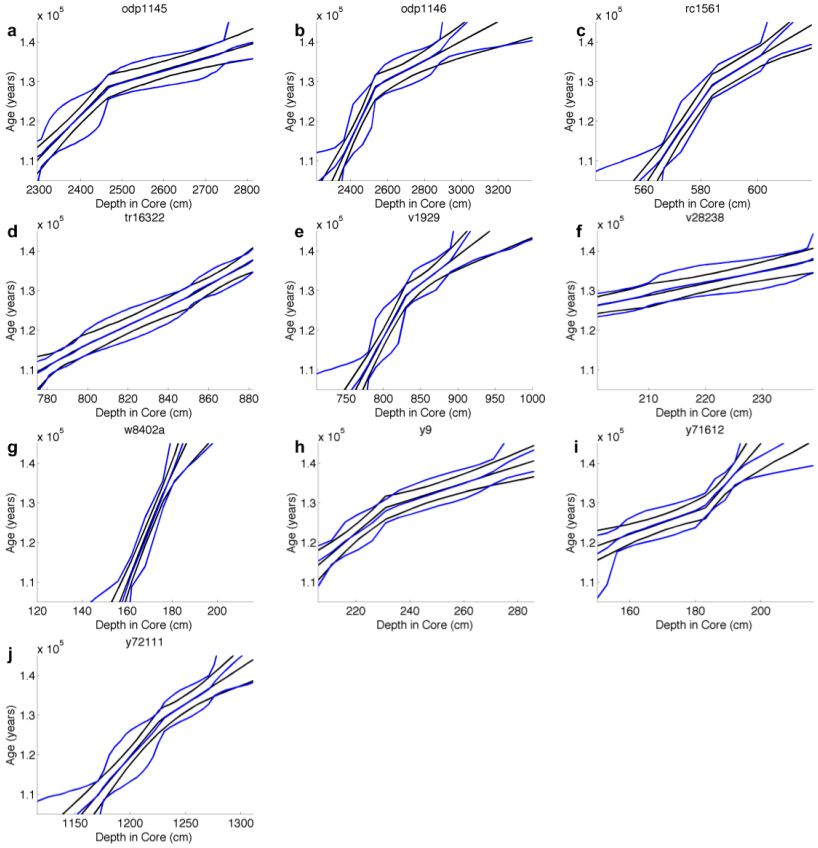

Fig. S34

Time series of calibrated SSTs for Pacific Ocean basin cores. Core sites are listed at the top of each panel and metadata is available for each site in Table S1&S2. In all figures the mean and 95% confidence intervals are shown. Green vertical lines demarcate the 125ka and 120ka time intervals.

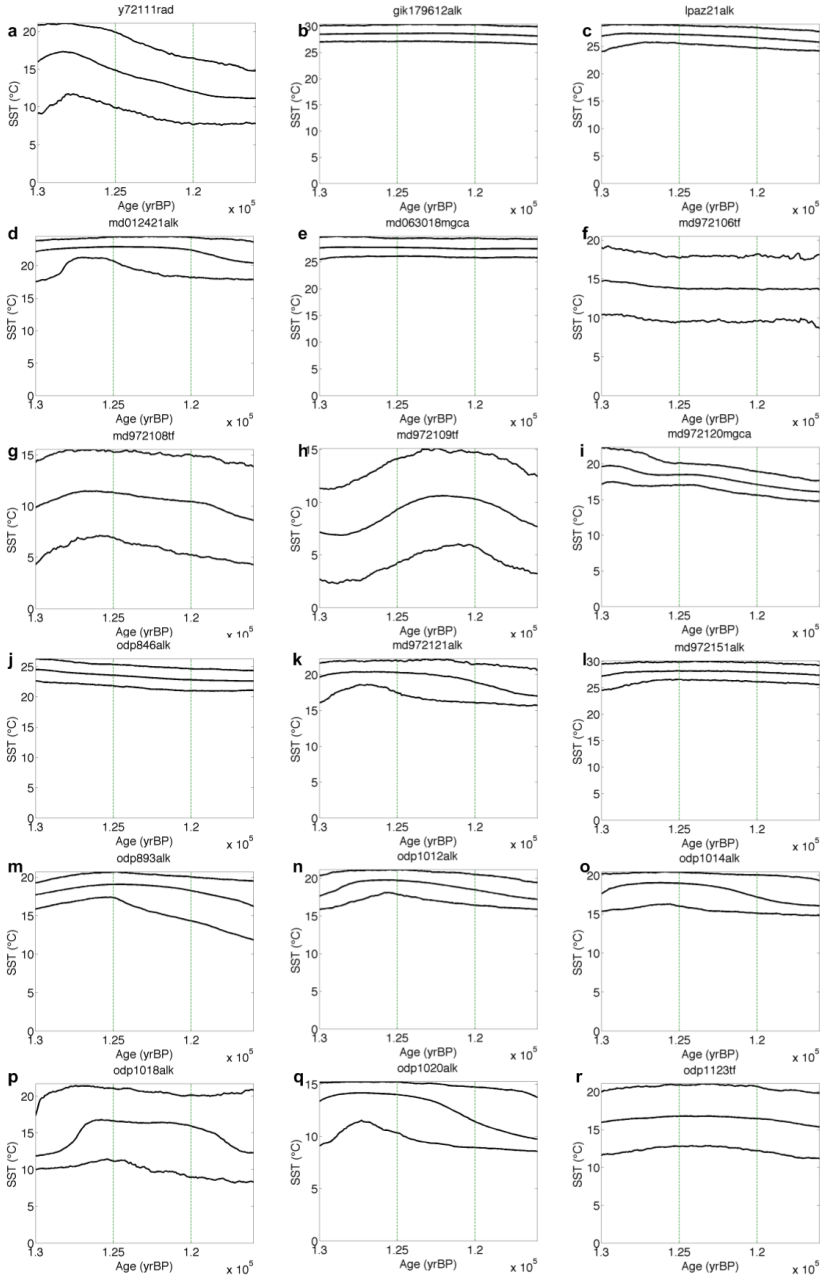

Fig. S35

Additional time series of calibrated SSTs for Pacific Ocean basin cores. Core sites are listed at the top of each panel and metadata is available for each site in Table S1&S2. In all figures the mean and 95% confidence intervals are shown. Green vertical lines demarcate the 125ka and 120ka time intervals.

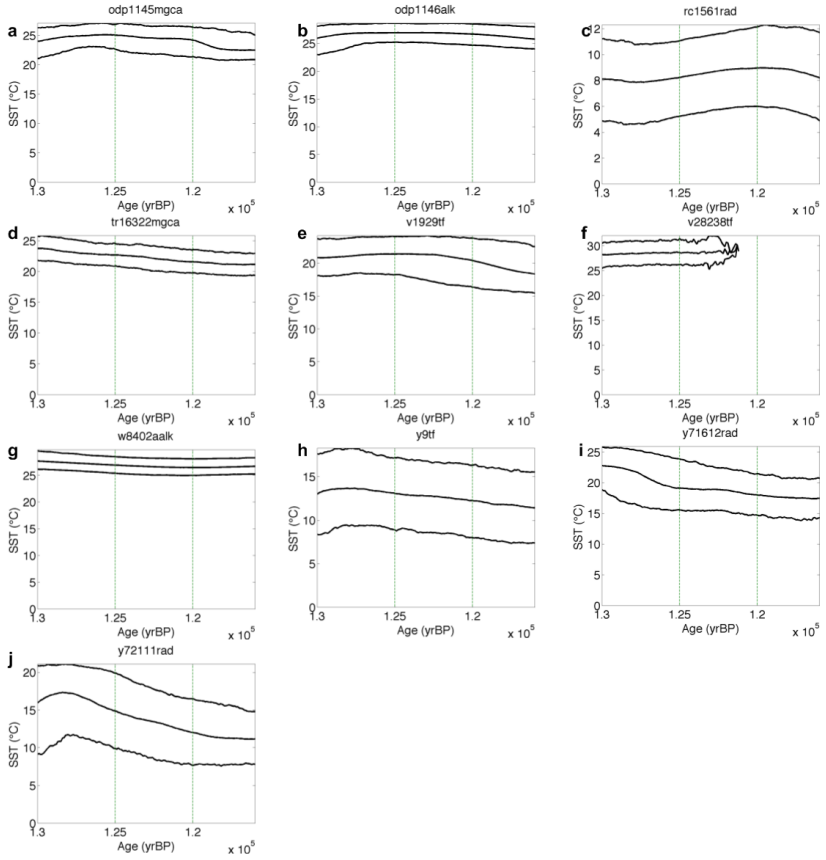

Fig. S36

Benthic $\delta^{18}O$ alignments for the North Atlantic basin. In all figures the blue time series is the benthic $\delta^{18}O$ time series from MD01-2444 (*39*) on the "Speleo-Age" model developed from the tie-points in Figure S5. Correlation coefficients (R^2) are also shown. Metadata for the cores on their depth scales is available in Tables S1 and S2. a) M23414 b) NEAP18k c) V23-82 d) ODP980 e) NA87-25 f) V27-20 g) M23323 h) V28-14 i) EW9302-JPC8

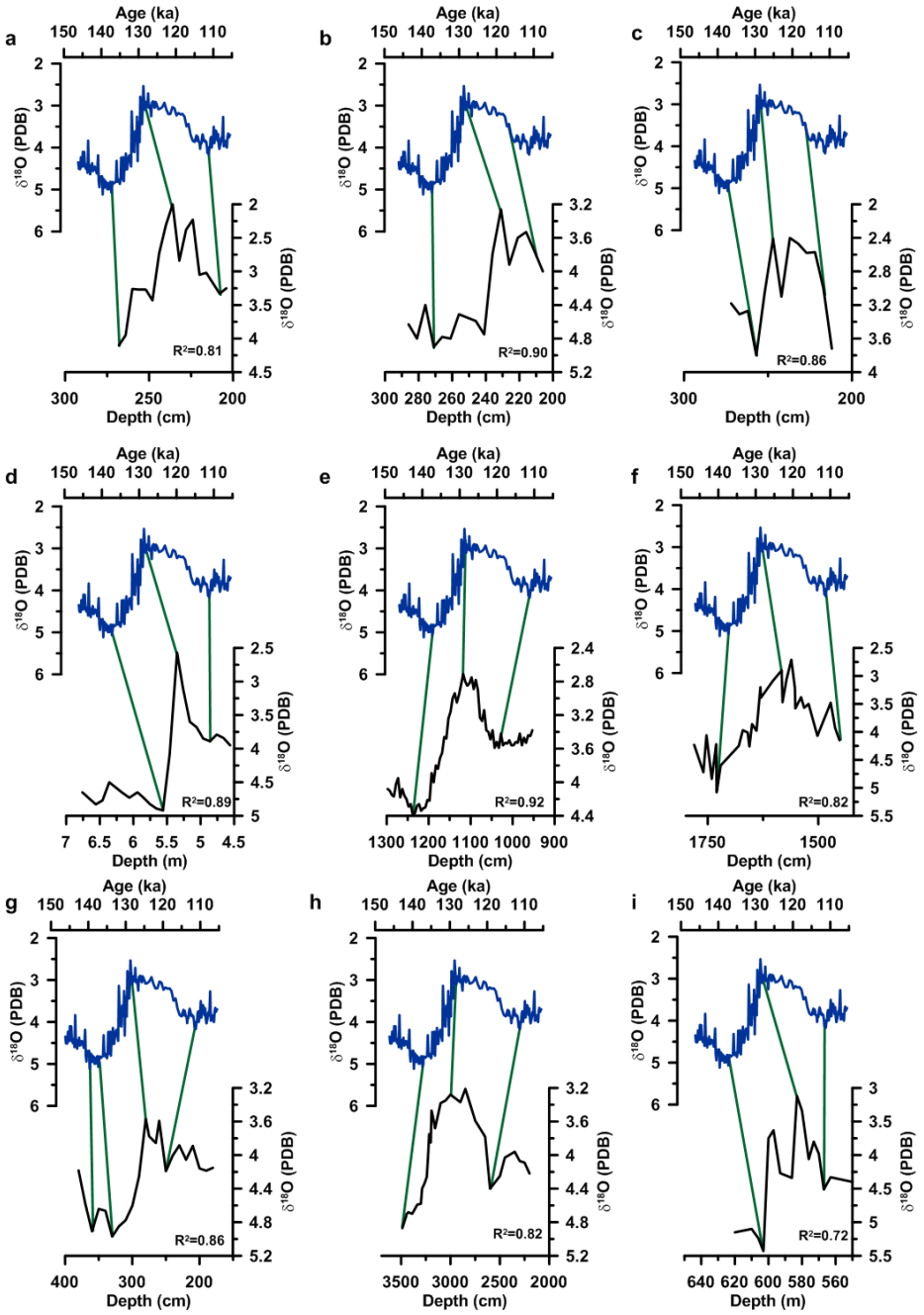

Fig. S37

Additional benthic $\delta^{18}O$ alignments for the North Atlantic basin. In all figures the blue time series is the benthic $\delta^{18}O$ time series from MD01-2444 (*39*) on the "Speleo-Age" model developed from the tie-points in Figure S5. Correlation coefficients (R^2) are also shown. Metadata for the cores on their depth scales is available in Tables S1 and S2. a) V30-97 b) MD95-2040 c) SU90-03 d) SU92-03 e) D-117 f) CH69K09 g) K708-1 h) MD04-2845 i) V29-179.

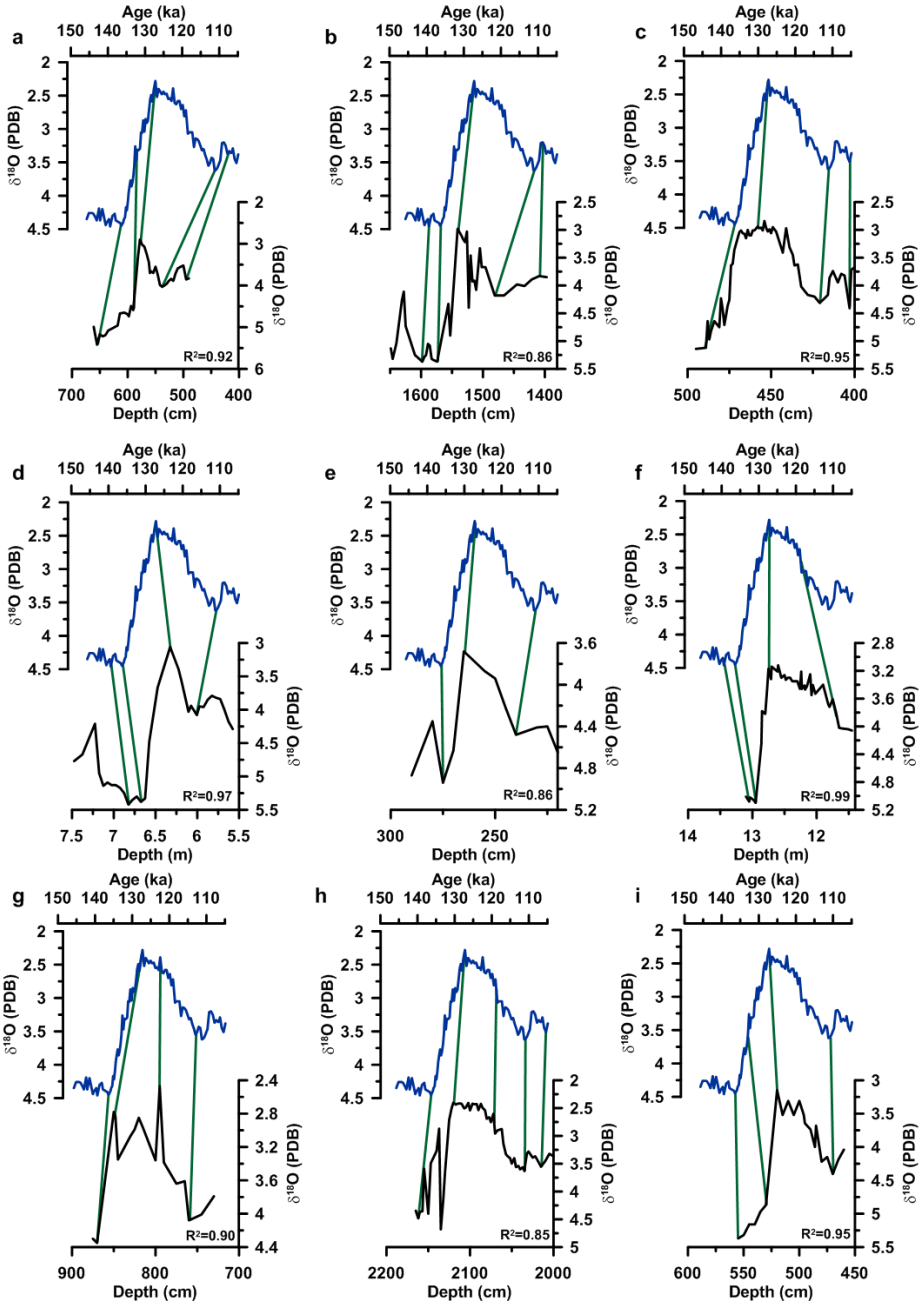

Fig. S38

Additional benthic $\delta^{18}O$ alignments for the North Atlantic basin. In all figures the blue time series is the benthic $\delta^{18}O$ time series from MD01-2444 (*39*) on the "Speleo-Age" model developed from the tie-points in Figure S5. Correlation coefficients (R^2) are also shown. Metadata for the cores on their depth scales is available in Tables S1 and S2. a)TR126-23 b) M35027-1 c) V22-196 d) GIK-15637 e) M12391-2 f) TR126-29 g) MD95-2036 h) KNR140-JPC37 i) MD02-2575.

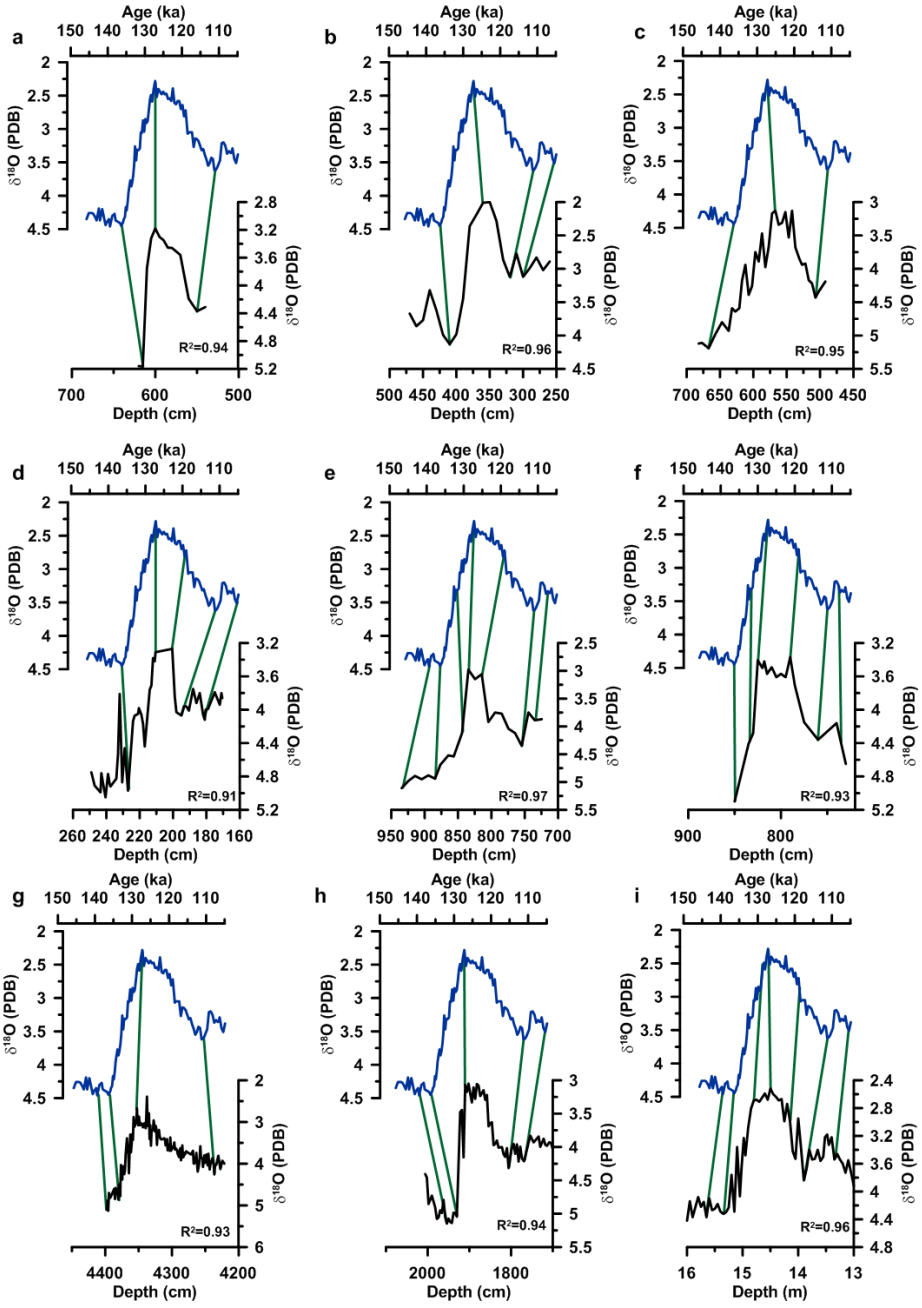

Fig. S39

Additional benthic $\delta^{18}O$ alignments for the North Atlantic basin. In all figures the blue time series is the benthic $\delta^{18}O$ time series from MD01-2444 (*39*) on the "Speleo-Age" model developed from the tie-points in Figure S5. Correlation coefficients (R^2) are also shown. Metadata for the cores on their depth scales is available in Tables S1 and S2. a) V28-127 b) MD03-2707 c) V25-59.

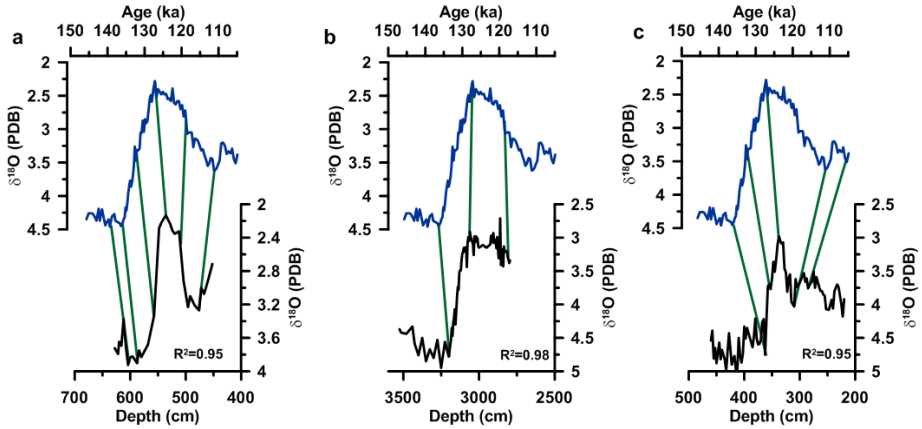

Fig. S40

Age models for North Atlantic basin cores. In all figures the blue lines are the mean and 95% confidence interval for age models predicted using Bchron (*16*). In all figures the black lines are the mean and 95% confidence intervals using the age model uncertainty propagation method from (*10*). Each plot gives the core site and metadata on these cores is available in Table S1 & S2.

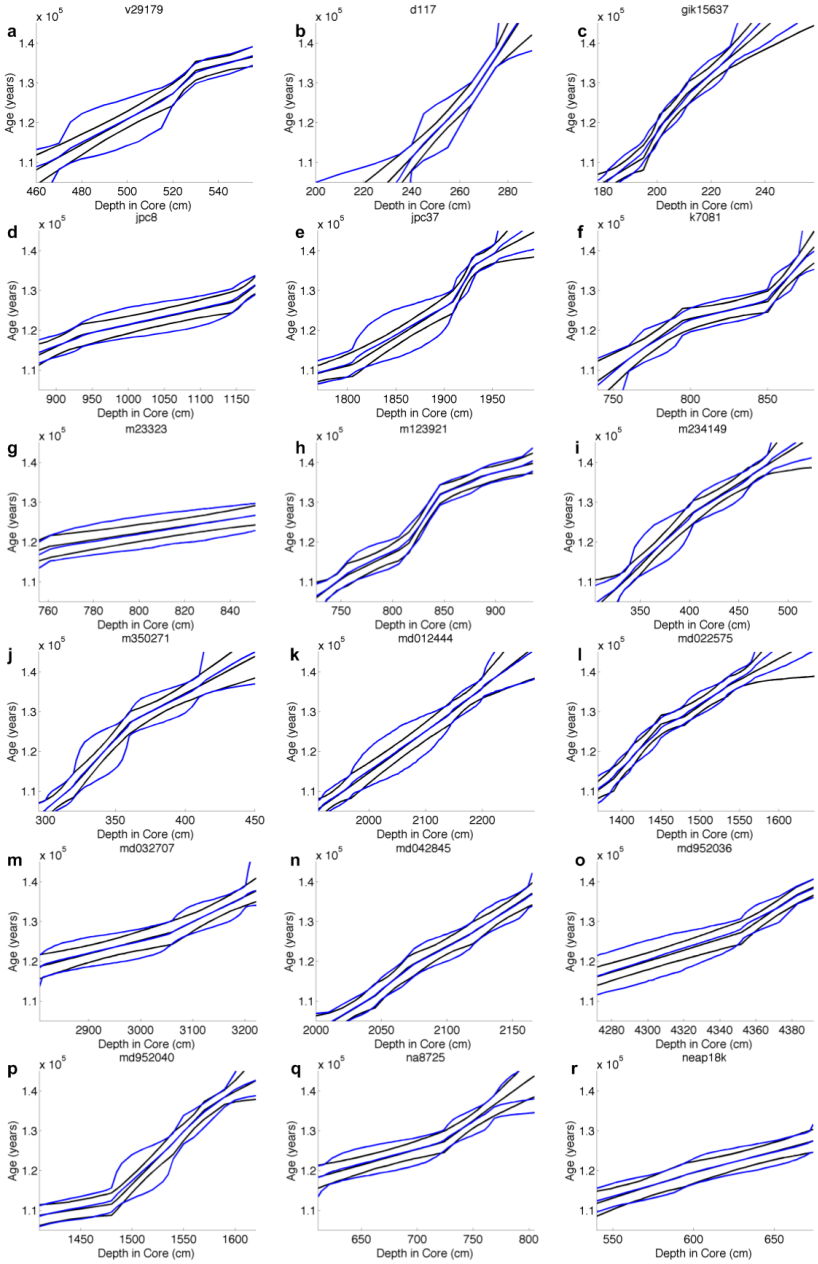

Fig. S41

Additional age models for North Atlantic basin cores. In all figures the blue lines are the mean and 95% confidence interval for age models predicted using Bchron (*16*). In all figures the black lines are the mean and 95% confidence intervals using the age model uncertainty propagation method from (*10*). Each plot gives the core site and metadata on these cores is available in Table S1 & S2.

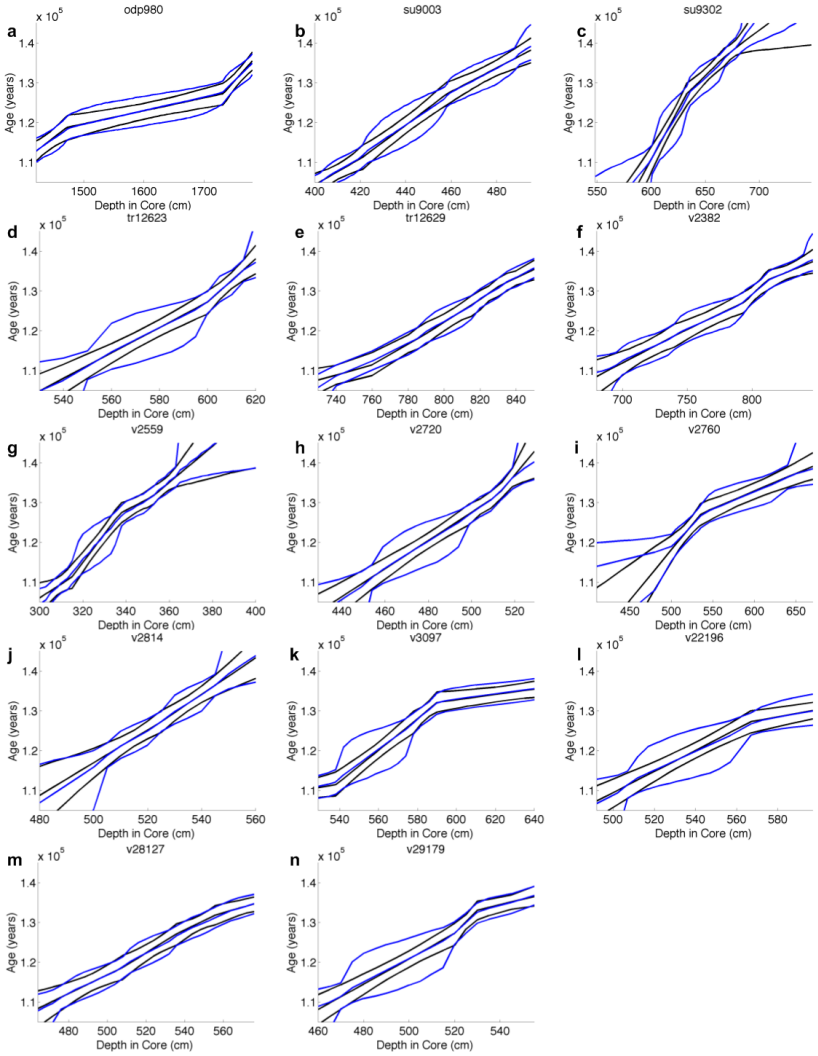

Fig. S42

Time series of calibrated SSTs for North Atlantic basin cores. Core sites are listed at the top of each panel and metadata is available for each site in Table S1&S2. In all figures the mean and 95% confidence intervals are shown. Green vertical lines demarcate the 125ka and 120ka time intervals.

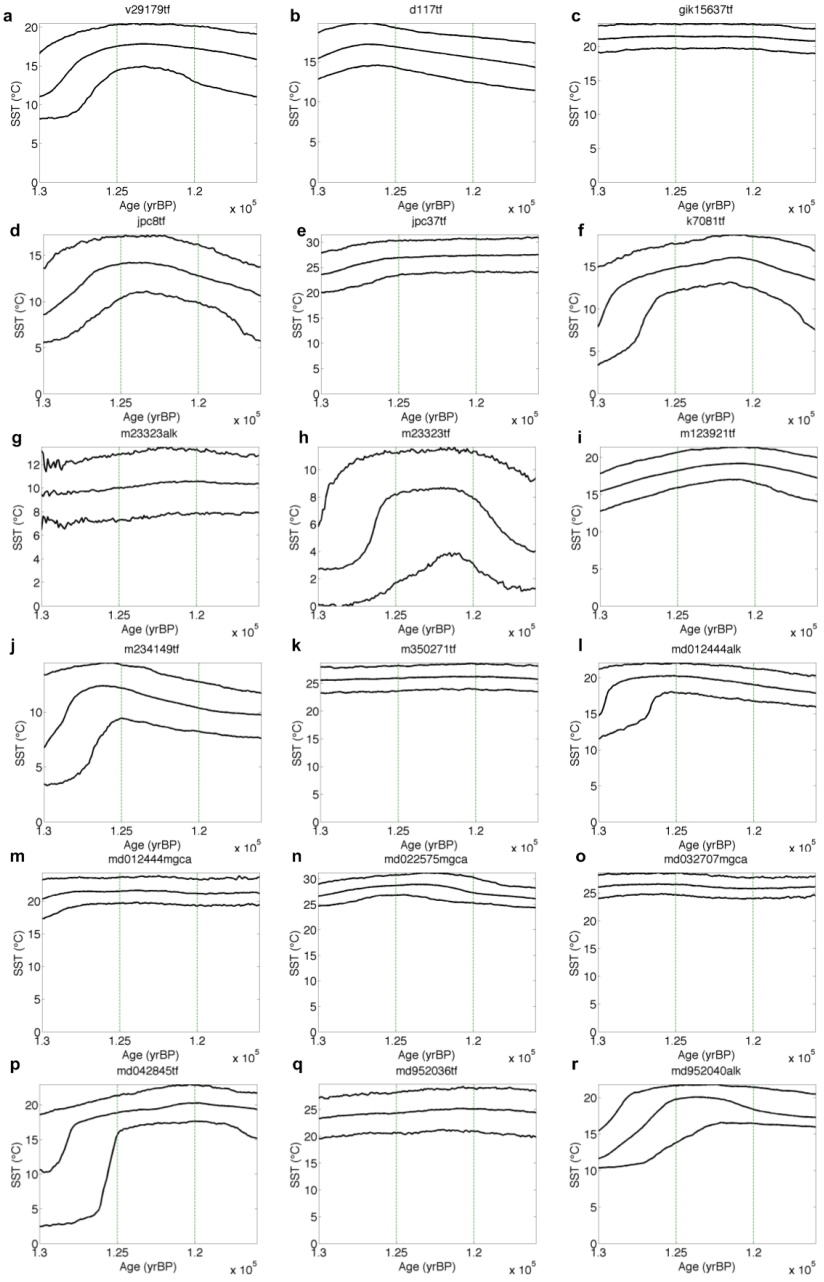

Fig. S43

Additional time series of calibrated SSTs for North Atlantic basin cores. Core sites are listed at the top of each panel and metadata is available for each site in Table S1&S2. In all figures the mean and 95% confidence intervals are shown. Green vertical lines demarcate the 125ka and 120ka time intervals.

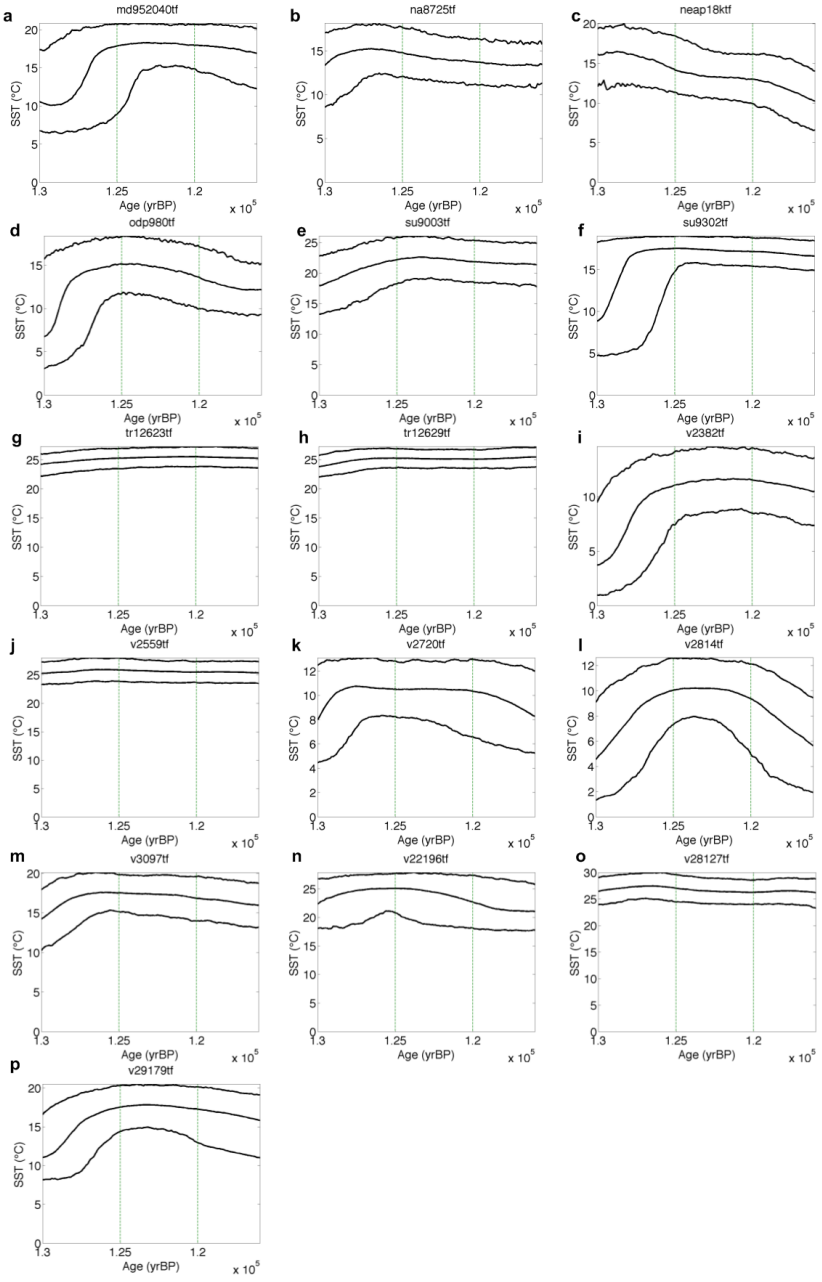

Table S1.
Metadata for the sediment core locations compiled for this study. Sites in bold represent basin reference core sites for their ocean basin as defined in this study. Annual* is a site with averaged summer/winter temperatures (see supplementary text).

#	CORE	LOCATION	BASIN	LATITUDE	LONGITUDE	DEPTH (m)	PUBLISHED RESOLUTION (YEARS)	SEA SURFACE TEMPERATURE PROXY	INFERRED PROXY SIGNAL
1	M23323-1	Norwegian Sea - Vøring Plateau	N_ATL	67.77	5.92	1286	110	Foraminiferal Census Counts - SIMMAX	Summer
2	M23323-1	Norwegian Sea - Vøring Plateau	N_ATL	67.77	5.92	1286	186	UK'37	Annual
3	V28-14	Irminger Basin	N_ATL	64.78	-29.57	1855	2100	Foraminiferal Transfer Function, FA13'	Annual*
4	EW9302-JPC8	Iceland Basin	N_ATL	61.42	-25.00	1917	570	Foraminiferal Census Counts - SIMMAX	Summer
5	ODP 980	Feni Drift	N_ATL	55.48	-14.70	2179	260	% N. pachyderma (s)	Summer
6	NA87-25	Feni Ridge	N_ATL	55.18	-14.73	2320	450	Foraminiferal Census Counts - SIMMAX	Summer
7	V27-20	Labrador Sea	N_ATL	54.00	-46.20	3510	1625	Foraminiferal Transfer Function, FA13'	Annual*
8	GIK/M23414-9	Rockall Plateau	N_ATL	53.53	-20.29	2196	320	Foraminiferal Census Counts, MAT/RAM/TFT	Annual*
9	NEAP18k	Charlie-Gibbs Fracture Zone	N_ATL	52.76	-30.35	3275	450	Foraminiferal Census Counts - SIMMAX	Summer
10	V23-82	Rockall Plateau	N_ATL	52.58	-21.93	3974	650	Foraminiferal Census Counts, FA3	Annual*
11	K708-1	Northeast Atlantic	N_ATL	50.00	-23.74	4053	680	Foraminiferal Transfer Function, FA13'	Annual*
12	MD04-2845	Bay of Biscay	N_ATL	45.35	-5.22	4100	1180	Foraminiferal Census Counts - SIMMAX	Summer
13	V29-179	Central North Atlantic	N_ATL	44.00	-23.51	3331	1100	Foraminiferal Transfer Function, FA13'	Annual*
14	Y7211-1	Northeast Pacific Margin	PAC	43.25	-126.38	3000	1100	Radiolarian Transfer Function RP8	Annual*
15	SU92-03	Iberian Margin	N_ATL	43.20	-10.11	3005	1625	Foraminiferal Census Counts - SIMMAX	Summer
16	D117	Western North Atlantic	N_ATL	42.10	-52.75	3300	1850	Foraminiferal Transfer Function, FA13	Annual*
17	CH69-K09	Western North Atlantic	N_ATL	41.76	-47.35	4100	375	% N. pachyderma (s)	Summer
18	V30-97	Central North Atlantic	N_ATL	41.00	-32.93	3371	1100	Foraminiferal Transfer Function, FA13'	Annual*
19	ODP 1020	California Margin	PAC	41.00	-126.43	1783	2000	UK'37	Annual
20	MD95-2040	Iberian Margin	N_ATL	40.58	-9.86	2465	500	UK'37	Annual
21	MD95-2040	Iberian Margin	N_ATL	40.58	-9.87	2465	450	Foraminiferal Census Counts - SIMMAX	Summer
22	SU90-03	Central North Atlantic	N_ATL	40.50	-32.05	2475	375	Foraminiferal Census Counts - SIMMAX	Summer
23	**MD01-2444**	**Iberian Margin**	**N_ATL**	**37.57**	**-10.13**	**2637**	**300**	**UK'37**	Annual
24	MD01-2444	Iberian Margin	N_ATL	37.57	-10.13	2637	470	Planktic Mg/Ca	Annual
25	ODP 1018	Guide Seamount	PAC	36.99	-123.27	2477	830	UK'37	Annual
26	MD01-2421	Japan Trench	PAC	36.02	141.78	2224	1600	UK'37	Annual
27	ODP 893	Santa Barbara Basin	PAC	34.28	-120.03	575	4000	UK'37	Annual
28	MD95-2036	Bermuda Rise	N_ATL	33.68	-57.57	4461	280	Foraminiferal Census Counts - SIMMAX	Summer
29	ODP 1014A	California Margin	PAC	32.80	-118.90	1165	1600	UK'37	Annual
30	ODP 1012	East Cortez Basin	PAC	32.28	-118.38	1783	980	UK'37	Annual
31	KNR140-37JPC	Blake Outer Ridge	N_ATL	31.68	-75.42	2972	600	Foraminiferal Census Counts - SIMMAX	Summer
32	MD02-2575	Gulf of Mexico	N_ATL	29.00	-87.11	847	800	Planktic Mg/Ca	Annual
33	GIK15637-1	Northeast Atlantic	N_ATL	27.00	-18.98	3849	890	Foraminiferal Census Counts - SIMMAX	Annual*
34	GIK/M12392-1	Northeast Atlantic	N_ATL	25.16	-16.85	2573	1850	Foraminiferal Transfer Function	Annual*
35	LAPAZ21P	Gulf of California	PAC	22.98	-109.47	624	1130	UK'37	Annual
36	TR126-29	Gulf of Mexico	N_ATL	21.33	-93.95	2700	1300	Foraminiferal Transfer Function FG6	Annual*
37	TR126-23	Gulf of Mexico	N_ATL	20.48	-95.62	2410	1850	Foraminiferal Transfer Function FG6	Annual*
38	ODP 1145	South China Sea	PAC	19.53	117.63	3175	400	Planktic Mg/Ca	Annual
39	ODP 1146	South China Sea	PAC	19.45	116.27	2092	2500	UK'37	Annual
40	M35027-1	Caribbean Sea	N_ATL	17.64	-67.17	1814	870	Foraminiferal Census Counts - SIMMAX	Annual
41	V34-88	Arabian Sea	IND	16.52	59.53	2100	1200	Foraminiferal Transfer Function, FI2	Annual*
42	V22-196	NW Africa - Cape Verde	N_ATL	13.83	-18.97	3728	1625	Foraminiferal Transfer Function, FA13	Annual*
43	V28-127	Caribbean Sea	N_ATL	11.65	-80.13	3227	1200	Foraminiferal Transfer Function, FA13	Annual*
44	RC12-339	Bay of Bengal	IND	9.13	90.03	3010	950	Foraminiferal Transfer Function, FI2	Annual*
45	MD97-2151	South China Sea	PAC	8.73	109.87	1598	180	UK'37	Annual
46	GIK17961-2	South China Sea	PAC	8.50	112.33	1968	3200	UK'37	Annual
47	MD03-2707	Gulf of Guinea	N_ATL	2.50	9.39	1295	220	Planktic Mg/Ca	Annual
48	V25-59	Equatorial Atlantic	N_ATL	1.37	-33.48	3824	1200	Foraminiferal Transfer Function, FA13	Annual*
49	V28-238	Western Equatorial Pacific	PAC	1.02	160.48	3120	870	Foraminiferal Transfer Function, FP12E	Annual*
50	W8402a	Central Equatorial Pacific	PAC	0.95	-138.95	4287	4000	UK'37	Annual

Table S1. (continued)

#	CORE	LOCATION	BASIN	LATITUDE	LONGITUDE	DEPTH (m)	PUBLISHED RESOLUTION (YEARS)	SEA SURFACE TEMPERATURE PROXY	INFERRED PROXY SIGNAL
51	TR163-22	Eastern Equatorial Pacific	PAC	0.50	-92.40	2830	560	Planktic Mg/Ca	Annual
52	V22-182	Central Equatorial Atlantic	S_ATL	-0.55	-17.27	3937	1200	Foraminiferal Transfer Function FA20	Annual*
53	V22-182	Central Equatorial Atlantic	S_ATL	-0.55	-17.27	3937	1625	Coccolithophore Transfer Function CA8	Annual*
54	ODP 662	Eastern Equatorial Atlantic	S_ATL	-1.38	-11.74	3824	2400	UK'37	Annual
55	GeoB 1105	Eastern Equatorial Atlantic	S_ATL	-1.67	-12.43	3225	1400	UK'37	Annual
56	GeoB 1105	Eastern Equatorial Atlantic	S_ATL	-1.67	-12.43	3225	2600	Foraminiferal Transfer Function	Annual*
57	GeoB 1105	Eastern Equatorial Atlantic	S_ATL	-1.67	-12.43	3225	2600	Planktic Mg/Ca	Annual
58	RC13-205	Eastern Equatorial Atlantic	S_ATL	-2.28	5.18	3731	1300	Radiolarian Transfer Function RSA1	Annual*
59	RC13-205	Eastern Equatorial Atlantic	S_ATL	-2.28	5.18	3731	1300	Foraminiferal Transfer Function FA2OU5	Annual*
60	ODP 846	Eastern Equatorial Pacific	PAC	-3.08	-90.82	3296	3000	UK'37	Annual
61	V19-29	Eastern Equatorial Pacific	PAC	-3.57	-83.22	3157	2200	Radiolarian Transfer Function RP7	Annual
62	GeoB 1112	Southeastern Atlantic - W. African Margin	S_ATL	-5.77	-10.74	3122	1650	Planktic Mg/Ca	Annual
63	GeoB 1112	Southeastern Atlantic - W. African Margin	S_ATL	-5.77	-10.74	3122	3300	Foraminiferal Census Counts - SIMMAX	Annual
64	GeoB 10038-4	Mentawai Basin	IND	-5.94	103.25	1819	700	Planktic Mg/Ca	Annual
65	GeoB 10038-4	Mentawai Basin	IND	-5.94	103.25	1819	700	UK'37	Annual
66	V22-38	Brazil Margin	S_ATL	-9.51	-34.25	3797	1450	Foraminiferal Transfer Function FA20	Annual*
67	V22-38	Brazil Margin	S_ATL	-9.51	-34.25	3797	1100	Coccolithophore Transfer Function CA8	Annual*
68	V22-174	Central South Atlantic	S_ATL	-10.07	-12.82	2630	1200	Foraminiferal Transfer Function FA20	Annual*
69	V22-174	Central South Atlantic	S_ATL	-10.07	-12.82	2630	1100	Coccolithophore Transfer Function CA8	Annual*
70	MD01-2378	Timor Sea	IND	-13.08	121.79	1783	260	Planktic Mg/Ca	Annual
71	Y71-6-12	Nazca Plate	PAC	-16.45	-77.57	2734	1450	Radiolarian Transfer Function RP8	Annual*
72	V28-345	Timor Sea	IND	-17.67	117.95	1904	1450	Foraminiferal Transfer Function, FI2	Annual*
73	RC13-228	Southeastern Atlantic - W. African Margin	S_ATL	-22.33	11.20	3204	1000	Coccolithophore Transfer Function CA8	Annual*
74	RC13-228	Southeastern Atlantic - W. African Margin	S_ATL	-22.33	11.20	3204	1450	Foraminiferal Transfer Function FA2OU7	Annual*
75	RC13-228	Southeastern Atlantic - W. African Margin	S_ATL	-22.33	11.20	3204	1100	Radiolarian Transfer Function RSA1	Annual*
76	MD06-3018	Southwestern Pacific	PAC	-23.00	166.13	2470	3000	Planktic Mg/Ca	Annual
77	GeoB 1711-4	Benguela Current	S_ATL	-23.31	12.38	1967	740	UK'37	Annual
78	GeoB 1710-3	Benguela Current	S_ATL	-23.43	11.70	2987	1130	UK'37	Annual
79	RC13-229	Cape Basin	S_ATL	-25.50	11.30	4191	870	Radiolarian Transfer Function RSA1	Annual*
80	RC13-229	Cape Basin	S_ATL	-25.50	11.30	4191	1000	Foraminiferal Transfer Function FA2OU7	Annual*
81	RC11-86	Agulhas Retroflection	S_ATL	-35.78	18.45	2829	1000	Foraminiferal Transfer Function FA2OU7	Annual*
82	RC11-86	Agulhas Retroflection	S_ATL	-35.78	18.45	2829	1100	Coccolithophore Transfer Function CA8	Annual*
83	MD96-2080	Agulhas Retroflection	S_ATL	-36.32	19.47	2488	1100	Planktic Mg/Ca	Annual
84	RC12-294	Central South Atlantic	S_ATL	-37.27	-10.10	3308	770	Coccolithophore Transfer Function CA8	Annual*
85	RC12-294	Central South Atlantic	S_ATL	-37.27	-10.10	3308	770	Foraminiferal Transfer Function FA20	Annual*
86	MD97-2121	Chatham Rise	PAC	-40.38	177.98	3014	250	UK'37	Annual
87	RC15-61	Chilean Margin	PAC	-40.62	-77.20	3771	1200	Radiolarian Transfer Function RP8	Annual*
88	**ODP 1089**	**Cape Basin**	**S_ATL**	**-40.93**	**9.90**	**4621**	**600**	**UK'37**	Annual
89	ODP 1089	Cape Basin	S_ATL	-40.93	9.90	4621	690	Radiolarian Transfer Function	Summer
90	ODP 1123	North Chatham Drift	PAC	-41.79	-171.50	3290	2700	Foraminiferal Transfer Function	Annual
91	MD94-101	South Indian Ocean	IND	-42.50	79.42	2920	1100	% N. pachyderma (s)	Summer
92	PS2489-2	Central South Atlantic	S_ATL	-42.90	8.97	3794	2000	Foraminiferal Census Counts - SIMMAX/MAT	Summer
93	MD84-527	Southwestern Indian Ocean	IND	-43.49	51.20	3267	980	Diatom Transfer Function DTF 166/34/4	Summer
94	MD94-102	South Indian Ocean	IND	-43.50	79.83	3205	1300	% N. pachyderma (s)	Summer
95	MD73-025	South Indian Ocean	IND	-43.82	51.30	3284	930	Radiolarian Transfer Function RAN3	Annual*
96	MD97-2106	Tasman Sea	PAC	-45.15	146.29	1083	1280	Foraminiferal Transfer Function	Annual
97	DSDP site 594	Chatham Rise/Bounty Trough	PAC	-45.50	174.95	1204	1800	Foraminiferal Transfer Function	Annual
98	**MD97-2120**	**Chatham Rise**	**PAC**	**-45.52**	**174.93**	**1210**	**1000**	**Planktic Mg/Ca**	Annual
99	MD88-770	South Indian Ocean	IND	-46.01	96.47	3290	770	% N. pachyderma (s)	Summer
100	MD88-770	South Indian Ocean	IND	-46.01	96.47	3290	700	Diatom Transfer Function DTF 166/34/4	Annual
101	**MD02-2488**	**South Indian Ocean**	**IND**	**-46.45**	**88.02**	**3420**	**650**	**% N. pachyderma (s)**	Summer
102	Y9	South Pacific - Bounty Plateau	PAC	-48.24	177.34	1267	2400	Foraminiferal Transfer Function	Annual
103	MD97-2108	Tasman Sea - South Tasman Rise	PAC	-48.50	149.11	2150	3000	Foraminiferal Transfer Function	Annual
104	MD97-2109	South Pacific - Campbell Plateau	PAC	-50.63	169.38	560	3000	Foraminiferal Transfer Function	Annual

Table S2.
Additional metadata for the cores compiled for this study. Yellow highlights indicate sites where a mid-Holocene value from Hessler et al. (2014) (*55*) was used due to a missing core top or where there was a missing core top value and was supplemented by HadlSST1.1 1870-1889 mean value. Bold represents basin reference cores.

#	CORE	PROXY REFERENCE	ISOTOPE REFERENCE	1870-1889 (°C)	1995-2014 (°C)	CT (°C)	CT Proxy
1	M23323-1	Bauch et al. (2011)(*61*)	Bauch and Kandiano (2007)(*62*)	7.47	8.37	7.4	SIMMAX
2	M23323-1	Bauch et al. (2011)(*61*)	Bauch and Kandiano (2007)(*62*)	7.47	8.37	10.97	UK'37
3	V28-14	CLIMAP Project Members (1984) (*5*)	CLIMAP Project Members (1984) (*5*)	6.60	7.00	10.45	Forams
4	EW9302-JPC8	Cortijo et al. (1999) (*63*)	Oppo et al. (1997)(*64*)	9.38	9.45	8.5	Mg/Ca
5	ODP 980	Govin et al. (2012) (*9*)	Oppo et al. (2006)(*65*)	11.92	12.21	11.6	Forams
6	NA87-25	Cortijo et al. (1999) (*63*)	Oppo et al. (1997) (*64*)	11.92	12.21	11.6	Forams
7	V27-20	CLIMAP Project Members (1984) (*5*)	CLIMAP Project Members (1984) (*5*)	7.15	7.61	7.7	Forams
8	GIK/M23414-9	Bauch and Kandiano (2007) (*62*)	Bauch and Kandiano (2007) (*62*)	12.07	12.32	6.55	Forams
9	NEAP18k	Cortijo et al. (1999) (*63*)	Cortijo et al. (1999) (*63*)	10.90	10.95	10.6	Forams
10	V23-82	CLIMAP Project Members (1984) (*5*)	Ruddiman and McIntyre (1979)(*66*)	12.25	12.41	11.65	Forams
11	K708-1	CLIMAP Project Members (1984) (*5*)	Ruddiman and McIntyre (1979) (*66*)	13.39	13.68	14	Forams
12	MD04-2845	Sanchez-Goni et al. (2012)(*67*)	Sanchez-Goni et al. (2012) (*67*)	15.04	16.08	15.5	Forams
13	V29-179	CLIMAP Project Members (1984) (*5*)	Streeter and Shackleton (1979)(*68*)	16.15	16.60	15.05	Forams
14	Y7211-1	CLIMAP Project Members (1984) (*5*)	CLIMAP Project Members (1984) (*5*)	12.26	12.56	10.2	UK37
15	SU92-03	Salgueiro et al. (2010)(*69*)	Salgueiro et al. (2010) (*69*)	15.50	16.28	17.9	SIMMAX
16	D117	CLIMAP Project Members (1984) (*5*)	CLIMAP Project Members (1984) (*5*)	15.77	16.80	8.1	Dinocyst
17	CH69-K09	Govin et al. (2012) (*9*)	Cortijo et al. (1999) (*63*)	16.70	18.00	12.6	Forams
18	V30-97	CLIMAP Project Members (1984) (*5*)	CLIMAP Project Members (1984) (*5*)	18.34	18.77	18.05	Forams
19	ODP 1020	Herbert et al. (2001)(*70*)	Herbert et al. (2001) (*70*)	12.73	12.95	11.15	UK'37
20	MD95-2040	Pailler and Bard (2002)(*71*)	de Abreu et al. (2003)(*72*)	16.29	17.07	17.3	UK'37
21	MD95-2040	de Abreu et al. (2003)(*72*)	de Abreu et al. (2003)(*72*)	16.29	17.07	18.3	Forams
22	SU90-03	Cortijo et al. (1999) (*63*)	Chapman and Shackleton (1998)(*73*)	18.23	18.66	18.3	UK'37
23	**MD01-2444**	**Martrat et al. (2007)**(*74*) **Hodell et al. (2013)**(*39*)	**Skinner and Shackleton (2006)**(*75*) **Hodell et al. (2013)** (*39*)	**17.56**	**18.48**	**17.6**	**UK'37**
24	MD01-2444	Skinner and Shackleton (2006) (*75*)	Skinner and Shackleton (2006) (*75*)	17.56	18.48	17.6	UK'37
25	ODP 1018	Lyle et al. (2010) (*76*)	Andreasen et al. (2000) (*77*)	13.57	13.91	13.8	UK'37
26	MD01-2421	Oba et al. (2006)(*78*)	Oba et al. (2006) (*78*)	19.28	20.74	18.7	UK'37
27	ODP 893	Herbert et al. (2001) (*70*)	Kennett (1995)(*79*)	15.34	16.03	14.8	UK'37
28	MD95-2036	Cortijo et al. (1999) (*63*)	Cortijo et al. (1999) (*63*)	22.15	22.78	27.2	Forams
29	ODP 1014A	Yamamoto et al. (2007) (*80*)	Hendy and Kennett (2000)(*81*)	16.06	16.86	15.8	UK'37
30	ODP 1012	Herbert et al. (2001) (*70*)	Andreasen et al. (2000) (*77*)	16.52	17.38	16.6	UK'37
31	KNR140-37JPC	Cortijo et al. (1999) (*63*)	Cortijo et al. (1999) (*63*)	24.46	24.40	27.2	Forams
32	MD02-2575	Ziegler et al. (2008)(*82*)	Ziegler et al. (2008) (*82*)	25.04	25.16	25.9	Mg/Ca
33	GIK15637-1	Kiefer (1998)(*83*)	Zahn (1986)(*84*)	21.43	22.15	21.45	Forams
34	M12392-1	CLIMAP Project Members (1984) (*5*)	CLIMAP Project Members (1984) (*5*)	20.50	21.01	19.7	Forams
35	LAPAZ21P	Herbert et al. (2001) (*70*)	Herbert et al. (2001) (*70*)	24.78	25.59	25	UK'37
36	TR126-29	CLIMAP Project Members (1984) (*5*)	CLIMAP Project Members (1984) (*5*)	26.36	26.81	26	Forams
37	TR126-23	CLIMAP Project Members (1984) (*5*)	CLIMAP Project Members (1984) (*5*)	26.04	26.60	25.95	Forams
38	ODP 1145	Oppo and Sun (2005)(*85*)	Oppo and Sun (2005) (*85*)	26.46	27.12	27.8	Mg/Ca
39	ODP 1146	Clemens et al. (2008)(*86*)	Clemens et al. (2008) (*86*)	26.57	27.19	25.9	UK'37
40	M35027-1	Hüls (2000)(*87*)	Hüls (2000) (*87*)	27.45	27.94	26.9	Forams
41	V34-88	CLIMAP Project Members (1984) (*5*)	CLIMAP Project Members (1984) (*5*)	26.16	26.81	24.9	Forams
42	V22-196	CLIMAP Project Members (1984) (*5*)	CLIMAP Project Members (1984) (*5*)	24.71	25.62	21.7	Forams

43	V28-127	CLIMAP Project Members (1984) (*5*)	Oppo et al. (1990)(*88*)	27.67	28.33	26.4	Forams
44	RC12-339	CLIMAP Project Members (1984) (*5*)	CLIMAP Project Members (1984) (*5*)	28.22	28.76	27.7	Forams
45	MD97-2151	Zhao et al. (2006)(*89*)	Zhao et al. (2006) (*89*)	27.67	28.28	27.5	UK'37
46	GIK17961-2	Pelejero et al. (1999)(*90*)	Wang et al. (1999) (*91*)	27.89	28.53	27.7	UK'37
47	MD03-2707	Weldleab et al. (2007)(*92*)	Weldleab et al. (2007) (*92*)	27.35	27.96	26.2	Mg/Ca
48	V25-59	CLIMAP Project Members (1984) (*5*)	CLIMAP Project Members (1984) (*5*)	26.78	27.56	26.57	Forams
49	V28-238	CLIMAP Project Members (1984) (*5*)	CLIMAP Project Members (1984) (*5*)	28.96	29.43	30.25	Forams
50	W8402a	Jasper et al. (1994)(*93*)	Jasper et al. (1994) (*93*)	26.04	26.05	26.5	Forams
51	TR163-22	Lea et al. (2006)(*94*)	Lea et al. (2006) (*94*)	24.43	24.54	24.2	Mg/Ca
52	V22-182	CLIMAP Project Members (1984) (*5*)	CLIMAP Project Members (1984) (*5*)	25.65	26.39	25.05	Forams
53	V22-182	CLIMAP Project Members (1984) (*5*)	CLIMAP Project Members (1984) (*5*)	25.65	26.39	23.85	Coccoliths
54	ODP 662	Herbert et al. (2010)(*95*)	Herbert et al. (2010) (*95*)	25.44	26.14	25.7	UK'37
55	GeoB 1105	Schneider et al. (1996)(*96*)	Bickert and Wefer (1996)(*97*)	25.28	25.95	25.6	UK'37
56	GeoB 1105	Wefer et al. (1999)(*98*)	Bickert and Wefer (1996) (*97*)	25.28	25.95	24.8	Forams
57	GeoB 1105	Nürnberg et al. (2000)(*99*)	Bickert and Wefer (1996) (*97*)	25.28	25.95	24.2	Mg/Ca
58	RC13-205	CLIMAP Project Members (1984) (*5*)	CLIMAP Project Members (1984) (*5*)	25.96	26.68	23.4	Radiolaria
59	RC13-205	CLIMAP Project Members (1984) (*5*)	CLIMAP Project Members (1984) (*5*)	25.96	26.68	22.7	Forams
60	ODP 846	Lawrence et al. (2006)(*58*)	Mix et al. (1995) (*100*)	23.27	23.77	23	UK'37
61	V19-29	Pisias and Mix (1997)(*101*)	Pisias and Mix (1997) (*101*)	22.51	22.56	22.65	Radiolaria
62	GeoB1112	Nürnberg et al. (2000) (*99*)	Bickert and Wefer (1996) (*97*)	25.33	26.10	26.4	Mg/Ca
63	GeoB1112	Wefer et al. (1999) (*98*)	Bickert and Wefer (1996) (*97*)	25.33	26.10	25.8	Forams
64	GeoB10038-4	Mohtadi et al. (2010) (*102*)	Mohtadi et al. (2010) (*102*)	28.25	28.60	24.8	Mg/Ca
65	GeoB10038-4	Mohtadi et al. (2010) (*102*)	Mohtadi et al. (2010) (*102*)	28.25	28.60	27.6	UK'37
66	V22-38	CLIMAP Project Members (1984) (*5*)	CLIMAP Project Members (1984) (*5*)	26.83	27.51	25.4	Forams
67	V22-38	CLIMAP Project Members (1984) (*5*)	CLIMAP Project Members (1984) (*5*)	26.83	27.51	23.6	Coccoliths
68	V22-174	CLIMAP Project Members (1984) (*5*)	CLIMAP Project Members (1984) (*5*)	24.81	25.52	25.45	Forams
69	V22-174	CLIMAP Project Members (1984) (*5*)	CLIMAP Project Members (1984) (*5*)	24.81	25.52	24.85	Coccoliths
70	MD01-2378	Xu et al. (2006) (*103*)	Xu et al. (2006) (*103*)	28.30	28.65	27.7	Mg/Ca
71	Y71-6-12	CLIMAP Project Members (1984) (*5*)	CLIMAP Project Members (1984) (*5*)	19.64	20.01	22.95	Radiolaria
72	V28-345	CLIMAP Project Members (1984) (*5*)	CLIMAP Project Members (1984) (*5*)	27.23	27.75	27	Forams
73	RC13-228	CLIMAP Project Members (1984) (*5*)	CLIMAP Project Members (1984) (*5*)	18.67	19.35	17.5	Coccoliths
74	RC13-228	CLIMAP Project Members (1984) (*5*)	CLIMAP Project Members (1984) (*5*)	18.67	19.35	17.5	Forams
75	RC13-228	CLIMAP Project Members (1984) (*5*)	CLIMAP Project Members (1984) (*5*)	18.67	19.35	18.35	Radiolaria
76	MD06-3018	Russon et al. (2011) (*104*)	Russon et al. (2011) (*104*)	24.29	24.82	25.6	Mg/Ca
77	GeoB 1711-4	Kirst et al. (1999) (*105*)	Little et al. (1997) (*106*)	18.08	18.76	19.1	UK'37
78	GeoB 1710-3	Kirst et al. (1999) (*105*)	Bickert and Wefer (1996) (*97*)	18.08	18.76	18.6	UK'37
79	RC13-229	CLIMAP Project Members (1984) (*5*)	Oppo et al. (1990) (*88*)	18.58	19.15	16.9	Radiolaria
80	RC13-229	CLIMAP Project Members (1984) (*5*)	Oppo et al. (1990) (*88*)	18.58	19.15	19.15	Forams
81	RC11-86	CLIMAP Project Members (1984) (*5*)	CLIMAP Project Members (1984) (*5*)	17.56	18.37	19.3	Forams
82	RC11-86	CLIMAP Project Members (1984) (*5*)	CLIMAP Project Members (1984) (*5*)	17.58	18.40	19.05	Coccoliths
83	MD96-2080	Martinez-Mendez et al. (2010) (*107*)	Martinez-Mendez et al. (2010) (*107*)	16.05	16.45	16.4	Mg/Ca
84	RC12-294	CLIMAP Project Members (1984) (*5*)	CLIMAP Project Members (1984) (*5*)	15.12	16.10	14.75	Coccoliths
85	RC12-294	CLIMAP Project Members (1984) (*5*)	CLIMAP Project Members (1984) (*5*)	16.05	16.45	14.75	Forams
86	MD97-2121	Pahnke and Sachs (2006) (*56*)	Carter and Manighetti (2006) (*108*)	13.38	13.93	16.9	UK'37
87	RC15-61	CLIMAP Project Members (1984) (*5*)	CLIMAP Project Members (1984) (*5*)	11.66	13.06	14.9	UK'37
88	**ODP 1089**	**Pahnke and Sachs (2006)** (*56*)	**Hodell et al. (2003)** (*59*)	**11.66**	**13.06**	**18.1**	**UK'37**
89	ODP 1089	Cortese et al. (2007) (*45*)	Hodell et al. (2003) (*59*)	14.39	14.89	15.2	Radiolaria
90	ODP 1123	Cortese et al. (2013) (*109*)	Hall et al. (2001) (*110*)	11.70	12.24	15.7	Forams
91	MD94-101	Govin et al. (2009) (*40*)	Salvignac (1998) (*111*)	9.76	10.52	12.2	Forams

92	PS2489-2	Becquey and Gersonde (2002) (*112*)	Becquey and Gersonde (2002) (*112*)	9.20	10.35	9.8	Forams
93	MD84-527	Pichon et al. (1992) (*113*)	Pichon et al. (1992) (*113*)	10.62	11.20	6.8	Diatoms
94	MD94-102	Govin et al. (2009) (*40*)	Salvignac (1998) (*111*)	7.45	8.59	12.1	Forams
95	MD73-025	CLIMAP Project Members (1984) (*5*)	CLIMAP Project Members (1984) (*5*)	11.87	12.67	4	Radiolaria
96	MD97-2106	Cortese et al. (2013) (*109*)	Moy et al. (2006) (*114*)	10.86	11.18	10.86	HadISST1.1 1870-1889
97	DSDP 594	Cortese et al. (2013) (*109*)	Nelson et al. (1993) (*115*)	10.86	11.18	14.91	Forams
98	**MD97-2120**	**Pahnke et al. (2003)** (*44*)	**Pahnke and Zahn (2005)** (*60*)	**10.86**	**11.18**	**16.6**	**Mg/Ca**
99	MD88-770	Govin et al. (2009) (*40*)	Labeyrie et al. (1996) (*116*)	8.20	9.11	7.6	Forams
100	MD88-770	Sowers et al. (1993) (*42*)	Labeyrie et al. (1996) (*116*)	8.20	9.11	9.7	Diatoms
101	**MD02-2488**	**Govin et al. (2009)** (*40*)	**Govin et al. (2009)** (*40*)	**8.88**	**9.53**	**10.4**	**Forams**
102	Y9	Cortese et al. (2013) (*109*)	Neil et al. (2004) (*117*)	9.61	9.96	9.6	HadISST1.1 1870-1889
103	MD97-2108	Cortese et al. (2013) (*109*)	Sturm et al. (2004) (*118*)	9.50	9.89	9.5	HadISST1.1 1870-1889
104	MD97-2109	Cortese et al. (2013) (*109*)	Sturm et al. (2004) (*118*)	8.9	9.1	8.9	HadISST1.1 HadISST1.1

References and Notes

1. Past Interglacials Working Group of PAGES, Interglacials of the last 800,000 years. *Rev. Geophys.* **54**, 162–219 (2016). doi:10.1002/2015RG000482

2. A. Dutton, A. E. Carlson, A. J. Long, G. A. Milne, P. U. Clark, R. DeConto, B. P. Horton, S. Rahmstorf, M. E. Raymo, Sea-level rise due to polar ice-sheet mass loss during past warm periods. *Science* **349**, aaa4019 (2015). doi:10.1126/science.aaa4019 Medline

3. D. J. Lunt, A. Abe-Ouchi, P. Bakker, A. Berger, P. Braconnot, S. Charbit, N. Fischer, N. Herold, J. H. Jungclaus, V. C. Khon, U. Krebs-Kanzow, P. M. Langebroek, G. Lohmann, K. H. Nisancioglu, B. L. Otto-Bliesner, W. Park, M. Pfeiffer, S. J. Phipps, M. Prange, R. Rachmayani, H. Renssen, N. Rosenbloom, B. Schneider, E. J. Stone, K. Takahashi, W. Wei, Q. Yin, Z. S. Zhang, A multi-model assessment of last interglacial temperatures. *Clim. Past* **9**, 699–717 (2013). doi:10.5194/cp-9-699-2013

4. B. L. Otto-Bliesner, N. Rosenbloom, E. J. Stone, N. P. McKay, D. J. Lunt, E. C. Brady, J. T. Overpeck, How warm was the last interglacial? New model-data comparisons. *Phil. Trans. R. Soc. A.* **371**, 20130097–20130097 (2013). doi:10.1098/rsta.2013.0097 Medline

5. CLIMAP Project Members, W. F. Ruddiman, R. M. L. Cline, J. D. Hays, W. L. Prell, W. F. Ruddiman, T. C. Moore, N. G. Kipp, B. E. Molfino, G. H. Denton, T. J. Hughes, W. L. Balsam, C. A. Brunner, J.-C. Duplessy, J. L. Fastook, J. Ismbrie, L. D. Keigwin, T. B. Kellogg, A. McIntyre, R. K. Matthews, A. C. Mix, J. J. Morley, N. J. Shackleton, S. S. Streeter, P. R. Thompson, The last interglacial ocean. *Quat. Res.* **21**, 123–224 (1984). doi:10.1016/0033-5894(84)90098-X

6. P. U. Clark, P. Huybers, Global change: Interglacial and future sea level. *Nature* **462**, 856–857 (2009). doi:10.1038/462856a Medline

7. C. Turney, R. T. Jones, Does the Agulhas Current amplify global temperatures during super-interglacials? *J. Quaternary Sci.* **25**, 839–843 (2010). doi:10.1002/jqs.1423

8. N. P. McKay, J. T. Overpeck, B. L. Otto-Bliesner, The role of ocean thermal expansion in Last Interglacial sea level rise. *Geophys. Res. Lett.* **38**, (2011). doi:10.1029/2011GL048280

9. A. Govin, P. Braconnot, E. Capron, E. Cortijo, J.-C. Duplessy, E. Jansen, L. Labeyrie, A. Landais, O. Marti, E. Michel, E. Mosquet, B. Risebrobakken, D. Swingedouw, C. Waelbroeck, Persistent influence of ice sheet melting on high northern latitude climate during the early Last Interglacial. *Clim. Past* **8**, 483–507 (2012). doi:10.5194/cp-8-483-2012

10. E. Capron, A. Govin, E. J. Stone, V. Masson-Delmotte, S. Mulitza, B. Otto-Bliesner, T. L. Rasmussen, L. C. Sime, C. Waelbroeck, E. W. Wolff, Temporal and spatial structure of multi-millennial temperature changes at high latitudes during the Last Interglacial. *Quat. Sci. Rev.* **103**, 116–133 (2014). doi:10.1016/j.quascirev.2014.08.018

11. S. Barker, G. Knorr, R. L. Edwards, F. Parrenin, A. E. Putnam, L. C. Skinner, E. Wolff, M. Ziegler, 800,000 years of abrupt climate variability. *Science* **334**, 347–351 (2011). doi:10.1126/science.1203580 Medline

12. Materials and methods are available as supplementary materials.

13. L. Skinner, N. Shackleton, An Atlantic lead over Pacific deep-water change across Termination I: Implications for the application of the marine isotope stage stratigraphy. *Quat. Sci. Rev.* **24**, 571–580 (2005). doi:10.1016/j.quascirev.2004.11.008

14. L. E. Lisiecki, M. E. Raymo, Diachronous benthic $\delta^{18}O$ responses during late Pleistocene terminations. *Paleoceanography* **24**, (2009). doi:10.1029/2009PA001732

15. J. V. Stern, L. E. Lisiecki, Termination 1 timing in radiocarbon-dated regional benthic $\delta^{18}O$ stacks. *Paleoceanography* **29**, 1127–1142 (2014). doi:10.1002/2014PA002700

16. J. Haslett, A. Parnell, A simple monotone process with application to radiocarbon-dated depth chronologies. *J.R. Stat. Soc.* **57**, 399–418 (2008). doi:10.1111/j.1467-9876.2008.00623.x

17. N. A. Rayner, D. E. Parker, E. B. Horton, C. K. Folland, L. V. Alexander, D. P. Rowell, E. C. Kent, A. Kaplan, Global analyses of sea surface temperature, sea ice, and night marine air temperature since the late nineteenth century. *J. Geophys. Res.* **108** (D14), 4407 (2003). doi:10.1029/2002JD002670

18. N. J. Abram, H. V. McGregor, J. E. Tierney, M. N. Evans, N. P. McKay, D. S. Kaufman, PAGES 2k Consortium, Early onset of industrial-era warming across the oceans and continents. *Nature* **536**, 411–418 (2016). doi:10.1038/nature19082 Medline

19. A. Filippova, M. Kienast, M. Frank, R. R. Schneider, Alkenone paleothermometry in the North Atlantic: A review and synthesis of surface sediment data and calibrations. *Geochem. Geophys. Geosyst.* **17**, 1370–1382 (2016). doi:10.1002/2015GC006106

20. P. U. Clark, J. D. Shakun, S. A. Marcott, A. C. Mix, M. Eby, S. Kulp, A. Levermann, G. A. Milne, P. L. Pfister, B. D. Santer, D. P. Schrag, S. Solomon, T. F. Stocker, B. H. Strauss, A. J. Weaver, R. Winkelmann, D. Archer, E. Bard, A. Goldner, K. Lambeck, R. T. Pierrehumbert, G.-K. Plattner, Consequences of twenty-first century policy for multi-millennial climate and sea-level change. *Nat. Clim. Chang.* **6**, 360–369 (2016). doi:10.1038/nclimate2923

21. V. Masson-Delmotte *et al*., in *Climate Change 2013*: *The Physical Science Basis*. *Contribution of Working Group I to the Fifth Assessment Report of the Intergovernmental Panel on Climate Change*, T. F. Stocker *et al*., Eds. (Cambridge Univ. Press, 2013)

22. R. A. Pedersen, P. L. Langen, B. M. Vinther, The last interglacial climate: Comparing direct and indirect impacts of insolation changes. *Clim. Dyn.* 10.1007/s00382-016-3274-5 (2016).

23. M. J. Kelly, R. L. Edwards, H. Cheng, D. Yuan, Y. Cai, M. Zhang, Y. Lin, Z. An, High resolution characterization of the Asian Monsoon between 146,000 and 99,000 years B.P. from Dongge Cave, China and global correlation of events surrounding Termination II. *Palaeogeogr. Palaeoclimatol. Palaeoecol.* **236**, 20–38 (2006). doi:10.1016/j.palaeo.2005.11.042

24. V. Masson-Delmotte, B. Stenni, K. Pol, P. Braconnot, O. Cattani, S. Falourd, M. Kageyama, J. Jouzel, A. Landais, B. Minster, J. M. Barnola, J. Chappellaz, G. Krinner, S. Johnsen, R. Röthlisberger, J. Hansen, U. Mikolajewicz, B. Otto-Bliesner, EPICA Dome C record of glacial and interglacial intensities. *Quat. Sci. Rev.* **29**, 113–128 (2010). doi:10.1016/j.quascirev.2009.09.030

25. E. J. Stone, E. Capron, D. J. Lunt, A. J. Payne, J. S. Singarayer, P. J. Valdes, E. W. Wolff, Impact of meltwater on high-latitude early Last Interglacial climate. *Clim. Past* **12**, 1919–1932 (2016). doi:10.5194/cp-12-1919-2016

26. E. Böhm, J. Lippold, M. Gutjahr, M. Frank, P. Blaser, B. Antz, J. Fohlmeister, N. Frank, M. B. Andersen, M. Deininger, Strong and deep Atlantic meridional overturning circulation during the last glacial cycle. *Nature* **517**, 73–76 (2015). Medline

27. E. W. Wolff, C. Barbante, S. Becagli, M. Bigler, C. F. Boutron, E. Castellano, M. de Angelis, U. Federer, H. Fischer, F. Fundel, M. Hansson, M. Hutterli, U. Jonsell, T. Karlin, P. Kaufmann, F. Lambert, G. C. Littot, R. Mulvaney, R. Röthlisberger, U. Ruth, M. Severi, M. L. Siggaard-Andersen, L. C. Sime, J. P. Steffensen, T. F. Stocker, R. Traversi, B. Twarloh, R. Udisti, D. Wagenbach, A. Wegner, Changes in environment over the last 800,000 years from chemical analysis of the EPICA Dome C ice core. *Quat. Sci. Rev.* **29**, 285–295 (2010). doi:10.1016/j.quascirev.2009.06.013

28. M. D. Holloway, L. C. Sime, J. S. Singarayer, J. C. Tindall, P. Bunch, P. J. Valdes, Antarctic last interglacial isotope peak in response to sea ice retreat not ice-sheet collapse. *Nat. Commun.* **7**, 12293 (2016). doi:10.1038/ncomms12293 Medline

29. A. Timmermann, T. Friedrich, O. E. Timm, M. O. Chikamoto, A. Abe-Ouchi, A. Ganopolski, Modeling Obliquity and CO_2 Effects on Southern Hemisphere Climate during the Past 408 ka. *J. Clim.* **27**, 1863–1875 (2014). doi:10.1175/JCLI-D-13-00311.1

30. R. Schneider, J. Schmitt, P. Köhler, F. Joos, H. Fischer, A reconstruction of atmospheric carbon dioxide and its stable carbon isotopic composition from the penultimate glacial maximum to the last glacial inception. *Clim. Past* **9**, 2507–2523 (2013). doi:10.5194/cp-9-2507-2013

31. S. Eggleston, J. Schmitt, B. Bereiter, R. Schneider, H. Fischer, Evolution of the stable carbon isotope composition of atmospheric CO_2 over the last glacial cycle. *Paleoceanography* **31**, 434–452 (2016). doi:10.1002/2015PA002874

32. J. D. Shakun, P. U. Clark, F. He, S. A. Marcott, A. C. Mix, Z. Liu, B. Otto-Bliesner, A. Schmittner, E. Bard, Global warming preceded by increasing carbon dioxide concentrations during the last deglaciation. *Nature* **484**, 49–54 (2012). doi:10.1038/nature10915 Medline

33. S. A. Marcott, J. D. Shakun, P. U. Clark, A. C. Mix, A reconstruction of regional and global temperature for the past 11,300 years. *Science* **339**, 1198–1201 (2013). doi:10.1126/science.1228026 Medline

34. F. He, thesis, University of Wisconsin-Madison, Madison, WI (2011).

35. P. D. Jones, T. J. Osborn, K. R. Briffa, Estimating sampling errors in large-scale temperature averages. *J. Clim.* **10**, 2548–2568 (1997). doi:10.1175/1520-0442(1997)010<2548:ESEILS>2.0.CO;2

36. N. G. Pisias, D. G. Martinson, T. C. Moore Jr., N. J. Shackleton, W. Prell, J. Hays, G. Boden, High resolution stratigraphic correlation of benthic oxygen isotopic records spanning the last 300,000 years. *Mar. Geol.* **56**, 119–136 (1984). doi:10.1016/0025-3227(84)90009-4

37. D. G. Martinson, N. G. Pisias, J. D. Hays, J. Imbrie, T. C. Moore Jr., N. J. Shackleton, Age

dating and the orbital theory of the ice ages: Development of a high-resolution 0 to 300,000-year chronostratigraphy. *Quat. Res.* **27**, 1–29 (1987). doi:10.1016/0033-5894(87)90046-9

38. L. E. Lisiecki, M. E. Raymo, A Pliocene-Pleistocene stack of 57 globally distributed benthic $\delta^{18}O$ records. *Paleoceanography* **20**, (2005). 10.1029/2004PA001071

39. D. Hodell, S. Crowhurst, L. Skinner, P. C. Tzedakis, V. Margari, J. E. T. Channell, G. Kamenov, S. Maclachlan, G. Rothwell, Response of Iberian Margin sediments to orbital and suborbital forcing over the past 420 ka. *Paleoceanography* **28**, 185–199 (2013). doi:10.1002/palo.20017

40. A. Govin, E. Michel, L. Labeyrie, C. Waelbroeck, F. Dewilde, E. Jansen, Evidence for northward expansion of Antarctic Bottom Water mass in the Southern Ocean during the last glacial inception. *Paleoceanography* **24**, PA1202 (2009). doi:10.1029/2008PA001603

41. A. Govin, E. Capron, P. C. Tzedakis, S. Verheyden, B. Ghaleb, C. Hillaire-Marcel, G. St-Onge, J. S. Stoner, F. Bassinot, L. Bazin, T. Blunier, N. Combourieu-Nebout, A. El Ouahabi, D. Genty, R. Gersonde, P. Jimenez-Amat, A. Landais, B. Martrat, V. Masson-Delmotte, F. Parrenin, M.-S. Seidenkrantz, D. Veres, C. Waelbroeck, R. Zahn, Sequence of events from the onset to the demise of the Last Interglacial: Evaluating strengths and limitations of chronologies used in climatic archives. *Quat. Sci. Rev.* **129**, 1–36 (2015). doi:10.1016/j.quascirev.2015.09.018

42. T. Sowers, M. Bender, L. Labeyrie, D. Martinson, J. Jouzel, D. Raynaud, J. J. Pichon, Y. S. Korotkevich, A 135,000-year Vostok-Specmap Common temporal framework. *Paleoceanography* **8**, 737–766 (1993). doi:10.1029/93PA02328

43. C. Waelbroeck, J. Jouzel, L. Labeyrie, C. Lorius, M. Labracherie, M. Stiévenard, N. I. Barkov, A comparison of the Vostok ice deuterium record and series from Southern Ocean core MD 88-770 over the last two glacial-interglacial cycles. *Clim. Dyn.* **12**, 113–123 (1995). doi:10.1007/BF00223724

44. K. Pahnke, R. Zahn, H. Elderfield, M. Schulz, 340,000-year centennial-scale marine record of Southern Hemisphere climatic oscillation. *Science* **301**, 948–952 (2003). doi:10.1126/science.1084451 Medline

45. G. Cortese, A. Abelmann, R. Gersonde, The last five glacial-interglacial transitions: A high-resolution 450,000-year record from the subantarctic Atlantic. *Paleoceanography* **22**, n/a (2007). doi:10.1029/2007PA001457

46. T. F. Stocker, S. J. Johnsen, A minimum thermodynamic model for the bipolar seesaw. *Paleoceanography* **18**, 1087 (2003). doi:10.1029/2003PA000920

47. H. Cheng, R. L. Edwards, W. S. Broecker, G. H. Denton, X. Kong, Y. Wang, R. Zhang, X. Wang, Ice age terminations. *Science* **326**, 248–252 (2009). doi:10.1126/science.1177840 Medline

48. F. Parrenin, J. M. Barnola, J. Beer, T. Blunier, E. Castellano, J. Chappellaz, G. Dreyfus, H. Fischer, S. Fujita, J. Jouzel, K. Kawamura, B. Lemieux-Dudon, L. Loulergue, V. Masson-Delmotte, B. Narcisi, J.-R. Petit, G. Raisbeck, D. Raynaud, U. Ruth, J. Schwander, M. Severi, R. Spahni, J. P. Steffensen, A. Svensson, R. Udisti, C.

Waelbroeck, E. Wolff, The EDC3 chronology for the EPICA Dome C ice core. *Clim. Past* **3**, 485–497 (2007). doi:10.5194/cp-3-485-2007

49. Z. Liu, B. L. Otto-Bliesner, F. He, E. C. Brady, R. Tomas, P. U. Clark, A. E. Carlson, J. Lynch-Stieglitz, W. Curry, E. Brook, D. Erickson, R. Jacob, J. Kutzbach, J. Cheng, Transient simulation of last deglaciation with a new mechanism for Bolling-Allerod warming. *Science* **325**, 310–314 (2009). doi:10.1126/science.1171041 Medline

50. M. F. Loutre, T. Fichefet, H. Goosse, P. Huybrechts, H. Goelzer, E. Capron, Factors controlling the last interglacial climate as simulated by LOVECLIM1.3. *Clim. Past* **10**, 1541–1565 (2014). doi:10.5194/cp-10-1541-2014

51. D. Paillard, L. Labeyrie, P. Yiou, Macintosh Program performs time-series analysis. *Eos (Wash. D.C.)* **77**, 379–379 (1996). doi:10.1029/96EO00259

52. P. Anand, H. Elderfield, M. H. Conte, Calibration of Mg/Ca thermometry in planktonic foraminifera from a sediment trap time series. *Paleoceanography* **18**, n/a (2003). doi:10.1029/2002PA000846

53. P. J. Müller, G. Kirst, G. Ruhland, I. von Storch, A. Rosell-Melé, Calibration of the alkenone paleotemperature index $U^{K'}_{37}$ based on core-tops from the eastern South Atlantic and the global ocean (60°N-60°S). *Geochim. Cosmochim. Acta* **62**, 1757–1772 (1998). doi:10.1016/S0016-7037(98)00097-0

54. M. Kucera, A. Rosell-Melé, R. Schneider, C. Waelbroeck, M. Weinelt, Multiproxy approach for the reconstruction of the glacial ocean surface (MARGO). *Quat. Sci. Rev.* **24**, 813–819 (2005). doi:10.1016/j.quascirev.2004.07.017

55. I. Hessler, S. P. Harrison, M. Kucera, C. Waelbroeck, M.-T. Chen, C. Anderson, A. de Vernal, B. Fréchette, A. Cloke-Hayes, G. Leduc, L. Londeix, Implication of methodological uncertainties for mid-Holocene sea surface temperature reconstructions. *Clim. Past* **10**, 2237–2252 (2014). doi:10.5194/cp-10-2237-2014

56. K. Pahnke, J. P. Sachs, Sea surface temperatures of southern midlatitudes 0-160 kyr B.P. *Paleoceanography* **21**, n/a (2006). doi:10.1029/2005PA001191

57. K. T. Lawrence, Z. Liu, T. D. Herbert, Evolution of the eastern tropical Pacific through Plio-Pleistocene glaciation. *Science* **312**, 79–83 (2006). doi:10.1126/science.1120395 Medline

58. D. A. Hodell, C. D. Charles, J. H. Curtis, P. G. Mortyn, U. S. Ninnemann, K. A. Venz, in *Proc. ODP*, *Sci. Results*, R. Gersonde, D. A. Hodell, P. Blum, Eds. (Ocean Drilling Program, College Station, TX, 2003), vol. 177, pp. 1–26.

59. K. Pahnke, R. Zahn, Southern Hemisphere water mass conversion linked with North Atlantic climate variability. *Science* **307**, 1741–1746 (2005). doi:10.1126/science.1102163 Medline

60. H. A. Bauch, E. S. Kandiano, J. Helmke, N. Andersen, A. Rosell-Mele, H. Erlenkeuser, Climatic bisection of the last interglacial warm period in the Polar North Atlantic. *Quat. Sci. Rev.* **30**, 1813–1818 (2011). doi:10.1016/j.quascirev.2011.05.012

61. H. A. Bauch, E. S. Kandiano, Evidence for early warming and cooling in North Atlantic surface waters during the last interglacial. *Paleoceanography* **22**, n/a (2007). doi:10.1029/2005PA001252

62. E. Cortijo, S. Lehman, L. Keigwin, M. Chapman, D. Paillard, L. Labeyrie, Changes in meridional temperature and salinity gradients in the North Atlantic Ocean (30°–72°N) during the last interglacial period. *Paleoceanography* **14**, 23–33 (1999). doi:10.1029/1998PA900004

63. D. W. Oppo, M. Horowitz, S. J. Lehman, Marine core evidence for reduced deep water production during Termination II followed by a relatively stable substage 5e (Eemian). *Paleoceanography* **12**, 51–63 (1997). doi:10.1029/96PA03133

64. D. W. Oppo, J. F. McManus, J. L. Cullen, Evolution and demise of the Last Interglacial warmth in the subpolar North Atlantic. *Quat. Sci. Rev.* **25**, 3268–3277 (2006). doi:10.1016/j.quascirev.2006.07.006

65. W. F. Ruddiman, A. McIntyre, Warmth of the subpolar North Atlantic Ocean during northern hemisphere ice-sheet growth. *Science* **204**, 173–175 (1979). doi:10.1126/science.204.4389.173 Medline

66. M. F. Sánchez Goñi, P. Bakker, S. Desprat, A. E. Carlson, C. J. Van Meerbeeck, O. Peyron, F. Naughton, W. J. Fletcher, F. Eynaud, L. Rossignol, H. Renssen, European climate optimum and enhanced Greenland melt during the Last Interglacial. *Geology* **40**, 627–630 (2012).

67. S. S. Streeter, N. J. Shackleton, Paleocirculation of the deep North Atlantic: 150,000-year record of benthic foraminifera and oxygen-18. *Science* **203**, 168–171 (1979). doi:10.1126/science.203.4376.168 Medline

68. E. Salgueiro, A. H. L. Voelker, L. de Abreu, F. Abrantes, H. Meggers, G. Wefer, Temperature and productivity changes off the western Iberian margin during the last 150 ky. *Quat. Sci. Rev.* **29**, 680–695 (2010). doi:10.1016/j.quascirev.2009.11.013

69. T. D. Herbert, J. D. Schuffert, D. Andreasen, L. Heusser, M. Lyle, A. Mix, A. C. Ravelo, L. D. Stott, J. C. Herguera, Collapse of the California Current during glacial maxima linked to climate change on land. *Science* **293**, 71–76 (2001). doi:10.1126/science.1059209 Medline

70. D. Pailler, E. Bard, High frequency palaeoceanographic changes during the past 140000 yr recorded by the organic matter in sediments of the Iberian Margin. *Palaeogeogr. Palaeoclimatol. Palaeoecol.* **181**, 431–452 (2002). doi:10.1016/S0031-0182(01)00444-8

71. L. de Abreu, N. J. Shackleton, J. Schonfeld, M. Hall, M. Chapman, Millennial-scale oceanic climate variability off the Western Iberian margin during the last two glacial periods. *Mar. Geol.* **196**, 1–20 (2003). doi:10.1016/S0025-3227(03)00046-X

72. M. R. Chapman, N. J. Shackleton, Millennial-scale fluctuations in North Atlantic heat flux during the last 150,000 years. *Earth Planet. Sci. Lett.* **159**, 57–70 (1998). doi:10.1016/S0012-821X(98)00068-5

73. B. Martrat, J. O. Grimalt, N. J. Shackleton, L. de Abreu, M. A. Hutterli, T. F. Stocker, Four climate cycles of recurring deep and surface water destabilizations on the Iberian margin. *Science* **317**, 502–507 (2007). doi:10.1126/science.1139994 Medline

74. L. C. Skinner, N. J. Shackleton, Deconstructing Terminations I and II: Revisiting the glacioeustatic paradigm based on deep-water temperature estimates. *Quat. Sci. Rev.* **25**,

3312–3321 (2006). doi:10.1016/j.quascirev.2006.07.005

75. M. Lyle, L. Heusser, C. Ravelo, D. Andreasen, A. Olivarez Lyle, N. Diffenbaugh, Pleistocene water cycle and eastern boundary current processes along the California continental margin. *Paleoceanography* **25**, n/a (2010). doi:10.1029/2009PA001836

76. D. H. Andreasen, M. Flower, M. Harvey, S. Chang, A. C. Ravelo, in *Proc. ODP*, *Sci. Results*, M. Lyle, I. Koizumi, C. Richter, T. C. Moore, Jr., Eds. (Ocean Drilling Program, College Station, TX, 2000), vol. 167, pp. 141–144.

77. T. Oba, T. Irino, M. Yamamoto, M. Murayama, A. Takamura, K. Aoki, Paleoceanographic change off central Japan since the last 144,000 years based on high-resolution oxygen and carbon isotope records. *Global Planet. Change* **53**, 5–20 (2006). doi:10.1016/j.gloplacha.2006.05.002

78. J. P. Kennett, in *Proc. ODP, Sci. Results*, J. P. Kennett, J. G. Baldauf, M. E. Lyle, Eds. (Ocean Drilling Program, College Station, TX, 1995), vol. 146, pp. 3–18.

79. M. Yamamoto, M. Yamamuro, Y. Tanaka, The California current system during the last 136,000 years: Response of the North Pacific High to precessional forcing. *Quat. Sci. Rev.* **26**, 405–414 (2007). doi:10.1016/j.quascirev.2006.07.014

80. I. L. Hendy, J. P. Kennett, in *Proc. ODP, Sci. Results*, M. Lyle, I. Koizumi, C. Richter, T. C. Moore, Jr., Eds. (Ocean Drilling Program, College Station, TX, 2000), vol. 167, pp. 129–140.

81. M. Ziegler, D. Nürnberg, C. Karas, R. Tiedemann, L. J. Lourens, Persistent summer expansion of the Atlantic Warm Pool during glacial abrupt cold events. *Nat. Geosci.* **1**, 601–605 (2008). doi:10.1038/ngeo277

82. T. Kiefer, thesis, Geologisch-Paläontologisches Institut der Universität Kiel, Kiel, Germany (1998).

83. R. Zahn, thesis, Kiel University, Kiel, Germany (1986).

84. D. W. Oppo, Y. Sun, Amplitude and timing of sea-surface temperature change in the northern South China Sea: Dynamic link to the East Asian monsoon. *Geology* **33**, 785 (2005). doi:10.1130/G21867.1

85. S. C. Clemens, W. L. Prell, Y. B. Sun, Z. Y. Liu, G. S. Chen, Southern Hemisphere forcing of Pliocene delta(18)O and the evolution of Indo-Asian monsoons. *Paleoceanography* **23**, n/a (2008). doi:10.1029/2008PA001638

86. M. Hüls, thesis, GEOMAR Research Center for Marine Geosciences, Christian Albrechts University in Kiel, Kiel, Germany (2000).

87. D. W. Oppo, R. G. Fairbanks, A. L. Gordon, N. J. Shackleton, Late Pleistocene Southern Ocean $\delta^{13}C$ variability. *Paleoceanography* **5**, 43–54 (1990). doi:10.1029/PA005i001p00043

88. M. Zhao, C.-Y. Huang, C.-C. Wang, G. Wei, A millennial-scale $U^{K'}_{37}$ sea-surface temperature record from the South China Sea (8°N) over the last 150 kyr: Monsoon and sea-level influence. *Palaeogeogr. Palaeoclimatol. Palaeoecol.* **236**, 39–55 (2006). doi:10.1016/j.palaeo.2005.11.033

89. C. Pelejero, J. O. Grimalt, S. Heilig, M. Kienast, L. J. Wang, High-resolution K'_{37} temperature reconstructions in the South China Sea over the past 220 kyr. *Paleoceanography* **14**, 224–231 (1999). doi:10.1029/1998PA900015

90. L. Wang, M. Sarnthein, H. Erlenkeuser, J. Grimalt, P. Grootes, S. Heilig, E. Ivanova, M. Kienast, C. Pelejero, U. Pflaumann, East Asian monsoon climate during the Late Pleistocene: High-resolution sediment records from the South China Sea. *Mar. Geol.* **156**, 245–284 (1999). doi:10.1016/S0025-3227(98)00182-0

91. S. Weldeab, D. W. Lea, R. R. Schneider, N. Andersen, 155,000 years of West African monsoon and ocean thermal evolution. *Science* **316**, 1303–1307 (2007). doi:10.1126/science.1140461 Medline

92. J. P. Jasper, J. M. Hayes, A. C. Mix, F. G. Prahl, Photosynthetic fractionation of ^{13}C and concentrations of dissolved CO_2 in the central equatorial Pacific during the last 255,000 years. *Paleoceanography* **9**, 781–798 (1994). doi:10.1029/94PA02116 Medline

93. D. W. Lea, D. K. Pak, C. L. Belanger, H. J. Spero, M. A. Hall, N. J. Shackleton, Paleoclimate history of Galapagos surface waters over the last 135,000 yr. *Quat. Sci. Rev.* **25**, 1152–1167 (2006). doi:10.1016/j.quascirev.2005.11.010

94. T. D. Herbert, L. C. Peterson, K. T. Lawrence, Z. Liu, Tropical ocean temperatures over the past 3.5 million years. *Science* **328**, 1530–1534 (2010). doi:10.1126/science.1185435 Medline

95. R. R. Schneider *et al*., in *The South Atlantic: Present and Past Circulation* (Springer Berlin Heidelberg, 1996), pp. 527–551.

96. T. Bickert, G. Wefer, in *The South Atlantic: Present and Past Circulation* (Springer Berlin Heidelberg, 1996), pp. 599–620.

97. G. Wefer, W. H. Berger, J. Bijma, G. Fischer, *Clues to Ocean History: A Brief Overview of Proxies* (Springer Berlin Heidelberg, 1999).

98. D. Nürnberg, A. Muller, R. R. Schneider, Paleo-sea surface temperature calculations in the equatorial east Atlantic from Mg/Ca ratios in planktic foraminifera: A comparison to sea surface temperature estimates from $U^{K'}_{37}$, oxygen isotopes, and foraminiferal transfer function. *Paleoceanography* **15**, 124–134 (2000). doi:10.1029/1999PA000370

99. A. C. Mix, J. Le, N. J. Shackleton, in *Proc. ODP, Sci. Results*, N. G. Pisias, L. A. Mayer, T. R. Janecek, A. Palmer-Julson, T. H. van Andel, Eds. (Ocean Drilling Program, College Station, TX, 1995), vol. 138, pp. 839–854.

100. N. Pisias, A. Mix, Spatial and temporal oceanographic variability of the eastern equatorial Pacific during the late Pleistocene: Evidence from Radiolaria microfossils. *Paleoceanography* **12**, 381–393 (1997). doi:10.1029/97PA00583

101. M. Mohtadi, A. Lückge, S. Steinke, J. Groeneveld, D. Hebbeln, N. Westphal, Late Pleistocene surface and thermocline conditions of the eastern tropical Indian Ocean. *Quat. Sci. Rev.* **29**, 887–896 (2010). doi:10.1016/j.quascirev.2009.12.006

102. J. Xu, W. Kuhnt, A. Holbourn, N. Andersen, G. Bartoli, Changes in the vertical profile of the Indonesian Throughflow during Termination II: Evidence from the Timor Sea. *Paleoceanography* **21**, n/a (2006). doi:10.1029/2006PA001278

103. T. Russon, M. Elliot, A. Sadekov, G. Cabioch, T. Corrège, P. De Deckker, The mid-Pleistocene transition in the subtropical southwest Pacific. *Paleoceanography* **26**, PA1211 (2011). doi:10.1029/2010PA002019

104. G. J. Kirst, R. R. Schneider, P. J. Müller, I. von Storch, G. Wefer, Late Quaternary temperature variability in the Benguela Current system derived from alkenones. *Quat. Res.* **52**, 92–103 (1999). doi:10.1006/qres.1999.2040

105. M. G. Little, R. R. Schneider, D. Kroon, B. Price, T. Bickert, G. Wefer, Rapid palaeoceanographic changes in the Benguela Upwelling System for the last 160,000 years as indicated by abundances of planktonic foraminifera. *Palaeogeogr. Palaeoclimatol. Palaeoecol.* **130**, 135–161 (1997). doi:10.1016/S0031-0182(96)00136-8

106. G. Martínez-Méndez, R. Zahn, I. R. Hall, F. J. C. Peeters, L. D. Pena, I. Cacho, C. Negre, Contrasting multiproxy reconstructions of surface ocean hydrography in the Agulhas Corridor and implications for the Agulhas Leakage during the last 345,000 years. *Paleoceanography* **25**, n/a (2010). doi:10.1029/2009PA001879

107. L. Carter, B. Manighetti, Glacial/interglacial control of terrigenous and biogenic fluxes in the deep ocean off a high input, collisional margin: A 139 kyr-record from New Zealand. *Mar. Geol.* **226**, 307–322 (2006). doi:10.1016/j.margeo.2005.11.004

108. G. Cortese, G. B. Dunbar, L. Carter, G. Scott, H. Bostock, M. Bowen, M. Crundwell, B. W. Hayward, W. Howard, J. I. Martínez, A. Moy, H. Neil, A. Sabaa, A. Sturm, Southwest Pacific Ocean response to a warmer world: Insights from Marine Isotope Stage 5e. *Paleoceanography* **28**, 585–598 (2013). doi:10.1002/palo.20052

109. I. R. Hall, I. N. McCave, N. J. Shackleton, G. P. Weedon, S. E. Harris, Intensified deep Pacific inflow and ventilation in Pleistocene glacial times. *Nature* **412**, 809–812 (2001). doi:10.1038/35090552 Medline

110. M. E. Salvignac, thesis, University of Bordeaux I, Talence, France (1998).

111. S. Becquey, R. Gersonde, Past hydrographic and climatic changes in the Subantarctic Zone of the South Atlantic–The Pleistocene record from ODP Site 1090. *Palaeogeogr. Palaeoclimatol. Palaeoecol.* **182**, 221–239 (2002). doi:10.1016/S0031-0182(01)00497-7

112. J. J. Pichon, L. D. Labeyrie, G. Bareille, M. Labracherie, J. Duprat, J. Jouzel, Surface water temperature changes in the high latitudes of the Southern Hemisphere over the last glacial-interglacial cycle. *Paleoceanography* **7**, 289–318 (1992). doi:10.1029/92PA00709

113. A. D. Moy, W. R. Howard, M. K. Gagan, Late Quaternary palaeoceanography of the Circumpolar Deep Water from the South Tasman Rise. *J. Quaternary Sci.* **21**, 763–777 (2006). doi:10.1002/jqs.1067

114. C. S. Nelson, P. J. Cooke, C. H. Hendy, A. M. Cuthbertson, Oceanographic and climatic changes over the past 160,000 years at Deep Sea Drilling Project Site 594 off southeastern New Zealand, southwest Pacific Ocean. *Paleoceanography* **8**, 435–458 (1993). doi:10.1029/93PA01162

115. L. Labeyrie, M. Labracherie, N. Gorfti, J. J. Pichon, M. Vautravers, M. Arnold, J.-C. Duplessy, M. Paterne, E. Michel, J. Duprat, M. Caralp, J.-L. Turon, Hydrographic changes of the southern ocean (southeast Indian sector) over the last 230 kyr.

Paleoceanography **11**, 57–76 (1996). doi:10.1029/95PA02255

116. H. L. Neil, L. Carter, M. Y. Morris, Thermal isolation of Campbell Plateau, New Zealand, by the Antarctic Circumpolar Current over the past 130 kyr. *Paleoceanography* **19**, n/a (2004). doi:10.1029/2003PA000975

117. A. Sturm, thesis, Christian-Albrechts-Universität, Kiel, Germany (2004).